

Acid ceramidase and sphingosine-1-phosphate lyase as biomarkers and therapeutic targets in cancer

(Ceramidasa ácida y Esfingosina-1-fosfato Liasa como biomarcadores y dianas terapéuticas en cáncer)

Luz del Carmen Camacho Castillo

ADVERTIMENT. La consulta d'aquesta tesi queda condicionada a l'acceptació de les següents condicions d'ús: La difusió d'aquesta tesi per mitjà del servei TDX (www.tdx.cat) ha estat autoritzada pels titulars dels drets de propietat intel·lectual únicament per a usos privats emmarcats en activitats d'investigació i docència. No s'autoritza la seva reproducció amb finalitats de lucre ni la seva difusió i posada a disposició des d'un lloc aliè al servei TDX. No s'autoritza la presentació del seu contingut en una finestra o marc aliè a TDX (framing). Aquesta reserva de drets afecta tant al resum de presentació de la tesi com als seus continguts. En la utilització o cita de parts de la tesi és obligat indicar el nom de la persona autora.

ADVERTENCIA. La consulta de esta tesis queda condicionada a la aceptación de las siguientes condiciones de uso: La difusión de esta tesis por medio del servicio TDR (www.tdx.cat) ha sido autorizada por los titulares de los derechos de propiedad intelectual únicamente para usos privados enmarcados en actividades de investigación y docencia. No se autoriza su reproducción con finalidades de lucro ni su difusión y puesta a disposición desde un sitio ajeno al servicio TDR. No se autoriza la presentación de su contenido en una ventana o marco ajeno a TDR (framing). Esta reserva de derechos afecta tanto al resumen de presentación de la tesis como a sus contenidos. En la utilización o cita de partes de la tesis es obligado indicar el nombre de la persona autora.

WARNING. On having consulted this thesis you're accepting the following use conditions: Spreading this thesis by the TDX (www.tdx.cat) service has been authorized by the titular of the intellectual property rights only for private uses placed in investigation and teaching activities. Reproduction with lucrative aims is not authorized neither its spreading and availability from a site foreign to the TDX service. Introducing its content in a window or frame foreign to the TDX service is not authorized (framing). This rights affect to the presentation summary of the thesis as well as to its contents. In the using or citation of parts of the thesis it's obliged to indicate the name of the author.



UNIVERSITAT DE BARCELONA



Departamento de Genética de la Facultad de Biología de la Universidad de Barcelona
Programa de Genética 2006-2008

Acid ceramidase and sphingosine-1-phosphate lyase as biomarkers and therapeutic targets in cancer

(Ceramidasa ácida y Esfingosina-1-fosfato Liasa como biomarcadores y
dianas terapéuticas en cáncer)

Memoria presentada por Luz del Carmen Camacho Castillo para optar al grado
de Doctora por la Universidad de Barcelona

Esta tesis fue realizada en el Instituto de Química Avanzada de Cataluña en las
instalaciones del Centro de Investigación y Desarrollo (CID-CSIC)

Dra. Gemma Fabriàs Domingo
Directora

Dra. Gemma Marfany Nadal
Tutora

Luz del Carmen Camacho Castillo

2011

CONTENT

I. INTRODUCTION

I.1. SPHINGOLIPIDS	3
I.1.1 Sphingolipid metabolism.....	4
I.1.2 Compartmentalization and transport of sphingolipids.....	6
I.2. SPHINGOSINE-1-PHOSPHATE	8
I.2.1 Biophysical properties of S1P.....	8
I.2.2 Biological functions of S1P.....	8
I.2.2.1 S1P as a receptor ligand.....	8
I.2.2.2 S1P as an intracellular signaling molecule.....	9
I.2.2.3 S1P and sphingolipid rheostat.....	10
I.3. SPHINGOSINE PHOSPHATE LYASE	11
I.3.1 Structure, expression and cellular localization of SPL.....	11
I.3.2 Tissue distribution of SPL.....	12
I.3.3 SPL and human disease.....	13
I.3.3.1 SPL in cell growth and cancer.....	13
I.3.3.2 SPL in immunological disorders.....	15
I.3.4 SPL activity assays.....	17
I.3.5 SPL inhibitors.....	18
I.3.5.1 Substrate and cofactor analogs.....	18
I.3.5.2 THI and analogs.....	19
I.3.5.3 FTY720.....	19
I.3.5.4 LX2931.....	20
I.4. CERAMIDE	21
I.4.1 Biophysical properties.....	21
I.4.2 Biological effects of ceramide.....	21
I.5. CERAMIDASES	22
I.5.1 Role of ceramidases in regulating cellular responses.....	22
I.5.1.1 Neutral ceramidase.....	22
I.5.1.2 Alkaline ceramidase 1.....	23
I.5.1.3 Alkaline ceramidase 2.....	24
I.5.1.4 Alkaline ceramidase 3.....	24
I.5.2 Acid ceramidase.....	25
I.5.2.1 AC and human diseases.....	25
I.5.2.1.1 Farber Disease.....	25
I.5.2.1.2 AC and cancer.....	26
I.5.2.1.3 AC and other complex diseases.....	27
I.5.3 AC inhibitors.....	28
I.5.3.1 NOE.....	28
I.5.3.2 Compound B13 and analogs.....	29
I.5.3.3 Compound B13 and analogues.....	30
I.5.4 Methods to determine ceramidase activity.....	32
I.5.4.1 Fluorogenic assay.....	34

I.6. CELL CYCLE	35
I.6.1 Cell cycle regulation.....	36
I.7. APOPTOSIS	37
I.7.1 The extrinsic apoptotic pathway.....	38
I.7.2 The intrinsic apoptotic pathway.....	39
I.8. CERAMIDE MEDIATED CELL CYCLE ARREST AND APOPTOSIS	41
I.9. CANCER	44
I.9.1 Prostate cancer.....	46
I.9.1.1 The prostate.....	46
I.9.1.2 PC detection.....	47
I.9.1.3 Stages of prostate cancer.....	47
I.9.1.4 PC treatments.....	49
I.9.1.5 PC epidemiology	49
I.9.2 Acid ceramidase and prostate cancer.....	50
I.9.2.1 Role of AC in tumor progression and metastasis.....	51
I.9.2.2 Role of AC in resistance to radiation therapy.....	52
II. OBJECTIVES	55
III. RESULTS AND DISCUSSION	
III.1. Development of enzyme assays for sphingosine-1-phosphate lyase.....	59
III.1.1. Determination of sphingosine-1-phosphate lyase activity by fluorimetry.....	59
III.1.2. Expression of recombinant SPL.....	67
III.1.3. Determination of sphingosine-1-phosphate lyase activity by gas chromatography coupled to mass spectrometry.....	69
III.2. Optimization and use of a fluorogenic enzyme assay for the acid ceramidase.....	78
III.2.1. Optimization of the chemical steps.....	78
III.2.1.1. Aminodiol oxidation by sodium periodate (NaIO ₄) in acid conditions.....	78
III.2.1.2 Oxidation in basic conditions with different amounts of NaIO ₄	80
III.2.2. Determination of the AC activity-dependence on the substrate <i>N</i> -acyl chain length.	83
III.2.2.1. Activity of AC over the RBM14 analogues both in intact cells and cell lysates.....	84
III.2.2.2. Hydrolysis of RBM14 analogues by other CDases in intact cells.	85
III.2.2.3. In vitro hydrolysis of RBM14 analogues by other CDases....	87
III.2.2.4. Dose dependence of RBM14 hydrolysis by CDases.....	88
III.2.3. Application to the diagnosis of Farber Disease.....	89
III.2.4. Application to screening of AC activity in cancer cells.....	99
III.2.4.1. Hydrolysis of RBM14 analogues in intact cancer cells.....	99
III.2.4.2. In vitro hydrolysis of RBM14 analogues by cancer cell lysates	101
III.2.4.3. Metabolism of RBM 14 and its analogues.....	103

III.2.5.	Application to screening, identification and characterization of AC inhibitors.....	106
III.2.5.1.	Compounds RBM2-1.....	106
III.2.5.1.1	Effect of RBM2-1B AND RBM2-1D on the sphingolipidome.....	108
III.2.5.2.	Compounds RBM1.....	113
III.2.5.2.1.	RBM1 compounds over NC <i>in vitro</i> activity.....	114
III.2.5.2.2.	Dose response of compounds RBM1.....	115
III.3.	Study of the contribution of the acid ceramidase to the invasiveness of prostate cancer cells.....	115
III.3.1.	Genetic inhibition of the <i>ASAH1</i> gene.	117
III.3.1.1.	Sphingolipid profile of PC3/Mc_ <i>ASAH1</i> knockdown cells.....	118
III.3.1.2.	Effect of <i>ASAH1</i> silencing on cell growth.....	119
III.3.1.3.	Effect of <i>ASAH1</i> silencing on the cell cycle.....	120
III.3.1.4.	Effect of <i>ASAH1</i> silencing on invasiveness	121
III.3.1.5.	Effect of <i>ASAH1</i> silencing on 3D growth and tumor formation.....	122
III.3.1.6.	Effect of <i>ASAH1</i> silencing on lung colonization.....	124
III.3.2.	Chemical inhibition of AC in PC intact cells.....	126
III.3.2.1.	Sphingolipid profile of PC3/Mc cells treated with AC inhibitors.....	127
III.3.2.2.	Effect of AC inhibitors on cell growth.....	129
III.3.2.3.	Effect of AC inhibitors on invasiveness.....	130
III.3.2.4.	Effect of AC inhibitors on 3D growth.....	131
III.3.2.5.	Toxicity of SABRAC.....	132
IV.	CONCLUSIONS.....	135
V.	GENERAL MATERIALS AND METHODS	
V.1	Materials.....	141
V.2	Buffers.....	142
V.3	Plasmids.....	143
V.4	Antibodies.....	144
V.5	Biochemistry and Molecular Biology.....	145
V.5.1	Enzyme activity assays	145
V.5.1.1	Ceramidase activity.....	145
A)	Fluorogenic assay	145
	Cell lysates	145
	Intact cells.....	145
B)	Hydrolysis of CerC12NBD.....	146
	Cell lysates.....	146
	Intact cells.....	146
C)	Quantification of So by NDA derivatization.....	146
V.5.1.2	SPL activity.....	148
A)	Fluorogenic assay.....	148
B)	GC/MS.....	148
V.5.2	Lipid extraction and processing.....	149
V.5.3	Protein quantification.....	149
V.5.4	Western blot analysis.....	150
V.5.5	Plasmids amplification.....	151
V.5.5.1	SPL expression in <i>E. coli</i>	151
V.5.6	Total RNA isolation and RT-PCR.....	152
V.5.7	Real-time PCR (qPCR).....	152

V.8. Cell Biology	
V.8.1 Cell lines.....	153
V.8.2 Transient transfection of fibroblasts.....	153
V.8.3 Cell viability assay (MTT).....	154
V.8.4 Production and transduction of retroviral particles.....	154
V.8.5 Cell cycle analysis.	155
V.8.6 Anchorage-independent growth assays.....	155
V.8.7 <i>In vitro</i> invasiveness assays.....	155
V.8.8 <i>In vivo</i> tumor formation.....	156
V.8.9 Toxicity of SABRAC in mice.....	156
V.9 Instrumental analysis.....	157
V.9.1 Sphingolipid analysis by UPLC/MS.....	157
V.9.2 Gas Chromatography-coupled to Mass Spectrometry.....	157
V.9.3 HPLC/ fluorescence detection.....	158
V.10 Statistical analysis	158
VI. REFERENCES.....	161
VII. RESUMEN.....	175
Appendix I	

Abbreviations

AC	Acid ceramidase
ACER1	Alkaline ceramidase 1
ACER2	Alkaline ceramidase 2
ACER3	Alkaline ceramidase 3 or phytoceramidase
Acyl-CoA	Acyl-coenzyme A
AKT	Serine/threonine protein kinase PKB
ASAH1	Acid ceramidase gene
ASAH2	Neutral ceramidase gene
ASAH3	Alkaline ceramidase 1 gene
ASAH3L	Alkaline ceramidase 2 gene
a.u.	Arbitrary units
BODIPY	Boron dipyrromethene difluoride
BSA	Bovine serum albumin
C1P	Ceramide-1-phosphate
CAPPs	Cer-activated protein phosphatases
CDase	Ceramidase
Cdks	Cyclin dependent kinases
Cer	Ceramide
CerK	Ceramide kinase
CerS	Ceramide synthase
DHCD	Dihydroceramide desaturase
DHCer	Dihydroceramide
DHSo	Dihydrosphingosine
DISC	Death-inducing signaling complex
DOP	Deoxypyridoxine
Dpl1p	Yeast ortholog of human SPL gene
DR	Death receptor
ER	Endoplasmic reticulum

ERK	Extracellular signal regulated kinase
FADD	Fas-Associated protein with Death Domain
FD	Farber disease
FTY720	S1P receptor agonist
GlcCer	Glucosylceramide
GSK-3β	Glycogen synthase kinase beta
GSL	Glycosphingolipids
HF	Fluorhydric acid
JNK	c-Jun N terminal kinase
MAMs	Mitochondria associated membranes
MAPK	Mitogen-activated protein kinase
MEK	MAPK/ERK kinase
MOMP	Mitochondrial outer membrane permeabilization
NBD	7-Nitro-2-1,3-benzoxadiazol
NC	Neutral ceramidase
NDA	Naphthalene-2,3-dialdehyde, derivatizing agent
NOE	AC inhibitor N-oleoylethanolamine
PC	Prostate cancer
PDGF	Platelet-derived growth factor
PHCA	Alkaline ceramidase 3
PHSo	Phytosphingosine
PI3K	Phosphoinositide 3-kinase
PKC	Protein kinase C
PP1 and PP2	Serine/threonine phosphatases
pRb	Retinoblastoma protein
PSA	Prostate specific antigen
RBM14	Fluorogenic substrate of acid ceramidase
RBM13	Fluorogenic substrate of sphingosine-1-phosphate lyase
SLs	Sphingolipids

SM	Sphingomyelin
SMase	Sphingomyelinase
aSMase	Acid sphingomyelinase
nSMase	Neutral sphingomyelinase
SMS	Sphingomyelin synthase
S1P	Sphingosine-1-phosphate
Sa	Sphinganine
SGPL1	Human sphingosine phosphate lyase 1 gene
So	Sphingosine
SPL	Sphingosine phosphate lyase
SPT	Serine palmitoyltransferase
THI	Food colorant tetrahydroxybutylimidazole
TLC	Thin layer chromatography
TNF-α	Tumor necrosis factor- α
TRAIL	TNF-related apoptosis inducing ligand

I. INTRODUCTION

I.1. SPHINGOLIPIDS

Sphingolipids (SLs) as well as phospholipids are the major components of eukaryotic plasma membrane. They were first considered only to play a structural role, however, it is now known that they are also involved in controlling cellular processes such as proliferation, growth, migration, differentiation, senescence and apoptosis¹. The family of bioactive sphingolipids includes mainly, ceramide (Cer), sphingomyelin (SM), ceramide-1-phosphate (C1P), sphingosine (So) and sphingosine-1-phosphate (S1P) among others. Chemically, SLs are composed of a polar head group and two nonpolar tails: the long-chain amino alcohol and the *N*-acyl moiety attached through an amide bond. The C4-C5 unsaturated core long chain base is sphingosine (So), while the saturated counterpart is sphinganine (Sa). The head groups range from a simple hydrogen (for So, Sa and (DH)Cer) to more complex species such phosphocholine (for SM) or the glycans of glycosphingolipids². Some examples of polar heads are shown in Figure 1.

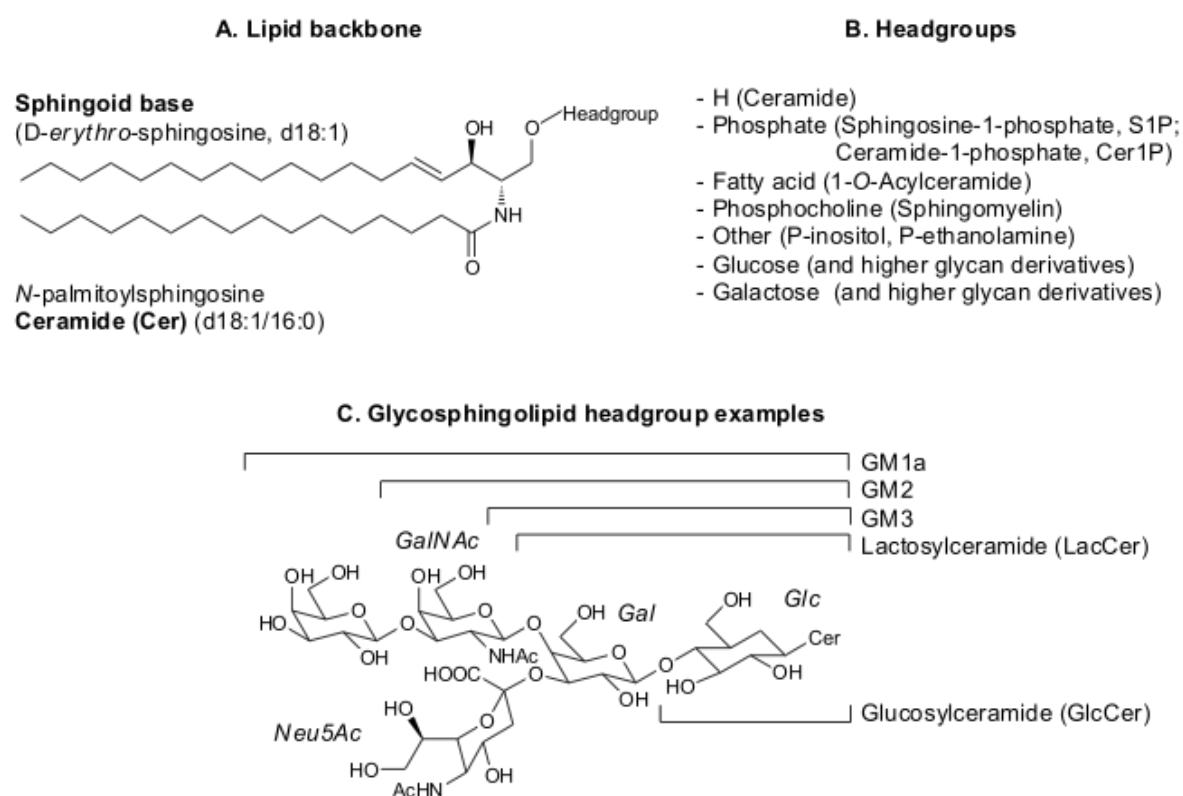


Figure 1. Basic structures of sphingolipid backbones and head groups. A) An example of Cer including names of the components; B) common head groups for mammalian sphingolipids; C) an example of a complex glycosphingolipid, ganglioside GM1a, and the names of the components. Modified from².

I.1.1 Sphingolipid metabolism

Cer is considered to be the central core of sphingolipid metabolism. As shown in Figure 2, Cer can be generated by two major mechanisms:

a) The *de novo* pathway, which is an anabolic pathway beginning with the condensation of serine and palmitoyl-CoA to form 3-ketosphinganine (or 3-ketodihydrosphingosine), a reaction that is catalyzed by serine palmitoyltransferase (SPT)³. Then, reduction of 3-ketosphinganine to Sa and acylation of Sa to dihydroceramide (DHCer) subsequently follow. The latter reaction is catalyzed by DHCer/Cer synthase (also known as Lass or CerS). Up to date, six different CerS have been identified. These enzymes show distinct preferences for the different fatty acyl-CoA substrates and therefore, they generate distinct ceramide species. The different (dihydro)ceramides may localize to distinct cell compartments and may intervene in the regulation of different cell functions⁴.

The last step of the *de novo* pathway includes desaturation of dihydroceramide through introduction of a trans-4,5 double bond to yield ceramide. In turn, ceramide can be acted upon by different biosynthetic enzymes, such as glycosyltransferases to form glycosphingolipids such as cerebrosides or gangliosides, or can incorporate a phosphocholine head group from phosphatidylcholine (PC) to form SM through the action of SM synthases (SMS)⁵. Importantly, SMS has been implicated in cell regulation and transformation through its ability to modulate the levels of ceramide and diacylglycerol, two essential bioactive lipids⁶. In addition, ceramide can be directly phosphorylated by ceramide kinase (CerK) to form C1P (Figure 2), which is a key regulator of cell homeostasis and has been implicated in the inflammatory response^{7,8}.

b) The catabolic pathway involves sphingomyelinase (SMase) activation to form ceramide directly (Figure 2). SMase catalyzes the conversion of SM to Cer and phosphocholine. Mammalian cells utilize three distinct forms of SMases that can be discriminated *in vitro* by their pH optima as: acid, neutral and alkaline SMases.

Both, acid SMase (aSMase) and neutral SMase (nSMase) are known to be involved in signal transduction, whereas alkaline SMase is mainly responsible for digestion of dietary SM in the intestine⁹.

Moreover, in the catabolic pathway Cer is also formed from complex glycosphingolipids, which are degraded by specific hydrolases. This mainly leads to formation of glucosylceramide or galactosylceramide¹⁰. Then specific β -glycosidases and galactosidases produce ceramide by cleavage of their sugar moieties.

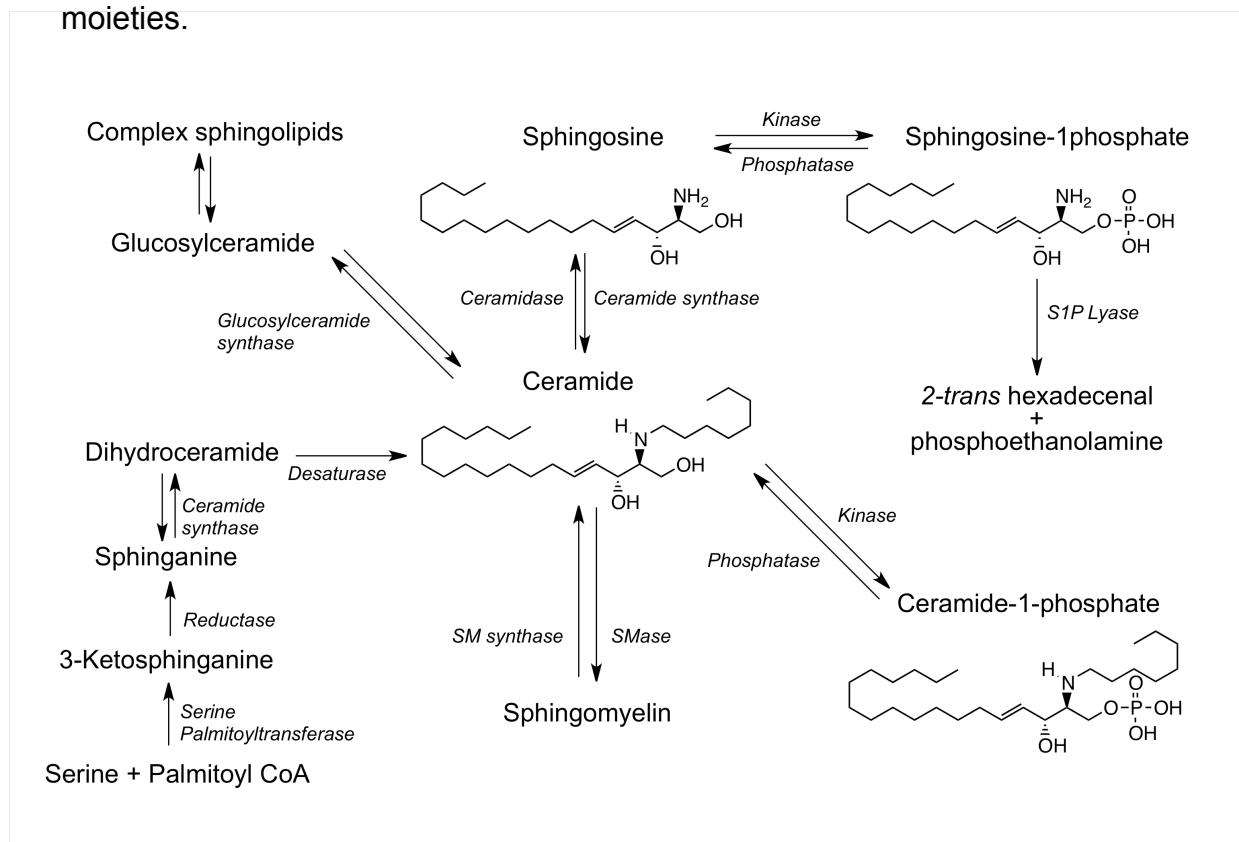


Figure 2. Formation of bioactive sphingolipids in mammalian cells. Modified from ³

Another important pathway that can control ceramide levels in cells is the So salvage pathway, in which So is recycled to ceramide through the action of CerS. Once generated, Cer can be also catabolized to So by the action of the specific ceramidases (CDases), and So, in turn, can be readily phosphorylated to S1P¹¹. Two sphingosine kinases (SphK1 and SphK2) differing in function and subcellular location have so far been identified in mammalian cells¹².

Furthermore, S1P can be dephosphorylated by specific phosphatases to regenerate So, which can be either recycled through the salvage pathway, or can be irreversibly cleaved by sphingosine phosphate lyase (SPL)² (Figure 2).

I.1.2 Compartmentalization and transport of sphingolipids

Sphingolipid biosynthesis and turnover are complex processes that involve not only the production of bioactive compounds, but also the correct balancing between *de novo* and recycling routes and the trafficking of compounds to the appropriate intracellular and extracellular destinations¹³. Most enzymes of sphingolipid metabolism show specific but multiple subcellular localizations, which coupled with the poor solubility of some sphingolipids in cells, establish distinct functional responses depending on the site of the generation and transport of the bioactive sphingolipid¹⁴.

The initial steps of *de novo* synthesis of sphingolipids occur in the endoplasmic reticulum (ER) and in mitochondria associated membranes (MAMs), while synthesis of more complex SL metabolites like SM and GlcCer takes place in the Golgi apparatus (Figure 3). Cer formed in the ER has two known specific transport pathways from the ER to the Golgi: a) through the action of the transfer protein CERT, which is required for SM synthesis but not for GlcCer synthesis¹⁵, or b) vesicle transport, which is needed for Cer delivery for GlcCer synthesis (Figure 3). Afterwards, transfer of GlcCer from the cytosolic surface of the Golgi to the luminal side for the synthesis of complex glycosphingolipids (GSL) requires the action of the transport protein FAPP2^{13,16} (Figure 3).

Subsequently, SM and complex GSL are transported to the plasma membrane via vesicular trafficking. Once in the plasma membrane, SM can be metabolized to Cer, either by aSMase on the outer leaflet of the membrane or by nSMase, which resides in the inner leaflet of the bilayer¹⁷ (Figure 3).

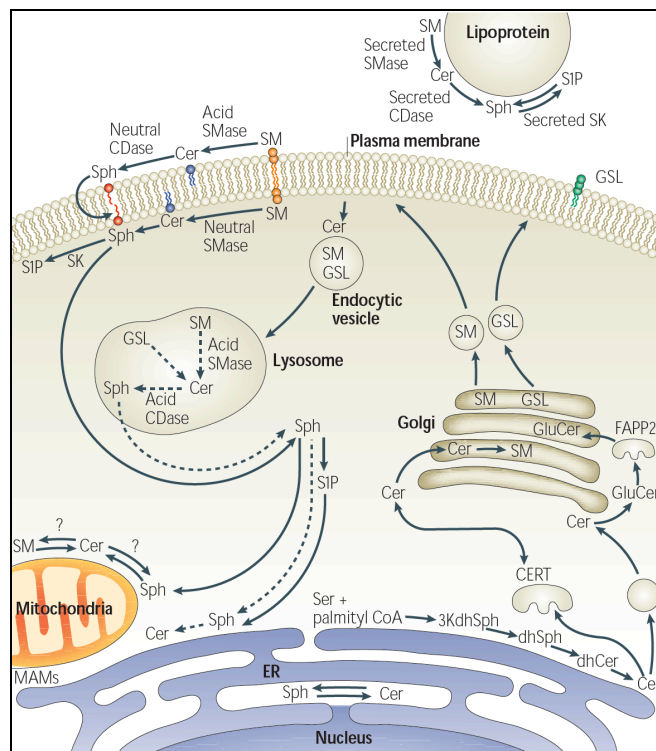


Figure 3. Sphingolipid compartmentalization and transport. The salvage pathway is shown by the dashed arrows. Modified from 13.

From the plasma membrane, SLs may be recirculated through the endosomal pathway. Once inside the cells, SM and GlcCer are metabolized to Cer in the lysosomal compartment by aSMase and glucosidases, and Cer is then hydrolyzed by acid CDase to form So. Due to its ionizable positive charge So is able to leave the lysosome and is sufficiently soluble to move across the cytosol reaching the ER, where it is available for recycling¹⁸.

I.2. SPHINGOSINE-1-PHOSPHATE

I.2.1 Biophysical properties of S1P

Since S1P possesses a lipidic nature, it must exert its regulatory role essentially at the membrane level, as is the case of ceramides and other related lipids. However, because of its amphiphilic nature, S1P also gives rise to stable dispersions in water. Consequently, as with any other soluble amphiphile in the presence of membranes, S1P will exist in equilibrium between the aqueous and membranous compartments².

I.2.2 Biological functions of S1P

S1P has important roles in regulation of cell migration, differentiation, survival and other complex physiological processes¹⁹. S1P signaling plays diverse roles in physiology, generally enhancing cell survival in response to stressful conditions, promoting vascular maturation and vascular permeability by fostering homotypic and heterotypic cell-cell interactions, and regulating lymphocyte egress from the thymus and peripheral lymphoid organs²⁰. S1P carries out its function acting as both an extracellular receptor ligand and an intracellular second messenger.

I.2.2.1 S1P as a receptor ligand

S1P functions primarily by activating a subgroup of the endothelial differentiation gene (EDG) family of G-protein coupled cell surface receptors now referred to as S1P₁₋₅. They bind to S1P with high affinity and also to dihydro-S1P with similar or slightly lower affinity²¹.

In mammals, S1P₁, S1P₂ and S1P₃, are expressed ubiquitously, whereas S1P₄, and S1P₅ are restricted to lymphoid tissues and brain respectively. The biological effects of S1P receptor signaling involve several pathways.

Upon binding of S1P to S1P receptors, S1P activates downstream signaling pathways (Figure 4), leading to a variety of cellular responses including mitogen-activated protein kinase (MAPK), c-Jun N terminal kinase (JNK), extracellular signal regulated kinase (ERK), phosphoinositide 3-kinase (PI3K), phospholipase C, phospholipase D and other downstream mediators²⁰⁻²².

I.2.2.2 S1P as an intracellular signaling molecule

A variety of studies performed in organisms lacking identifiable S1P receptors have shown that disrupting S1P metabolism can result in marked changes in cell migration, Ca⁺² mobilization, stress responses, endocytosis, tissue homeostasis, infectivity, viability and reproduction²³ (Figure 4). These effects could be explained by the direct interaction of S1P with intracellular targets.

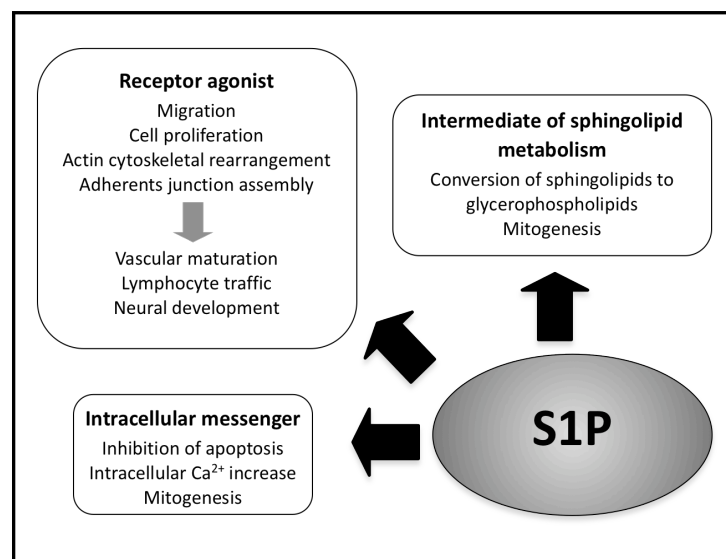


Figure 4. S1P biological functions. Modified from²¹

However, since most cellular responses elicited by intracellular S1P resemble those induced through S1P receptors, it has been suspected that intracellular S1P might be released into the extracellular space to then bind to a S1P receptor in an autocrine or paracrine manner. Indeed, the so-called “inside-out signaling” has been observed in PDGF-induced cell motility²⁴. Thus, the possible intracellular signaling has remained a controversial issue, due to a lack of information regarding intracellular target molecules.

I.2.2.3 S1P and the sphingolipid rheostat

Unlike Cer and So, S1P promotes cell growth and inhibits apoptosis. The antagonistic effects of these metabolites are regulated by enzymes that interconvert Cer, So, and S1P²⁵. Thus, conversion of Cer and So to S1P simultaneously removes pro-apoptotic signals and creates a survival signal, and *vice versa*. This led to the proposal of a “sphingolipid rheostat” as a critical factor determining cell fate²⁶ (Figure 5). According to this hypothesis, it is not the absolute levels but the relative amounts of these antagonistic metabolites that determines cell fate. In agreement, it has been shown that increased S1P protects against Cer-induced apoptosis, and depletion of S1P enhances Cer-induced apoptosis²⁷. Cells overexpressing acid ceramidase are protected from tumor necrosis factor- α (TNF- α)-induced apoptosis, presumably by shunting Cer to S1P²⁸.

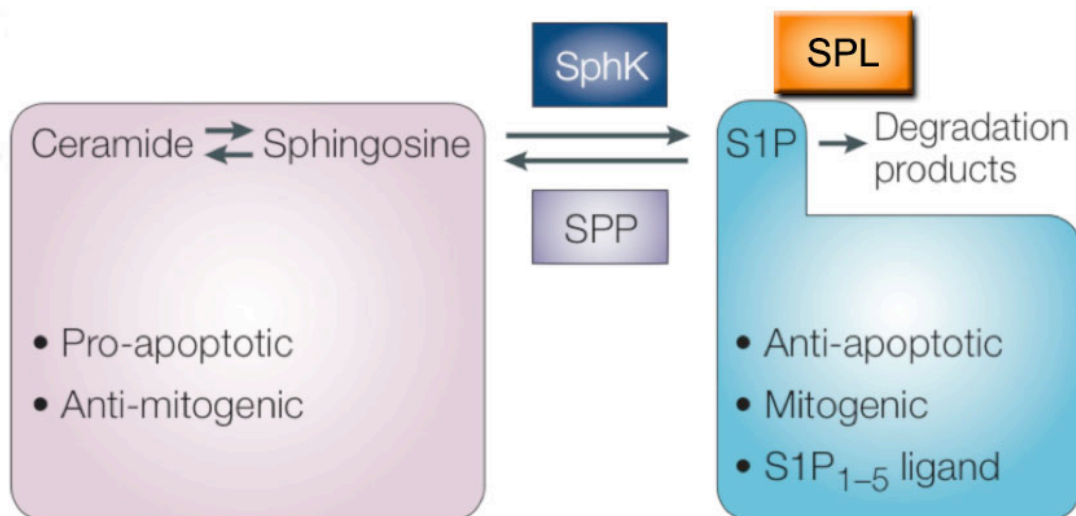


Figure 5. The sphingolipid rheostat. Modified from¹⁹

The intracellular levels of S1P are regulated through the balance between its synthesis by So kinases and its degradation by S1P phosphatases or S1P lyase (SPL).

I.3 SPHINGOSINE PHOSPHATE LYASE

The enzyme SPL irreversibly degrades S1P by cleaving the long chain base between C2 and C3. This reaction results in the formation of a C16-aldehyde and ethanolamine phosphate and depletion of intracellular S1P.

I.3.1 Structure, expression and cellular localization of SPL

The human SPL gene, *sphingosine phosphate lyase 1 (SGPL1)*, located on chromosome 10q21, encodes a protein of 568 amino acids with a predicted molecular mass of 63.5 kDa²⁹. Human SPL displays 84% amino acid identity and 91% similarity to the mouse ortholog³⁰. This enzyme is located primarily in the endoplasmic reticulum as a membrane protein with the catalytic and pyridoxal phosphate binding domains facing the cytosol thereby facilitating the availability of the substrate to the active site. Furthermore, there is only one transmembrane segment close to the N-terminus, which faces the ER lumen³¹.

Several conserved amino acid residues have been mapped to the C-terminal domain of human SPL, including a 20 amino-acid stretch spanning positions 344–364, which contains predicted cofactor binding lysine residues at position K353 and K359. Site-directed mutagenesis of human SPL revealed the importance of two conserved cysteine residues at positions C218 and C317, which are required for proper enzymatic activity³².

Interestingly, recombinant SPL lacking the transmembrane domain and the ER luminal sequence was fully active *in vitro* when expressed in bacteria³². Conversely, a mutagenesis study conducted on the yeast ortholog Dpl1p revealed the important role of the N-terminal domain³³. In this study, the luminal domain of Dpl1p appears to be required to maintain protein stability, and a Dpl1p NΔ57 mutant lacking the entire luminal domain was completely inactive when evaluated using an *in vivo* complementation assay in yeast.

Dpl1p has been shown to form higher order complexes that are required for its *in vivo* function. Polar amino acid residues in the transmembrane domain of Dpl1p play an important role in protein oligomerization³³.

More recently Bourquin et al.³⁴ have succeeded in crystallizing the SPL homologue proteins encoded by Dpl1p (*Saccharomyces cerevisiae*) and StSPL (*Symbiobacterium thermophilum*) genes, as well as in characterizing these proteins both structurally and functionally. They demonstrated that truncation of luminal domain in mutant Dpl1p Δ 1-57 reduces only partially the SPL activity³⁴. Moreover, in this work the authors also propose a mechanism of S1P cleavage by SPL, identifying Y482 as a critical residue for activity. However, further analysis is required to understand completely the reaction mechanism of SPL.

1.3.2 Tissue distribution of SPL

SPL is expressed in many mammalian tissues to variable degrees. In mice and rats, SPL activity and expression is highest in the small intestine, colon, thymus, and spleen, whereas moderate expression is observed in liver, kidney, lung, stomach and testis. SPL expression is lowest in the heart, skeletal muscle and brain, with the exception of the olfactory mucosal epithelium, where the enzyme is highly enriched^{30,35,36}.

SPL expression is low in lymphocytes and absent in erythrocytes and platelets, which are major sources of plasma S1P^{37,38}. SPL is expressed in some inflammatory cells, but its activity in macrophages, monocytes, dendritic cells and neutrophils has not been characterized to date. SPL expression seems to be high in tissues characterized by rapid cell turnover. This is exemplified by the pronounced expression and activity of SPL in intestinal epithelial cells, which are renewed every 12 hours³⁰. Another example is the high SPL expression in the olfactory mucosa, a unique neuronal tissue that is subject to high rates of apoptosis due to inhaled toxic-induced cell damage³⁵.

In addition, the high expression of SPL in the thymus might be required to maintain low tissue S1P levels compared to the surrounding plasma. The S1P concentration gradient between thymus and the plasma enables T cell egress from thymus into the circulation³⁹.

I.3.3 SPL and human disease

The involvement of S1P in diverse essential cellular processes necessitates precise control and regulation of its intracellular and extracellular levels. The importance of SPL in modulating the levels of S1P, other sphingolipid intermediates and cell fate is likely to contribute to tissue homeostasis and its dysregulation could contribute to the pathophysiology of disease. In support of this notion, genetically modified mice lacking SPL expression in all tissues demonstrate stunted growth and early mortality with defects reported in the kidney, bone and vasculature⁴⁰, as well as myeloid cell hyperplasia, and significant lesions in the lung, heart and urinary tract⁴¹. The potential role of SPL in specific disease states is described below.

I.3.3.1 SPL in cell growth and cancer

Sphingolipids regulate various aspects of cell growth, proliferation, and cell death⁴². Ceramide generation is considered to be a key mechanism by which chemotherapeutic agents induce apoptosis in cancer cells. On the other hand, S1P promotes cell growth, migration, tumor angiogenesis, invasion and metastasis. Consistent with its key roles in the regulation of cancer growth and therapy, genetic changes acquired by malignant cells that result in either a reduction in ceramide generation and/or an accentuation of S1P generation are implicated in the development of resistance to drug-induced apoptosis and escape from cell death⁴³. SPL has the ability to shift the balance towards cell death by attenuating the proliferative S1P signal.

A potential role of SPL in regulating cell fate and stress responses has been investigated in several model systems. For example, an insertional mutagenesis study revealed that mutations in the *Dictyostelium sgIA* gene, which encodes SPL, confers resistance to the anticancer drug cisplatin⁴⁴. Conversely, overexpression of SPL enhanced the sensitivity of *Dictyostelium* cells to the drug⁴⁵.

Enforced expression of SPL in malignant and non-transformed human cells sensitizes these cells to platinum-based chemotherapy drugs (cisplatin and carboplatin), daunorubicin and etoposide^{39,46,47}. The ability of SPL to potentiate cell death requires the actions of p53 and p38 MAPK signaling pathways. Conversely, knockdown of endogenous SPL expression in HEK293 cells by siRNA results in diminished apoptosis in etoposide treated cells³⁹.

Furthermore, elevation in *Sgpl1* mRNA levels has been associated with testicular degeneration caused by increased apoptosis due to leptin deficiency in mice⁴⁸. Conversely, SPL deficiency can also lead to cell death, as evidenced by increased apoptosis observed in the reproductive organs of *Drosophila Sply* null mutant⁴⁹. The sphingolipid metabolite responsible for this effect is unknown, although these tissues show a profound accumulation of long-chain bases including $\Delta 4,6$ -sphingadienes, which are found to promote apoptosis in *Drosophila* cell lines⁵⁰. Interestingly, it has been proposed that accumulation of intracellular S1P above a certain threshold can also induce apoptosis. Cerebellar granule neurons isolated from SPL-deficient mice showed a similar elevation in the intracellular S1P levels upon treatment with either sphingosine or exogenous S1P. However, only S1P addition to the cells induces apoptosis⁵¹.

Consistent with a role for S1P in various processes associated with tumorigenesis⁴², SPL expression and activity are downregulated during intestinal tumor development in the *ApcMin/+* mouse model of intestinal tumorigenesis, as well as in human colon cancer specimen compared with normal adjacent tissues³⁹. In agreement with these findings, administration of a monoclonal S1P antibody substantially reduced tumor progression and angiogenesis in murine xenograft and allograft models⁵².

SGPL1 is among a set of genes downregulated in metastatic tumor tissues compared to primary tumors from the same patients⁵³. Additionally, Colié *et al.*⁵⁴ have found that the lack of SPL leads to upregulation of the antiapoptotic proteins Bcl-2 and Bcl-xL and consequently protects against apoptosis induced by chemotherapeutic agents. Moreover, SPL-deficient cells isolated from *sgpl1*^{-/-} mouse embryos showed an increase in cell growth rate in culture, colony formation in soft agar, and tumor progression in nude mice compared with cells isolated from wild-type embryos⁵⁴.

Conversely, upregulation of SPL expression has been observed in ovarian cancer. SGPL1 was also identified in a group of genes whose expression is upregulated in ovarian tumors that were resistant to chemotherapy⁵⁵.

These findings suggest that SPL may act as tumor suppressor and may be involved in cancer surveillance pathways. Presumably SPL would act by preventing intracellular S1P accumulation, whereas loss of SPL expression or activity might promote tumorigenesis through activation of S1P-mediated signaling.

I.3.3.2 SPL in immunological disorders

S1P levels in the blood and lymph are high (0.1–1.0 μM) compared with those in most tissues, which maintain baseline levels in the range of 0.5 to 75 pmol/mg^2 . This difference establishes an S1P concentration gradient between circulatory fluids (lymph and blood) and lymphoid organs⁵⁶, which is tightly maintained by SPL activity in the tissues. This S1P gradient is essential for lymphocyte egress from lymphoid organs. Inhibition of SPL activity by the food colorant tetrahydroxybutylimidazole (THI) or by reducing hematopoietic cell SPL expression through RNA interference-mediated knockdown prevents lymphocyte egress from thymus and secondary lymphoid organs⁵⁶. Inhibition of SPL by THI raised the bioavailable S1P levels ~100–1000-fold in thymus and secondary lymphoid organs without altering plasma S1P levels, thereby causing a disruption of the S1P gradient.

The critical role of SPL in lymphocyte trafficking was recently confirmed in a study showing that genetically modified mice lacking *Sgpl1* expression exhibit lymphopenia, with sequestration of mature T cells in the thymus and lymph nodes⁴¹. Furthermore, humanized knock-in mice lacking murine *Sgpl1* expression but harboring one or two alleles of human *Sgpl1* also exhibited immune defects.

Replacement of the human SPL gene in the *Sgpl1* null background resulted in SPL expression at 10–20% of normal mouse SPL levels, yet failed to restore normal T-cell development and trafficking. These data suggest that immune functions including lymphocyte trafficking are exquisitely sensitive to alterations in SPL activity⁴¹.

Apart from its role in lymphocyte trafficking, S1P signaling plays a role in proliferation, survival and differentiation of lymphocytes. S1P treatment enhances the survival of B and T cells, inhibits both homeostatic proliferation and T-cell receptor-induced proliferation of T cells, and inhibits cytokine production²².

Importantly, it has recently been demonstrated that genetic ablation of *Sgpl1* in mice hampers B and T cell development in addition to lymphocyte egress⁴¹. *Sgpl1* knockout (*Sgpl1*^{-/-}) and humanized knock-in mice harboring one human allele (*Sgpl1H*⁻) mice showed severe hypocellularity and increased apoptosis of lymphocytes within the thymic cortex, as well as a paucity of T-cells in the splenic periarteriolar lymphoid sheaths and paracortical areas of lymph nodes. SPL deficiency also caused the vacuolization of thymic epithelial and stromal cells required for T- cell selection and maturation⁴¹.

These studies suggest that dysregulation of the S1P/ SPL axis could be important in mediating multiple aspects of some autoimmune and inflammatory diseases like multiple sclerosis, type I diabetes, atopic dermatitis and, on the other hand, may serve as target for therapeutic intervention³⁰.

Moreover, SPL represents a novel target for cancer therapy and immunosuppression in transplantation and autoimmunity. In this context, the discovery and characterization of new S1PL inhibitors is of interest, since it may finally lead to the development of new drugs to treat immune diseases.

1.3.4 SPL activity assays

The measurement of SPL activity was originally described using a radioactive assay in which conversion of a radiolabeled substrate to a long-chain aldehyde that retained the label was monitored.

The most accepted radiometric method for SPL activity involves the use of [4,5-³H]dihydrosphingosine phosphate³¹. SPL is solubilized in Triton X-100, which does not interfere with enzyme activity. The reaction mixture also contains pyridoxal 5' - phosphate cofactor, as well as phosphatase inhibitors. Radiolabeled products are separated by TLC and the regions of interest are scraped into scintillation vials and the radioactivity is counted. The drawback of this assay system is the necessity of using radioactive materials, the time required to develop the autoradiograms, and the lack of commercial sources of high quality substrate.

More recently, Bandhuvula *et al.*⁵⁷ have developed a fluorescence-based method to measure SPL activity, which uses 7-nitrobenz-2-oxa-1,3-diazole-sphingosine 1-phosphate (NBD-S1P) (Figure 6) as a substrate, leading to the production of phosphoethanolamine and NBD-hexadecenal, which is detected by HPLC coupled to a fluorescence detector⁵⁷.

Another method relies on a substrate containing a boron dipyrromethene difluoride (BODIPY) group (Figure 6). Advantages associated with the BODIPY fluorophore include better photochemical stability, high fluorescence intensity and insensitivity⁵⁸ to polarity and pH of the environment. In both cases, the fluorophore is attached to the omega carbon atom of the long chain base to avoid steric hindrance that could interfere with the SPL reaction⁵⁹. Finally, Berdyshev *et al.*⁶⁰ have developed a simple and highly sensitive protocol for SPL activity determination based on (*E*)-2-hexadecenal quantitation as a semicarbazone derivative by LC/MS.

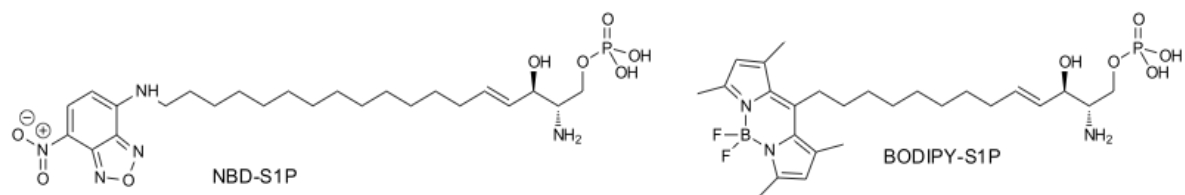


Figure 6. Chemical structures of the reported SPL substrates NBD-S1P and BODIPY-S1P.

I.3.5 SPL inhibitors

Modulation of SPL activity through the use of small molecule inhibitors appears to hold promise for therapeutic purposes, particularly for immunomodulation in the treatment of autoimmune disorders and for transplantation, as well as for enhancement of wound healing and protection of normal tissues from various insults such as radiation, hypoxia and ischemia. Different pharmacological categories of SPL inhibitors have been described.

I.3.5.1 Substrate and cofactor analogs

The substrate analogs include 1-desoxydihydrospingosine-1-phosphonate, the 2D,3L- isomer of DHS1P and 2-vinyldihydrospingosine-1-phosphate⁶¹ (Figure 7). These compounds have been shown to inhibit SPL activity, but generally they are not appropriate for *in vivo* use due to lack of specificity and high toxicity⁶². The second group of SPL inhibitors includes pyridoxal 5'-phosphate analogs or compounds that inhibit the binding of the cofactor. An example is the compound deoxypyridoxine (DOP), which inhibits the activity of SPL and other pyridoxal 5'-phosphate dependent enzymes. Interestingly, DOP is also known to induce lymphopenia, presumably by reducing the S1P gradient. SPL activity is profoundly inhibited in the thymus of DOP-treated mice, an effect which can be overcome by treatment with excess cofactor coincident with restoration of SPL activity⁵⁶.

Since DOP inhibition is not specific for SPL and affects the activity of many other enzymes including those involved in DNA synthesis, long-term exposure is associated with considerable toxicity²⁶. Additionally, SPL activity is also inhibited by divalent metal ions such as Ca^{2+} and Zn^{2+} , and by semicarbazide, cyanide, and bisulfite³¹.

I.3.5.2 THI and analogs

It was discovered that THI (Figure 7), a component of caramel food coloring, also produces lymphopenia through inhibition of lymphocyte trafficking, but in the latter case the effect appears to be due to inhibition of SPL, which results in attenuation of the S1P gradient⁶³. This observation revealed the potential of SPL to serve as a therapeutic target for immune modulation. Oral administration of THI results in reduced tissue SPL activity and elevated levels of tissue and circulating S1P; however, the drug does not inhibit SPL *in vitro*. It has been suggested that may require metabolism to an active state or may be dependent on the formation of a higher-order complex^{33,64,65}.

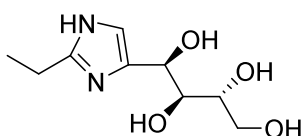
THI derivatives have been synthesized and screened for their ability to induce lymphopenia in mice⁶⁴. Several modifications were made to THI in the core heterocycle, in the side chain and in the position 2 of the imidazole ring. In the latter case, the α,α -difluoro analog exhibited remarkable ability to deplete lymphocyte levels but was highly toxic due to HF poisoning. Adding another heterocycle in this position depleted lymphocyte levels⁶³. Those compounds, however, have not been tested *in vitro* and their mechanism of action remains unknown.

I.3.5.3 FTY720

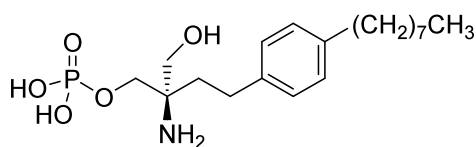
The S1P receptor agonist FTY720 (Figure 7) is a modest inhibitor of SPL activity both *in vivo* and *in vitro*⁶⁶. FTY720 has shown promise in preventing rejection with both standard and reduced cyclosporine exposure. However, the results of large multicenter clinical trials with FTY720 in renal transplant patients have been disappointing. Phase III clinical trial studies not only failed to show an advantage of FTY720 over standard immunosuppressive drugs but also demonstrated lower creatine clearance and increased risk of macular edema⁶⁷⁻⁶⁹. FTY720 was associated with higher incidence of bradycardia and respiratory disorders⁶⁸.

I.3.5.4 LX2931

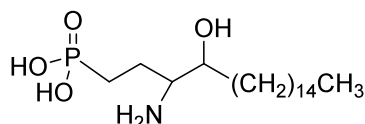
Despite the number of small molecules reported to inhibit SPL, none is specific and non-cytotoxic. However, Lexicon Pharmaceutical, Inc., The Woodlands, Texas, has developed an orally-deliverable small molecule inhibitor of SPL, which has completed Phase I clinical trial for the treatment of rheumatoid arthritis. Preclinical studies with LX2931 showed a consistent reduction in circulating lymphocyte counts in multiple species. In addition, LX2931 reduced joint inflammation and prevented arthritic destruction of joints in mouse and rat models of arthritis^{70,71}. These findings strongly suggest that SPL inhibitors could be a powerful addition to the arsenal of immunomodulatory therapy for autoimmune diseases.



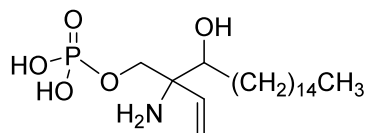
THI (2-acetyl-4-(1R,2S,3R,4-tetrahydroxybutyl)-imidazole)



FTY720 phosphate



1-desoxysphinganine-1-phosphonate



2-vinylsphinganine 1-phosphate

Figure 7. Chemical structure of known SPL inhibitors

Thus, a need remains for additional approaches to modulating S1P-mediated effects on the immune system with therapeutic purposes.

I.4 CERAMIDE

I.4.1 Biophysical properties

Chemically, ceramides (Cers), also named *N*-acylsphingosines, are the result of the *N*-acylation of sphingosine with fatty acids, which can vary in chain length (16-24 carbon atoms typically in humans). According with the current convention about the nomenclature of Cers, the fatty acyl chain length is usually presented as a prefix, such as C16-Cer for *N*-palmitoylsphingosine. Since both, the sphingoid base and fatty acid can be unsaturated, there is another clearer nomenclature that provides information about both chains; for example, d18:1/16:0 for *N*-palmitoylsphingosine⁷².

Natural Cers are highly hydrophobic and essentially insoluble in aqueous medium. When studies require the delivery of ceramides, the water-insolubility problem is bypassed using detergents, liposomes, organic solvents or short chain analogs (C2 to C8-Cer)⁷³. Despite that, when a short chain ceramide is added to cells, the fatty acid is removed and replaced with a long chain fatty acid through cellular metabolism, resulting in the production of small quantities of long chain ceramide. It is important to point out that the use of these short chain analogs is only informative, because most of the Cer remains as short chain Cer, displaying different biophysical and probably physiological properties⁷⁴.

I.4.2 Biological effects of ceramide.

Diverse studies have demonstrated that ceramide is implicated in the regulation of apoptosis, cell growth arrest, diabetes, insulin resistance, inflammation, neurodegenerative disorders, and atherosclerosis⁷⁵. The topology of ceramide generation is crucial for determination of its functions as a bioregulatory molecule, with compartmentalization being essential for separation of signaling and metabolic pools within cells⁷⁶. Therefore, Cer generation at the plasma membrane exerts distinct and specific functions including aggregation of the Fas receptor, and effects on protein kinase C (PKC), but not other effects mediated by endogenous ceramides such as apoptosis, or cell cycle arrest⁷⁷. The proposed molecular mechanisms and intracellular targets involved in ceramide biological functions will be addressed later.

1.5 CERAMIDASES *

CDases are ubiquitous amidohydrolases that catalyze the cleavage of Cers into So and fatty acids. According to their optimum pH, CDases are classified in three groups, acid, neutral and alkaline. Five human CDases that are encoded by five distinct genes have already been cloned: acid ceramidase (AC) or *ASAH1*, a neutral ceramidase (NC) or *ASAH2*, and three alkaline ceramidases, ACER1, ACER2 and ACER3 or *ASAH3*, *ASAH3L* and *PHCA* respectively³. Table 1 summarizes information about protein sequences, chromosomal locations, tissue distributions, and cellular localizations of the human CDases.

AC and NC are ubiquitously expressed and are found in lysosomes and plasma membrane, respectively⁷⁸. By contrast, ACER1 is exclusively expressed in the ER of skin cells⁷⁹. ACER2 is localized to the Golgi complex and, although it is expressed in all tissues⁸⁰, it is particularly abundant in placenta, which also contains high levels of the ACER3 alkaline enzyme. ACER3 was in fact the first alkaline ceramidase to be cloned in mammalian cells⁷⁸. ACER3 is localized to both the ER and the Golgi, and it hydrolyzes dihydroceramides and phytoceramides containing unsaturated acyl chains. An interesting feature of the three alkaline CDases is their activation by Ca^{2+} ions. CDases have also been identified in bacteria and yeast^{81,82}.

1.5.1 Role of ceramidases in regulating cellular responses

1.5.1.1 Neutral ceramidase

NC is mainly expressed in cell membrane; thus, Tani *et al.*⁸³ showed that overexpression of the mouse NC fails to alter the levels of ceramides, So, and S1P in CHOP cells, unless ceramides are released from sphingomyelin in the plasma membrane or in fetal bovine serum, suggesting that NC may be responsible for the generation of So and S1P by controlling the hydrolysis of ceramides in the plasma membrane and the extracellular space. It is unclear whether an increased generation of So and S1P by hNC has any effects on cell survival or apoptosis.

*Parts of this section are included in the review: Gangoiti P, Camacho L, Arana L, Ouro A, Granado MH, Brizuela L, Casas J, Fabriás G, Abad JL, Delgado A, Gómez-Muñoz A. Control of metabolism and signaling of simple bioactive sphingolipids: Implications in disease. *Prog Lipid Res.* 2010, 49, 316-34. A copy of the review is included in the Annexes section

Table 1

Protein	Gene	Chr	AA	Cellular localization	pH optimum	Substrate specificity	Tissue distribution
AC	<i>ASAH1</i>	8	395	Lysosome	4.5	C6 to C16 Cer	Ubiquitous Highly expressed in kidney, lung, heart and brain. Low expression in spleen, skeletal muscle and testes.
NC	<i>ASAH2</i>	10	782	Plasma membrane	7.0	C14 Cer	Ubiquitous High levels in kidney, liver and heart. Medium in brain, and lung. Low levels in spleen, skeletal muscle and testes.
ACER1	<i>ASAH3</i>	19	264	ER	8.5	C24:1 Cer	Highly expressed in skin. No detectable expression in other tissues.
ACER2	<i>ASAH3L</i>	9	275	Golgi	9.0	C14 Cer	Ubiquitous Highest levels in placenta.
ACER3	<i>PHCA</i>	11	267	ER/Golgi	9.5	C20:1 Cer (DHCer, PHCer)	Ubiquitous. Highest levels in placenta

Table 1. Human CDases. Chr, Chromosome; AA, number of amino acid. Modified from ⁷⁷

Moreover, Kono *et al.*⁸⁴ showed that knockout of the mouse NC impairs the catabolism of ceramides in the intestine, leading to an increase in ceramides but a decrease in So in this tissue, suggesting that the mouse NC plays an important role in the catabolism of dietary sphingolipids and regulation of ceramide and So in the intestinal tract. Interestingly, inactivation of the NC gene does not cause obvious abnormalities or major alterations in total ceramide in tissues other than the intestinal tract.

I.5.1.2 Alkaline ceramidase 1

ACER1 is mainly expressed in the skin. ACER1 appears to have anti-proliferating and pro-differentiating roles in epidermal keratinocytes by controlling the generation of So and/or S1P.

Lipid analysis demonstrated that ACER1 overexpression increases the levels of both sphingosine and S1P with a concomitant decrease in very long-chain ceramides (D-e-C24- ceramide and D-e-C24:1-ceramide) in human epidermal keratinocytes whereas its knockdown has opposing effects⁷⁹.

I.5.1.3 Alkaline ceramidase 2

ACER2 has dual roles. Its activation or upregulation promotes cell proliferation and survival by generating S1P while So is not aberrantly elevated by its action. On the other hand, ACER2 action may induce cell growth arrest and apoptosis by generating high cellular levels of So, whose anti-proliferative and pro-apoptotic effects may exceed the mitogenic and anti-apoptotic role of S1P. Therefore, the role of this ceramidase in cellular responses may be both cell type specific and stimulus dependent⁸⁰.

In a recent article, Mao et al.⁸⁵ demonstrated that ACER2 is responsible for the cytotoxicity of dihydrosphingosine produced in treatments with the synthetic retinoid *N*-(4-hydroxyphenyl)retinamide in tumor cells. The authors showed that this drug, an inhibitor of dihydroceramide desaturase (DHCD), increases the expression of ACER2, which catalyzes the hydrolysis of dihydroceramides, to generate dihydrosphingosine, and that ACER2 upregulation plays a key role in mediating the *N*-(4-hydroxyphenyl) retinamide-induced generation of DHS as well as the cytotoxicity of *N*-(4-hydroxyphenyl)retinamide in tumor cells.

I.5.1.4 Alkaline ceramidase 3

ACER3 catalyzes the hydrolysis of both unsaturated long-chain dihydroceramides and phytoceramides with a similar efficiency to the hydrolysis of unsaturated long-chain ceramides, suggesting that it has a role in regulating the generation of DHS_o and PHS_o and their phosphates, in addition to So and its phosphate⁸⁶. ACER3 is highly and ubiquitously expressed. In contrast, its endogenous substrates are scarce in most tissues. This inverse correlation between the enzyme and its substrates may suggest that ACER3 may act as a house-keeping enzyme responsible for the catabolism of a specific group of ceramides to generate basal levels of So, DHS_o, or PHS_o and their phosphates in cells and tissues⁸⁶.

I.5.2 Acid ceramidase

Acid ceramidase (AC) (N-acylsphingosine deacylase, EC 3.5.1.23) was originally identified in rat brain homogenates by Gatt in 1963⁸⁷, but the first substantial purification of the enzyme did not occur until 1995, when the protein was isolated from human urine and the full length 2,312 bp *ASAH1* gene was identified and confirmed by DNA sequencing⁸⁸.

AC is synthesized as a 55 kDa precursor polypeptide that is self cleaved in the lysosome to form the mature heterodimeric enzyme, composed of 2 subunits: a 13 kDa α subunit and a 40 kDa β subunit. The latter possesses 5 to 6 *N*-linked oligosaccharide chains, in contrast to the α subunit, which is not glycosylated⁸⁹.

Hydrolysis of ceramide with the purified active human enzyme occurred mostly at an acid pH in *in vitro* experiments (about 4.5). Interestingly, it was shown that the purified recombinant enzyme also synthesizes Cer from So and free fatty acids at an optimal pH of about 6.0⁹⁰. The synthesis of ceramide by AC is named 'reverse' ceramidase activity and suggests that AC plays a crucial role in controlling Cer and So levels.

In 2002 Li *et al.* generated a complete knockout mouse model and obtained F1 heterozygous mice. However, genotype analysis of the mice and embryos from heterozygous (+/-) intercrosses revealed that homozygous (-/-) mice had an embryonic lethal phenotype and that the embryos died before E8.5⁹¹. Interestingly, the progressive lipid storage and lamellar-like structures similar to Farber bodies were observed in several organs of +/- animals.

I.5.2.1 AC and human diseases

I.5.2.1.1 Farber Disease

A genetic deficiency in AC activity causes an accumulation of sphingolipids in lysosomes, leading to the lysosomal storage disorder Farber disease (FD), a very rare autosomal recessive disorder. To date a total of 17 different mutations in the AC gene have been found in FD patients.

The distinct clinical presentation of individual FD patients is likely due to the specific mutations inherited in the AC gene. In most cases the disease is detected early in life with typical symptoms including deformed joints, subcutaneous nodules, progressive hoarseness and early death. FD is diagnosed by the demonstration of reduced AC activity, abnormally high ceramide levels in cultured cells, biopsy samples or urine, and the presence of Farber bodies, “comma shaped” curvilinear tubular structures, by electron microscope analysis⁹². Although there is no treatment for Farber disease beyond palliative care, future therapy of this severe disorder can be envisioned using gene transfer approaches^{93,94}.

1.5.2.1.2 AC and cancer

Abnormal expression of endogenous AC has been reported in several human cancers; for example in prostate cancers and melanomas. Furthermore, several studies have suggested that the inhibition of AC activity may serve cell apoptosis in response to various stressful stimuli⁹⁵.

Increasing evidence points to important roles of ceramidases, specially AC, in the outcome and progression of cancer, and the response of tumors to therapy (reviewed in ^{92,96-98}). AC is overexpressed in several cancer cell lines and cancer tissues⁹⁹⁻¹⁰⁴, which appears to contribute to decrease the levels of ceramide and increase those of S1P, thereby resulting in resistance to cell death and enhancement of cell proliferation. In most cases, AC inhibition induced apoptosis. Multiple reports confirm the relationship between AC activity and radio or chemotherapy resistance, as well as the interest of AC inhibitors as anticancer drugs, either alone or in combination with other therapies.

High levels of AC expression were found in a radiation resistant glioblastoma cell line when exposed to gamma-radiation, and sensitivity to radiation was achieved by treatment with *N*-oleoylethanolamine (NOE) (see below), which significantly increased ceramide levels, caspase activation and apoptosis¹⁰⁵. Cells overexpressing AC show enhanced survival to TRAIL-induced caspase-independent cell death¹⁰⁶. Also head and neck squamous cell cancer (SCC) cell lines with low, medium, or high levels of AC revealed an inverse correlation between the levels of AC and their response to exogenous C6-ceramide.

Furthermore, over-expression of AC in SCC-1 cells increased resistance to Fas-induced cell killing, an action that was overridden by silencing the AC gene. Compound LCL204 (see below) also sensitized head and neck SCC cell lines to Fas-induced apoptosis both *in vitro* and in a xenograft model *in vivo*⁹⁸. The chicken anemia viral protein apoptin promotes apoptosis in many human cancers and transformed cell lines, by increased ceramide accumulation, enhanced aSMase expression and AC down-regulation⁵. AC is also involved in hepatocarcinogenesis and therefore, inhibitors of this enzyme activity may arise as a promising strategy to treat liver cancer.

I.5.2.1.3 AC and other complex diseases

In addition to cancer and FD, AC may play a role in the pathology of other important complex diseases. For example, it has been shown that AC activity and protein levels are significantly increased in Alzheimer's disease¹⁰⁷. Recently He *et al.*¹⁰⁸ demonstrated that both aSM and AC expression are increased, resulting in decreased SM and increased Cer levels. Another article reports that aSM and S1P levels are significantly correlated with the levels of amyloid beta (A β) peptide and hyperphosphorylated *tau* protein; it has been postulated that abnormalities in the two proteins can have an impact in Alzheimer's disease¹⁰⁹. Furthermore, an imbalance between aSMase and AC results in high ceramide levels in the respiratory tract of a cystic fibrosis murine model, which provokes pulmonary inflammation, respiratory epithelial cell death and high susceptibility to severe infections by *Pseudomonas aeruginosa*¹¹⁰⁻¹¹².

Another study reported that ceramide accumulation inhibits Akt/protein kinase B, a central regulator of glucose uptake and anabolic metabolism, leading to insulin resistance¹¹³. Moreover, overexpression of AC blocks the free fatty acid dependent inhibition of insulin signaling¹¹⁴. Recently, Samad *et al.*¹¹⁵ demonstrated that when aSM and AC levels are elevated, SM and Cer levels decreased, but S1P levels are increased in adipose tissues of genetically obese (*ob/ob*) mice.

Together, these reports suggest that sphingolipid metabolism, particularly Cer and S1P and enzymes regulating their metabolism play important roles in obesity and later insulin-resistant type 2 diabetes.

These overall studies suggest that ceramide and its regulating enzyme AC can be putative targets for treating and/or preventing obesity and type 2 diabetes.

I.5.3 AC inhibitors

Based on the important role(s) of ceramide and sphingosine-1-phosphate in regulating cell growth, these sphingolipids have become important targets in cancer therapy¹¹⁶. Moreover, since AC is one of the key enzymes regulating sphingolipid metabolism, several of these recent therapies have been focused on this enzyme, based on the fact that inhibitors of AC activity may lead to increased ceramide levels and stimulate apoptotic cell death.

I.5.3.1 NOE

Amongst the AC inhibitors, *N*-oleoylethanolamine (NOE) has been commonly used as pharmacological tool (Figure 8). However, its weak potency and poor selectivity preclude it from any therapeutic use. In addition, caution must be taken when using this compound, as its specificity versus other enzymes has not been studied.

In this regard, it has been reported that both acid and alkaline CDases are inhibited by NOE in keratinocytes¹¹⁷. Furthermore, NOE also inhibits glucosylation of naturally occurring ceramides in CHP-100 neuroepithelioma cells at non-toxic concentrations, which is accompanied by enhanced accumulation of ceramides and induction of apoptosis.

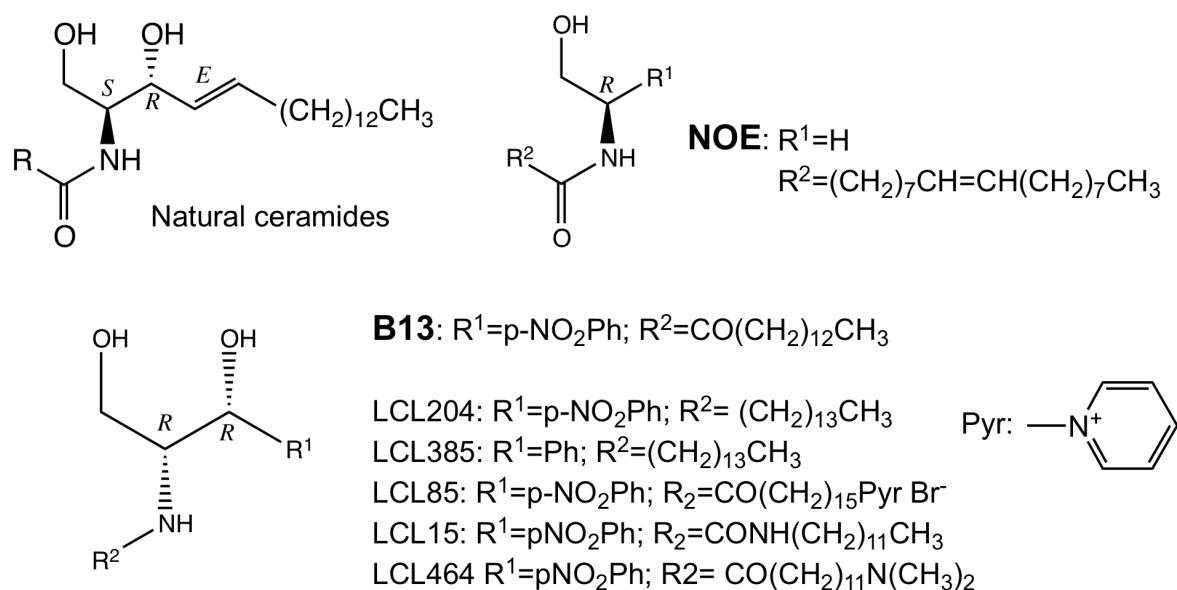


Figure 8. Selected reported acid ceramidase inhibitors. Modified from³

I.5.3.2 NOE analogues

Our group has developed several NOE analogues, some of which have been identified as AC inhibitors. Compounds Z- and E-tb, Z- and E-c7, Z- and E-tbph, C16 c7, tbph and tb, S16c7 have shown to be AC inhibitors when tested *in vitro*¹¹⁸ (Figure 9).

However, only pivaloylamides E-tb and C16-tb, the octanoylamide E-c7 and the *p-tert*-butylbenzamide C16-tbph caused a significant decrease of fluorescence from the substrate in intact FD fibroblasts expressing functional AC. The E-tb and E-c7 IC_{50} values in intact cells were 13.5 and 15.7 μM , respectively.

The compounds E-tb and SC16-tb were investigated further. Kinetic analysis revealed that AC inhibition by these compounds is competitive towards the substrate, with K_i values of 34 and 94 μM , respectively. Compound E-tb seemed to induce an increment in apoptosis when incubated at 50 μM in A549 cells. Additionally, none of the compounds inhibited the neutral ceramidase¹¹⁸.

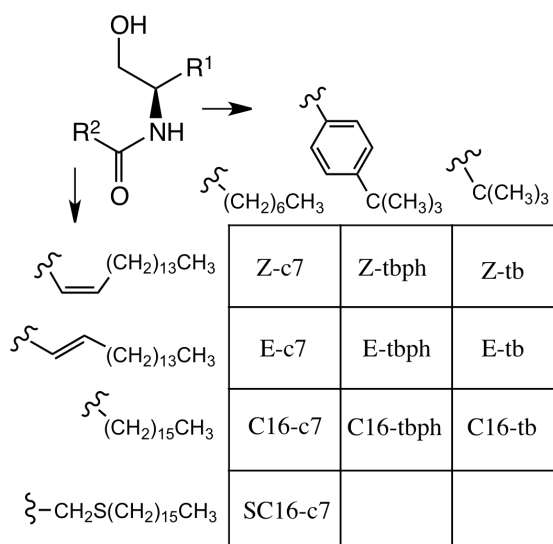


Figure 9. NOE analogues. Modified from ¹¹⁷

I.5.3.2 Compound B13 and analogues

Besides NOE and its analogues, compound B13 ((1*R*,2*R*)-2-(*N*-tetradecanoylamino)-1-(4-nitrophenyl)-1,3-propanediol) is another important AC inhibitor¹¹⁹⁻¹²¹ (Figure 8). It suppresses AC activity quite efficiently without altering the activity of the neutral and alkaline CDases. B13 induces ceramide accumulation and causes cell death in SW403 human adenocarcinoma¹¹⁹, melanoma¹²⁰, and prostate LNCaP and PC3 cells¹²¹. Furthermore, B13 prevented tumor growth *in vivo*¹¹⁹ and sensitized prostate tumors to radiation induced apoptosis¹²¹.

Because B13 is a neutral lipophilic molecule and thus it may not efficiently reach and accumulate in the acid compartment where AC is present, its chemical structure was modified to improve its cell targeting properties^{122,123}. This endeavor afforded three families of analogs (Figure 8) with different target organelles: lysosomotropic alkylamine analogs (i.e. LCL204), mitochondriotropic cationic analogs (i.e. LCL85) and a number of neutral analogs with no compartmental preferences (i.e. LCL15).

Amongst the lysosomotropic analogs, LCL204 ((1*R*,2*R*)-2-(*N*-(tetradecylamino)-1-(4'-nitrophenyl)-1,3-propanediol) specifically targeted the lysosomes, induced apoptosis in prostate cancer cells¹²⁴, and enhanced apoptin cytotoxicity in prostate cancer¹²⁵ and Fas-induced apoptosis of head and neck squamous cancer cells⁹⁸.

Interestingly, LCL204 was also used in an independent laboratory with the name of (AD2646)¹²⁶. In that study, the compound was able to dose- and time-dependently decrease the viability of Jurkat leukemia cells, which was accompanied by an accumulation of endogenous ceramide, caspase activation and triggering of mitochondrial apoptotic events¹²⁶. However, LCL204 (or AD2646) also caused induction of lysosomal destabilization and rapid cathepsin-dependent degradation of AC, which suggested a lack of tumor specificity.

A similar effect has also been reported for desipramine¹²⁷, which down-regulates AC by stimulating its cathepsin B/L-dependent proteolytic degradation, as well as for other amphiphilic agents (chlorpromazine, chloroquine) but not other lysosomotropic agents (ammonium chloride, bafilomycin A1).

Synthesis of a novel generation of lysosomotropic inhibitors of AC deprived of the lysosomal destabilization and AC proteolytic degradation properties of LCL204 has been reported¹²⁸. This class of inhibitors exhibits a ω -aminoacyl group and a combination of structural elements of B13 and LCL204 (or AD2646).

Amongst the new hybrids, the analog LCL464 ((1*R*,2*R*)-2-*N*-(12'-*N,N*-dimethyl-aminododecanoyl amino)-1-(4"-nitrophenyl)-1,3-propandiol) inhibited AC activity both *in vitro* and in cells, but it did not induce lysosomal destabilization or degradation of AC. Furthermore, it showed increased caspase-dependent apoptotic cell death in a wide range of different cancer cell lines¹²⁸.

1.5.4 Methods to determine ceramidase activity

Several methods have been developed to evaluate CDase activity both *in vitro* and *in situ*. The most common procedures are summarized in Table 2. The first assays were based on the hydrolysis of [³H]- or [¹⁴C]-labeled ceramides and subsequent determination of the amount of radioactivity present in the reaction product (released fatty acids). However, this method required separation of ceramide from the fatty acids by thin layer chromatography (TLC) prior to quantification of the radioactive product¹²⁹.

To avoid the use of radioactive substrates, a number of fluorescent ceramide analogues were designed. In these substrates, the fluorophore is bound to the end of the *N*-acyl chain, and ceramidase activity can be measured by following the release of the fluorescent fatty acid after separation by TLC and further fluorimetry or HPLC coupled to fluorescence detection¹³⁰. 7-Nitro-2-1,3-benzoxadiazol (NBD) and 4,4-difluoro-4-bora-3a,4a-diaza-s-indacene (BODIPY) are the most common fluorophores used in this kind of assays.

Initially, the Cer-C6-NBD, (Table 2) was used for determination of both acid and alkaline ceramidase activities *in vitro* and *in situ*. However, subsequent work demonstrated that Cer-C6-NBD was a poor substrate for these two enzymes¹³¹, and so, alternative NBD-ceramide substrates were used. It was found that Cer-C12-NBD, (Table 2) was a suitable substrate for both neutral and alkaline ceramidases, even better than the radioactive Cers not bearing the NBD moiety¹³².

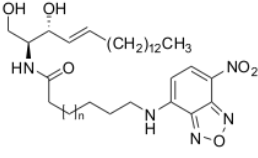
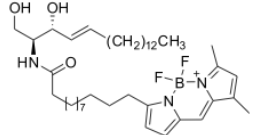
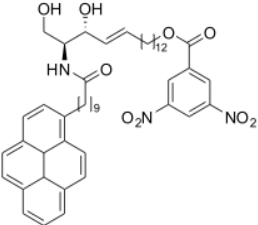
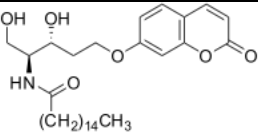
Another reported fluorescent ceramide substrate, Cer-C12-BODIPY, contained a terminal BODIPY unit (Table 2). This substrate has been almost exclusively used for determination of AC activity⁸⁸.

An additional substrate that can also be used for determination of ceramidase activities is a non-fluorescent ceramide analogue named Cer-C10-pyrene (Table 2). This compound becomes fluorescent upon Cer hydrolysis by ceramidases thereby allowing to follow the reaction with a fluorimeter¹³³. The latter assay has been mainly utilized for measurement of *Pseudomonas sp.* alkaline ceramidase activity.

An alternative approach for determination of ceramidase activity is the evaluation of sphingosine produced after derivatization with fluorescent compounds and its further isolation and determination by HPLC and fluorescence detection. Along this line, two derivatizing agents have been reported, *O*-phthaldehyde (OPA) and naphthalene-2,3-dialdehyde (NDA) (Table 2)¹³⁴.

Table 2

Methods to determine ceramidase activity

Substrate	ASAH Gene	N-Acyl chain	Features	Product detection	Ref.
[³ H] or [¹⁴ C] Ceramide	1, 2 and 3	C12 C16 C18	Lipid extraction and TLC separation needed	Image analyzer or scintillation counter	134-136
 <p>Cer-C6-NBD (n=1) Cer-C12-NBD (n=7)</p>	Mostly 2 and 3	C6-NBD C12-NBD	No extraction needed	HPLC-fluorimetry	131, 137, 138
 <p>Cer-C12-BODIPY</p>	1	C12-BODIPY	No extraction needed	HPLC-fluorimetry	88
 <p>Cer-C10-pyrene</p>	3	C10-pyrene	No extraction needed	Direct fluorimetry	139
 <p>Cer-coumarin</p>	1 and 2	C16	No extraction needed	Direct fluorimetry	117, 140
Ceramide	1, 2 and 3	C12	Sphingosine detection after OPA derivatization	HPLC-fluorimetry	74, 79
			Sphingosine detection after NDA derivatization	HPLC-fluorimetry	133

I.5.4.1 Fluorogenic assay

Our group published a versatile fluorimetric assay for determination of ceramidase activity that employs a coumarinic substrate (RBM14) (Table 2) in which the fluorogenic unit is located in the aminodiol moiety (Figure 10). This ceramide analogue can be hydrolyzed by ceramidases both *in vitro* and *in situ*; the released aminodiol group is then chemically oxidized and the resulting aldehyde undergoes a spontaneous β -elimination reaction to release umbelliferone (7-hydroxycoumarin), which can be easily detected by fluorimetry¹⁴¹. This assay is suitable for use in microtiter plates, thus being ideal for high-throughput screening¹¹⁷.

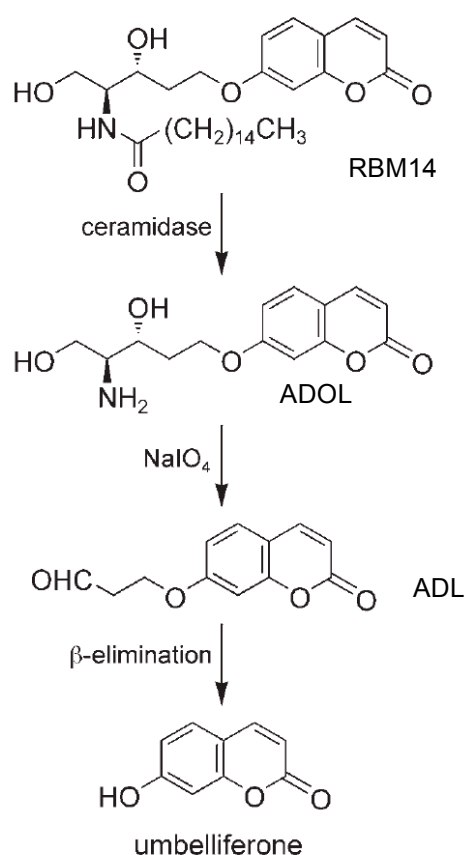


Figure 10. Enzymochemical transformation of RBM14 into fluorescent umbelliferone.

I.6 CELL CYCLE

The cell cycle is an intricate sequence of events, which enables cells to grow and replicate. Originally, cell division was divided into two stages: mitosis (M), the process of nuclear division, and interphase, the interlude between two M phases. Stages of mitosis include prophase, metaphase, anaphase and telophase. Under the microscope, during interphase cells simply grow in size, but different techniques revealed that the interphase includes G₁, S and G₂ phases¹⁴² (Figure 11).

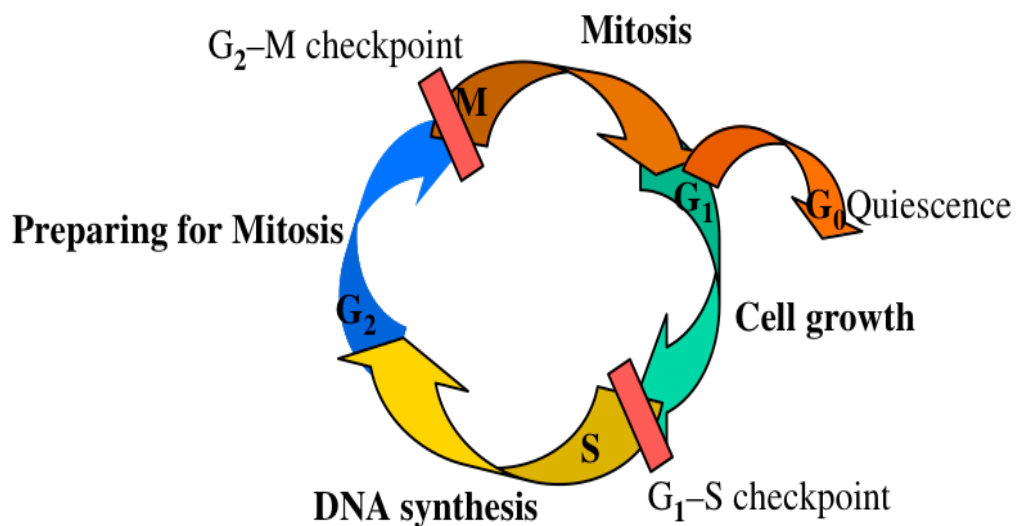


Figure 11. The cell cycle.

The G₁ and G₂ phases of the cycle represent the “gaps” in the cell cycle that occur between DNA synthesis and mitosis. In the first gap, G₁, the cell is preparing for DNA synthesis. Replication of DNA occurs in the S phase. The G₂ phase is the second gap during which the cell prepares for mitosis. G₁, S, G₂ and M phases are the traditional subdivisions of the standard cell cycle (Figure 11). Cells in G₁ can enter a resting state called G₀. Cells in G₀ account for the major part of the non-growing, non-proliferating cells in the human body¹⁴².

I.6.1 Cell cycle regulation

Cell cycle checkpoints regulate the complex network of interactions that determine cell growth, arrest or apoptosis¹⁴³ (Figure 12). Checkpoints are regulated by a small number of heterodimeric protein kinases, called cyclins. Their catalytic subunits are called cyclin dependent kinases (cdks) because they have no kinase activity unless they are associated with a cyclin. Each Cdk subunit can associate with different cyclins, and the associated cyclin determines which proteins are phosphorylated by the Cdk-cyclin complex. Because of their cyclic expression, cdks can be activated only at specific times during cell cycle. Thus, a cell enters and exits cell cycle phases in association with the synthesis and degradation of specific cyclins¹⁴³.

In G1, an important target of cdks is the retinoblastoma protein (pRb), which, acting as a switch in G1 (Figure 12), determines whether the cell enters the S phase. Progression through the cell cycle is determined by the phosphorylation of the pRb by cdk. In its hypophosphorylated state, pRb binds with and inhibits the transcription factor E2F. When pRb is phosphorylated by the cyclin-cdk complex, E2F is released and activates the transcription of genes required for entering in S phase¹⁴⁴.

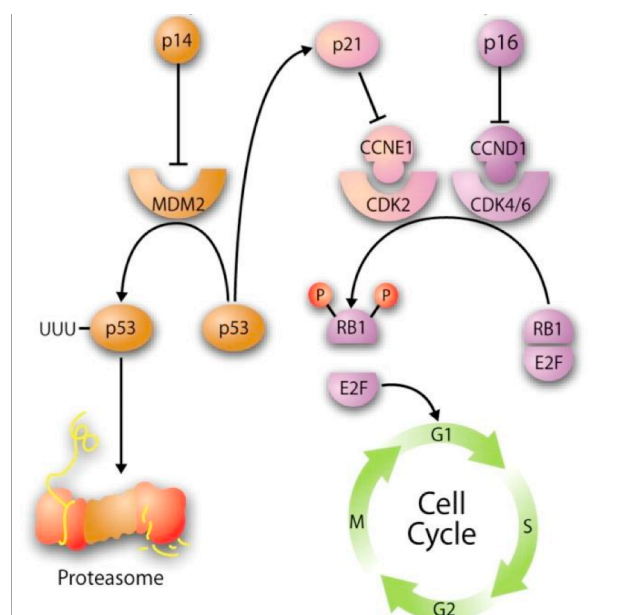


Figure 12. Cell cycle regulation

Cdk activity is checked and regulated by the cell cycle inhibitory proteins cdk inhibitors. These proteins belong to two distinct families, first, the ink4 family, which includes p15, p16, p18 and p19 proteins and second, p21, p27 and p57¹⁴⁵ comprise the Cip/Kip family.

Another checkpoint is found in the G2 to M transition. This checkpoint is sensitive to the exact duplication of DNA during the S phase and dictates the entry of the dividing cells into the M phase. An important regulator of this step of the cell cycle is p53, which is a ubiquitous transcription factor that performs its role by detecting DNA damage. Levels of p53 increase in response to DNA damage, affecting the G2-M transition through cyclin B downregulation or disruption of the Cdk1/Cyclin B complex, arresting the cell in G1 and allowing DNA repair or cell death. p53 also responds to DNA damage by increasing the transcription of p21, an inhibitor of cdk. Misregulation of cell cycle is a general event in diseases of uncontrolled growth, such as cancer¹⁴⁶.

I.7 APOPTOSIS

Apoptosis is the best understood mode of regulated cell death in multicellular organisms where is critical for sculpting tissue during development, and for maintaining homeostasis in the adult when infected, injured or aged cells have to be eliminated. When cells are exposed to a variety of stimuli, they undergo apoptosis in a tightly regulated and controlled manner, characterized by specific biochemical and morphological changes including cellular and nuclear reduction, chromatin condensation, cell membrane blebbing, formation of apoptotic bodies and DNA fragmentation¹⁴⁷. Two evolutionarily conserved central pathways are known to mediate apoptosis: the extrinsic pathway, which utilizes cell surface death receptor; and the intrinsic pathway, which involves the mitochondria and the endoplasmic reticulum (Figure 13).

I.7.1 The extrinsic apoptotic pathway

In the extrinsic pathway, the death ligands FasL (CD95 L), tumor necrosis factor α (TNF- α), TNF-related apoptosis inducing ligand (TRAIL) or TNF ligand superfamily member 10 (TNFSF10) interact with their respective death receptors (DR) Fas (CD95), TNF-receptor 1 (TNFR1), death receptor 4 (DR4) (TRAILR1) or DR5 (TRAILR2). The ligand-receptor binding leads to the formation of a multimolecular complex of proteins called death-inducing signaling complex (DISC)¹⁴⁸. Among the DR complexes, the CD95 DISC is the most extensively investigated and will be explained as an example.

The transduction of the apoptotic signal starts with the ligand-receptor association, which stimulates recruitment of adaptor protein Fas-associated via death domain (FADD), which then recruits procaspase-8 or 10 to form DISC. Thereafter procaspase-8 or 10 is cleaved, which leads to formation of active caspase 8/10¹⁴⁹. In cells type I, processed caspase-8/10 are sufficient to directly activate other downstream (effector) caspases and lead on to the execution phase of apoptosis.

In cells type II the DISC is formed quite poorly and, subsequently, active caspase-8 is generated in lower amounts, activation of effector caspases 3/7 depends further on an amplification loop where caspase-8 mediates cleavage of the pro-apoptotic Bcl-2 homology domain-3 (BH3) containing Bcl-2 family member Bid¹⁴⁶. This fragment links to the intrinsic pathway of apoptosis, inducing pro-apoptotic functions of mitochondria by causing aggregation of Bax and Bak, and release of cytochrome c from the mitochondrial intermembrane space. APAF-1, cytochrome C and ATP form a large protein complex, the “apoptosome”, a sort of cytosolic DISC at which caspase-9 as initiator caspase is activated¹⁵⁰.

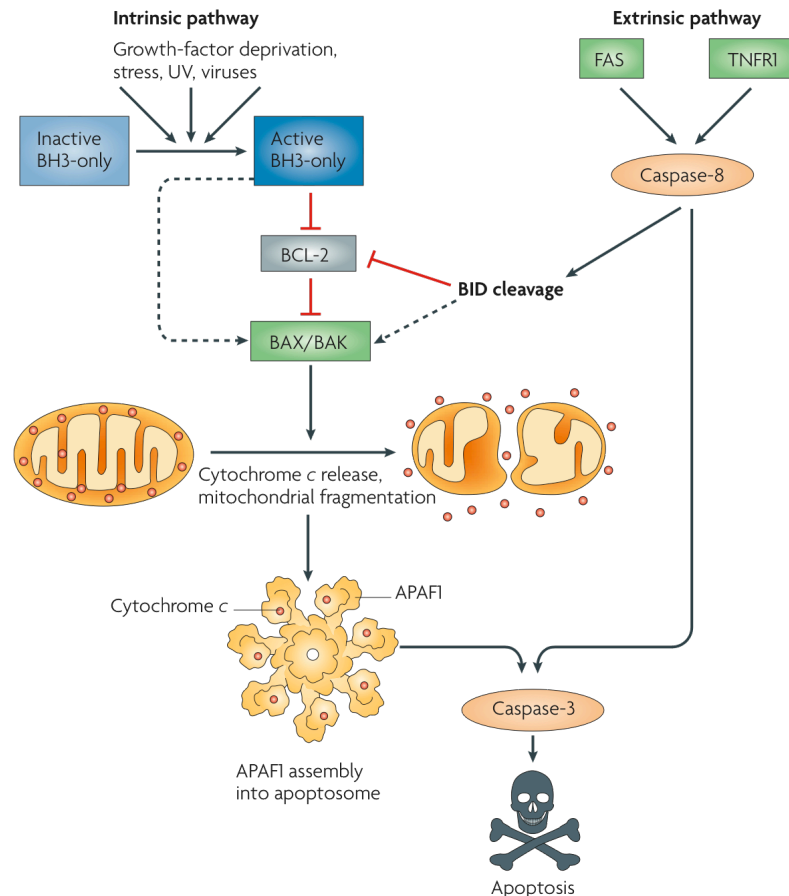


Figure 13. Scheme depicting intrinsic and extrinsic pathways of apoptosis. Apoptosis can be induced by cell surface receptors, such as Fas and tumor necrosis factor receptor-1 (TNFR1) (extrinsic pathway, right), or by various genotoxic agents, metabolic insults or transcriptional cues (intrinsic pathway, left).¹⁵¹

Induction of apoptosis is accomplished by activation of effector caspases like caspase-3. CD95- mediated apoptosis in type II cells is further affected by the expression of antiapoptotic members of the Bcl-2 family. Expression of Bcl2 or Bcl-XL renders type II cells resistant to CD95- mediated apoptosis. Type I cells are not protected against CD95 mediated apoptosis¹⁴⁶.

I.7.2 The intrinsic apoptotic pathway

The intrinsic pathway transduces a wide variety of extracellular and intracellular stimuli including toxins, radiation, hypoxia, oxidative stress, ischemia-reperfusion and DNA damage. Downstream signaling for each of these is unclear but all appear to converge on the consequent activation of the intrinsic pathway that involves central death machinery located at the mitochondria and endoplasmic reticulum.

At the mitochondria, mitochondrial outer membrane permeabilization (MOMP) is a pivotal event during apoptosis¹⁵². Following MOMP, pro-apoptotic factors (apoptogens) normally found in the space between the inner and outer membranes are irreversibly released into the cytoplasm. As MOMP is often found following a dissipation of the mitochondrial inner transmembrane potential, the mechanism leading to MOMP may arise from the pore opening in the inner membrane¹⁴⁸.

Although the composition of this mitochondrial permeability transition pore (MPTP) remains to be resolved, MPTP most likely consists of three components: these are adenosine nucleotide translocase (ANT) on the inner membrane, the voltage dependent anion transporter (VDAC) on the outer membrane and cyclophilin D. Cyclophilin D facilitates a conformational change of ANT, converting MPTP into an open pore¹⁴⁶.

A second mechanism for MOMP involves members of the Bcl-2 family of apoptosis-regulating proteins acting at the outer mitochondrial membrane. Bcl-2 family members share Bcl-2 homology (BH) domains. The BH123 (or multidomain) proteins Bax and Bak are pro-apoptotic family members that promote MOMP. Following apoptotic stimuli, Bax and Bak undergo a conformational change, oligomerize and translocate to the mitochondria. The other subfamily, BH3- only proteins (effectors) can either directly activate Bax and Bak or interfere with anti-apoptotic Bcl-2 family members (sensitizers)¹⁵³. Anti-apoptotic Bcl-2 family proteins such as Bcl-2, Bcl-xL and Mcl-1 prevent MOMP by sequestering pro-apoptotic BH3-only proteins. BH3-only proteins include Puma, Noxa, and Bad¹⁴⁸.

Other molecules have demonstrated to play a role during intrinsic apoptosis. The transcription factor p53 induces apoptosis in part by inducing expression of *Puma*. In addition, p53 appears to trigger MOMP and apoptosis independent of transcription through direct activation of Bax or Bak¹⁴⁶.

Following MOMP, a critical apoptogen that is released from the intermembrane mitochondria space is cytochrome C. When in the cytosol, cytochrome c binds to an adapter molecule Apaf-1, allowing dATP to gain access to a nucleotide binding

site on Apaf-1 which then induces an Apaf-1 conformational change. Apaf-1 then oligomerizes into an “apoptosome” which recruits and activates caspase 9¹⁵⁴. As with activated caspase 8/10 in the extrinsic pathway, activated caspase 9 activates downstream effector caspases and leads on to the execution phase of apoptosis.

Under unstressed conditions, effector caspases (caspase 3/7) are potentially inhibited by the endogenous X-linked inhibitor of apoptosis (XIAP). The release of another set of mitochondrial apoptogens, Smac/DIABLO and Omi/HtrA 2, allow direct activation of the effector caspases by binding of these apoptogenes to XIAP, and XIAP inactivation¹⁴⁸.

I.8 CERAMIDE MEDIATED CELL CYCLE ARREST AND APOPTOSIS.

As mentioned above, Cer has been implicated in differentiation, cell cycle arrest, apoptosis and senescence in several cell types¹⁵⁵.

Cer induces cell cycle arrest through the activation of Cer-activated protein phosphatases (CAPPs), which comprise the serine/threonine phosphatases PP1 and PP2A¹⁵⁶. These phosphatases produce the dephosphorylation of the retinoblastoma gene product (Rb). Cer also induces the activation of p21 and the cyclin dependent kinase 2 (CDK2)^{157,158}.

A key mechanism of Cer-induced senescence involves the inhibition of phospholipase D, diacylglycerol generation and protein kinase C activation¹⁵⁹. Additionally, a direct link between ceramide and senescence has been reported by establishing a role for ceramide in the regulation of telomerase activity and telomere¹⁶⁰. Interestingly, in the A549 human lung adenocarcinoma cell line, forced increases in endogenous levels of ceramide by either overexpression of sphingomyelinase, supply of exogenous precursor short-chain Cer, or using chemotherapeutic agents that induce ceramide (such as daunorubicin), caused significant inhibition of telomerase activity¹⁵⁵, resulting in senescence.

One of the most studied roles of ceramide is its function as a proapoptotic molecule; however, the mechanisms have not been fully defined. Ceramide plays a role leading to the apoptotic signaling pathway after death-stimuli, including death-receptor-mediated (TNF- α and CD95), chemotherapeutic agent-mediated (etoposide, cisplatin, doxorubicin, paclitaxel, and inostamycin), and irradiation-mediated (UV and γ -irradiation)^{161,162}.

Cell death via Cer signaling occurs through two main pathways. First, through the mitochondrial pathway, increased Cer levels activate PP2A, which dephosphorylates the proapoptotic proteins Bak and Bax, resulting in conformational change and activation¹⁶³, and the anti-apoptotic protein Bcl-2, resulting in proteasomal degradation¹⁵⁹ (Figure 14).

The second mechanism by which Cer induces apoptosis is activation of the stress-activated protein kinase (SAPK/p38MAPK) pathway¹⁶⁴. Functional signaling through both pathways has been shown to be required for induction of apoptosis in response to Cer accumulation^{116,165} (Figure 14).

Ceramide-enriched platforms are generated in plasma membrane after TNF and CD95-mediated receptor clustering and UV, γ irradiation, and anticancer treatment¹⁶⁶ (Figure 14). During TNF-induced apoptotic signaling, the increment in Cer levels caused by aSM activity may cause cathepsin D activation and Bid cleavage. Further, ceramide was shown to bind directly to cathepsin D, causing autocatalytic proteolysis of the pre-pro-cathepsin D to form the enzymatically active isoforms of the enzyme, thereby implicating ceramide in regulation of Bid processing¹⁶⁷.

Ceramide may block the cell survival pathway by reducing PI3K/AKT and MEK/ERK activation⁷⁵. Ceramide-activated PP1 and PP2A may activate GSK-3 β and regulate Bcl-2 family proteins, which includes upregulating Bax and Bad and downregulating Bcl-2 and Bcl-xL (Figure 14). These effects lead to mitochondrial apoptosis. In addition, ceramide induces apoptosis by sequentially activating caspase-2 and 8 upstream of mitochondria, which is followed by tBid expression

and translocation, mitochondrial transmembrane potential ($\Delta\Psi_m$) reduction, cytochrome C release, and caspase-9 and -3 activation. In this hypothetical scheme, how ceramide activates protein phosphatase is not known¹⁵⁵ (Figure 14). The role of GSK-3 β in ceramide-induced mitochondrial apoptosis needs further investigation.

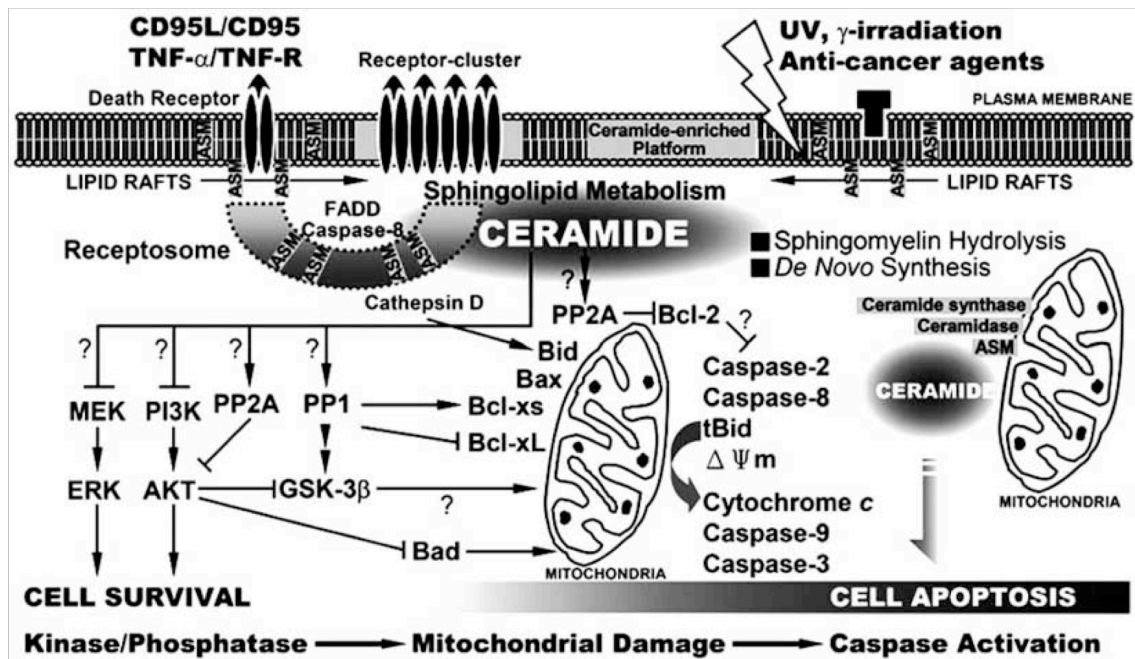


Figure 14 Ceramide-induced mitochondrial apoptosis pathways. Modified from¹⁶⁰.

Alterations in ceramide signaling have been observed in multiple human cancers, implicating ceramide dysregulation as an important determinant of tumor development and progression.

The exact mechanism by which Cer performs its biological functions is not completely understood. A number of findings suggest that changes in local membrane structure induced by ceramide accumulation are essential for its biological function¹⁶⁶. Ceramide-enriched domains alter the biophysical properties of a distinct domain of the cell membrane and, thus, permit a reorganization of receptor molecules and intracellular signaling molecules upon stimulation.

For instance, stimulation via FASL/CD95 results in trapping and clustering of the receptor within ceramide-enriched domains^{168,169}. Clustering of the receptor induces a very high density of the receptor within a described area of the membrane and facilitates the transmission of a positive signal into the cell. The comprehensive ceramide-enriched membrane platforms explains how ceramide can be involved in many signal transduction pathways and be required for cellular activation by many receptors with different biological functions¹⁷⁰.

I.9 CANCER

The current definition of cancer describes a class of diseases in which a group of cells display uncontrolled growth, ability to invade adjacent tissues and sometimes, metastatic properties¹⁴⁵.

Cancer comprises over 200 distinct entities differing in their genetic basis, etiology, clinical characteristics, patterns of progression, and final outcome. In broad terms, cancer can be classified into carcinomas and sarcomas according to the fetal germ layer from which tumors arise. Carcinomas arise within tissues derived from the fetal ectoderm or endoderm and include most of the common cancers in adults. Sarcomas are seen more frequently in children and arise from tissues originating from the fetal mesoderm, which generate tumors of the bone, muscle, connective tissues, and blood vessels. In developed countries, about 50% of all cancer cases are carcinomas of the lung, colon, prostate, and breast while hematological cancers (leukemias and lymphomas) account for about 8–10% of all cancer cases^{145,171}.

The genetic basis for cancer is well established through studies with tumor viruses, carcinogenesis models, molecular biology, somatic cell genetics, and genetic epidemiology. Cancer is the result of multiple mutations that occur in oncogenes, tumor suppressors and/or DNA repair genes of somatic cells¹⁷².

In 2000 Hanahan and Weinberg¹⁷³ proposed a model to understand the process of transformation through which a normal cell becomes into a cancer cell. They suggested that the vast catalog of cancer cell genotypes is a manifestation of six essential alterations in cell physiology (Figure 15): self sufficiency in growth signals, insensitivity to growth inhibitory (antigrowth) signals, evasion of programmed cell death (apoptosis), limitless replicative potential, sustained angiogenesis, and tissue invasion and metastasis. Based on this model, the authors believe that virtually all cancers must acquire the same six capabilities, but the order and the mechanism by which these capabilities are acquired seems to be quite variable across cancer types¹⁷³.

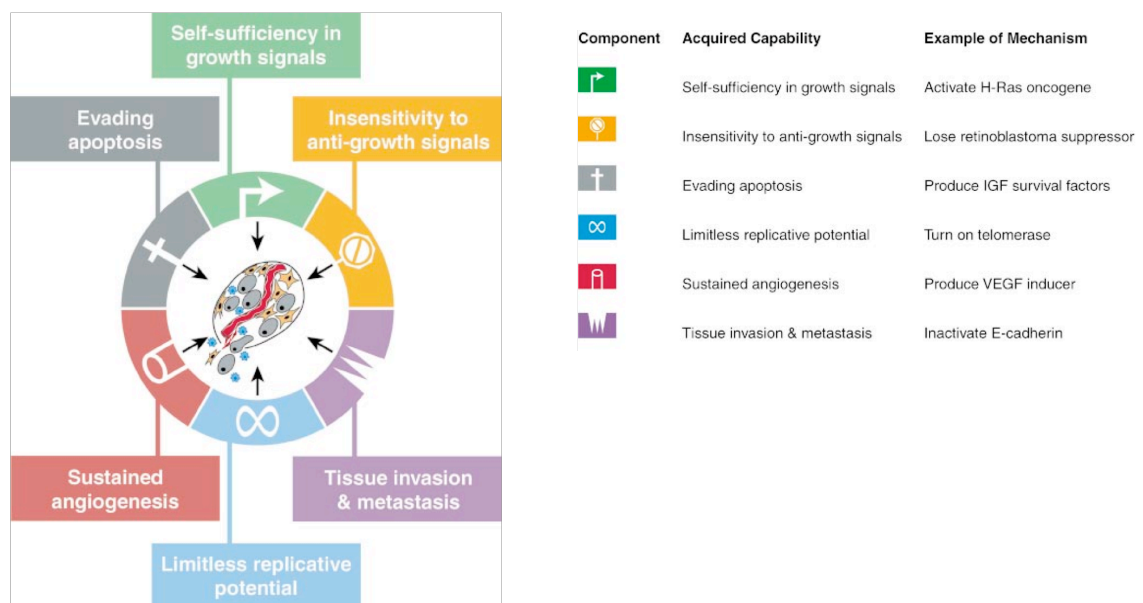


Figure 15. Acquired capabilities of cancer. Modified from¹⁷²

I.9.1 Prostate cancer

I.9.1.1 The prostate

The prostate is an exocrine gland of the male reproductive system and consists of glandular and muscular tissue. The prostate is a pyramid-shaped organ with apex (contact to the urethra and directed downward) and basis (contact to the bladder and directed upward). The prostate is located in front of the rectum. It weighs about 20 g (3 cm long, 4 cm wide, 2 cm thick), and lies below the urinary bladder, encircling the urethra¹⁷⁴ (Figure 16). The prostate produces a thin, milky, alkaline fluid that is secreted into the urethra at the time of semen emission, providing an added medium for the life and motility of sperm.

Although the adult prostate lacks discernible lobular structure, the classic work of McNeal¹⁷⁵ defined the human prostate as having a zonal architecture, corresponding to central, periurethral transition, and peripheral zones, together with an anterior fibromuscular stroma¹⁷⁶. Importantly, the outermost peripheral zone occupies the most volume and harbors the majority of prostate carcinomas. In contrast, benign prostatic hyperplasia (BPH), a common non-malignant condition found in older men, arises from the transition zone¹⁷³.

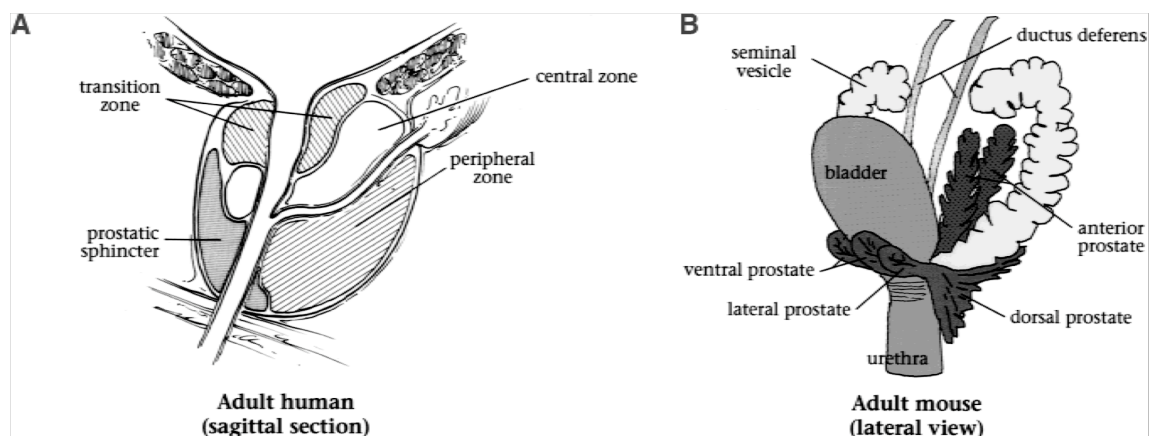


Figure 16. Schematic illustration of the anatomy of the human (A) and mouse (B) prostate.

Unlike the human prostate, the mouse prostate consists of multiple lobes that have distinct patterns of ductal branching, histological appearance, gene expression, and secretory protein expression¹⁷⁷ (Figure 16).

I.9.1.2 PC detection

Prostate cancer has been recognized as a clinical entity since antiquity, when it was first described by the ancient Egyptians, while surgical procedures to remove the prostate were developed >100 years ago¹⁷⁸. However, the availability of a highly accessible blood test for prostate specific antigen (PSA) has revolutionized the diagnosis of prostate cancer over the past three decades. PSA is a kallikrein related serine protease that is produced in normal prostate secretions, but is released into the blood as a consequence of disruption of normal prostate architecture¹⁷⁹. Men that have elevated PSA levels typically undergo biopsy to assess the potential presence of prostate cancer.

Following biopsy, histopathological grading of prostate tissue is performed by Gleason scoring, which classifies tumors from 2 to 10 (most to least differentiated) based on their most prevalent architecture, and assigns a combined score that is the sum of the two most common patterns¹⁸⁰. Patients are also diagnosed by the status of their primary tumors, from organ-confined to fully invasive (T1–4), with or without lymph node involvement (N0 or 1), and the presence and degree of distant metastases (M0 and 1a–c)¹⁸¹.

I.9.1.3 Stages of prostate cancer¹⁸²:

Stage I. Cancer is found in the prostate only (Figure 17). The tumor is not detected during a digital rectal exam, and it can't be seen on a sonogram. It is found by chance when surgery is done for another reason, usually for benign prostatic hyperplasia (BPH). The PSA level is lower than 10 and the Gleason score is 6 or lower.

Stage II. The tumor is more advanced but is not extended beyond the prostate (Figure 17). It may be felt during a digital rectal exam, or seen on a sonogram. PSA level is lower than 20 and Gleason score is ≤ 7 .

Stage III. The tumor is extended beyond the prostate. The tumor may have invaded the seminal vesicles, but cancer cells have not spread to the lymph nodes (Figure 17). The PSA can be any level and the Gleason score can range from 2 to 10.

Stage IV. The tumor has invaded the bladder, rectum, or nearby structures (beyond the seminal vesicles). It has spread to the lymph nodes, bones, or to other parts of the body (Figure 17).

Advanced prostate cancer has a propensity to metastasize to bone, which is primarily responsible for its effect on patient morbidity as well as mortality. Thus, unlike other epithelial tumors that occasionally metastasize to bone, metastatic prostate cancer almost invariably metastasizes to bone¹⁸³.

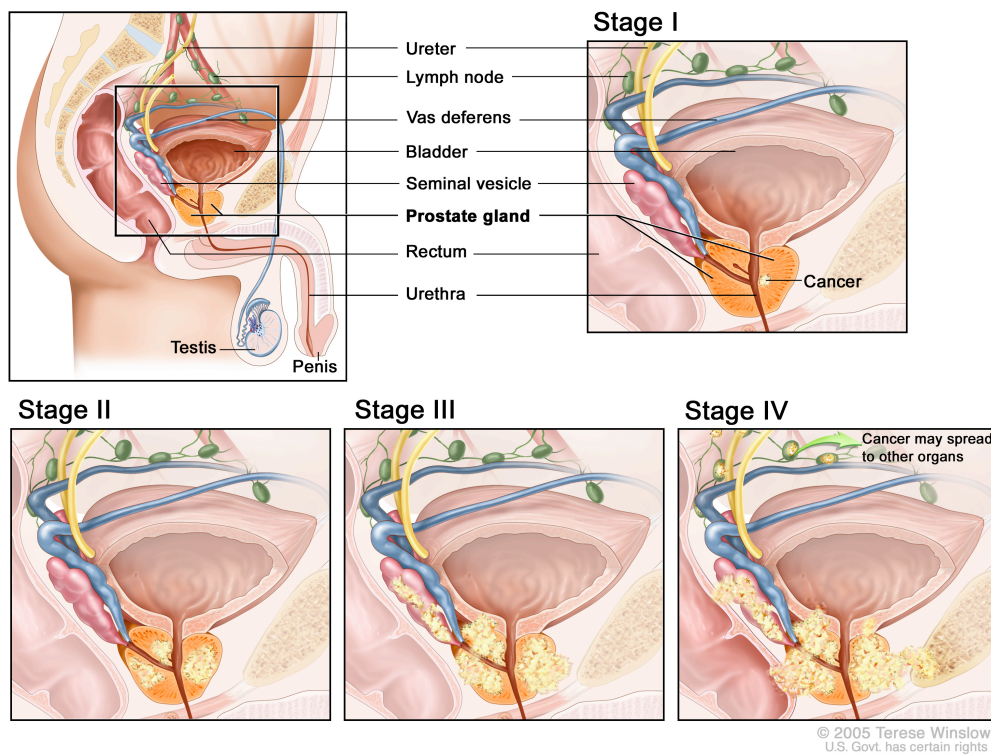


Figure 17. Prostate cancer stages. As prostate cancer progresses from Stage I to Stage IV, the cancer cells grow within the prostate, through the outer layer of the prostate into nearby tissue, and then to lymph nodes or other parts of the body.

Staging correlates with survival and provides an essential guide both to prognosis and to the design of treatment plans.

I.9.1.4 PC treatments

PC treatment options include surgical excision of the prostate (radical prostatectomy), irradiation through external beam therapy or implantation of radioactive “seeds” (brachytherapy), or androgen depletion. Treatment is selected depending on the stage of the disease, patient’s age and other coexisting medical conditions¹⁸². Conversely, androgen depletion, through removal of testicular androgens by surgical or chemical castration, is usually associated with the recurrence of prostate cancer, and this recurrent disease is termed “castration resistant”¹⁸⁴.

Unfortunately, castration resistant prostate cancer has been essentially untreatable, with the most effective standard chemotherapeutic regimens resulting in a mean increase in survival of 2 months¹⁸⁵. These facts highlight the importance of finding new therapeutic options.

I.9.1.5 PC epidemiology

In 2009, there were 192,280 new cases of prostate cancer reported and 27,360 related deaths in USA¹⁷⁰. During the last 10 years, prostate cancer has remained the second leading cause of cancer death in men in the United States. In Europe and worldwide, an estimated 913,000 men were diagnosed with prostate cancer in 2008, and more than two-thirds of cases are diagnosed in developed countries. The highest rates are in Australia/New Zealand, Western and Northern Europe, Northern America, largely because the practice of PSA testing and subsequent biopsy has become widespread in those regions^{185,186} (Figure 18).

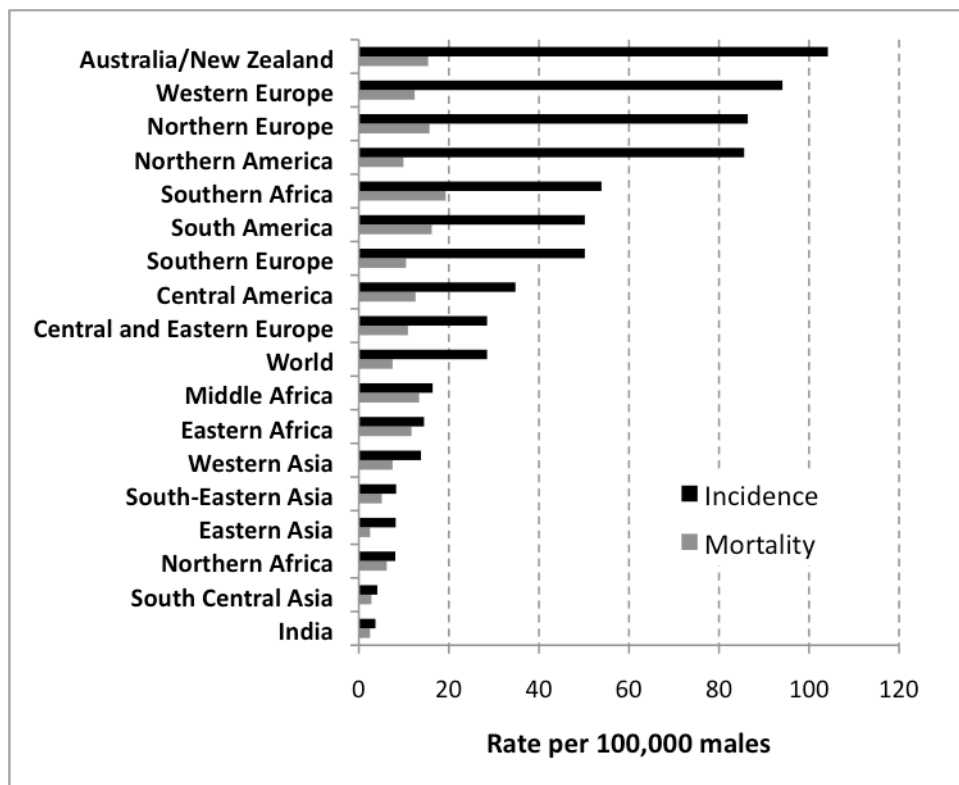


Figure 18. World age-standardized incidence and mortality rates for prostate cancer by world regions. Modified from ¹⁸⁴

I.9.2 Acid ceramidase and prostate cancer

Seelan *et al.*⁹⁹ first reported that AC is overexpressed in prostate cancer. Using RT-PCR they demonstrated AC overexpression in 40% of primary cancer tissue, with greater frequency in higher grade disease. Similar results were obtained by Liu *et al.*¹⁸⁷ using western blot analysis. These authors found out that over 60% of Gleason grades 5-6 and 80% of Gleason grade 8-10 cancers had elevated AC levels compared with patient matched normal tissue.

The mechanism of AC upregulation in prostate cancer is unknown and several hypotheses have been proposed. The first possibility is that the increase in AC is a feedback mechanism to keep levels of ceramide low following cellular exposure to systemic stress. This results in the selection of a subpopulation of cancer cells that exhibit higher AC levels and exhibit a growth survival advantage.

Second, increased AC may be a result of transcriptional control. It is known that the murine AC enhancer-promoter has a KLF6 binding motif embedded within a 43-base pair region that regulates AC expression. KLF6 is a transcription factor identified as a potential candidate tumor suppressor gene in prostate and other cancers¹⁸⁸; however, it is not yet clear if transcription is the primary mechanism for AC upregulation. Third, it is well known that AC maps to 8p22, the region of chromosome 8 most frequently deleted in prostate cancer¹⁸⁹. This has led to suggest that loss of heterozygosity may cause depletion of a chromosome region containing one or more micro-RNAs or other regulatory controls which lead to increased expression of AC by direct or indirect means.

I.9.2.1 Role of AC in tumor progression and metastasis

The functional consequences of AC upregulation on prostate cancer have been studied in diverse works^{102, 190}. In these studies, the authors demonstrated that cells expressing higher AC levels exhibited increased proliferation under nutrient-depleted conditions in cell culture, and displayed augmented tumorigenicity *in vivo*. AC overexpression also enhanced migration rates through collagen coated transwells and increased adhesion to fibronectin or collagen. Administration of AC inhibitors or AC siRNA reversed this aggressive behavior, directly linking AC to this phenotypic change.

In this context, stable clones of prostate cancer DU145 cells overexpressing AC exhibited enhanced proliferation and migration and subcutaneous injection of these cells into nude mice resulted in larger tumor volumes compared to controls. Moreover, the AC-overexpressing cells were more resistant to cell death induced by doxorubicin, cisplatin, etoposide, gemcitabine or C6-ceramide, while knock down of ASA1 sensitized the cells to these drugs¹⁰².

Nevertheless, the exact mechanism of increased tumorigenicity and enhanced cell migration induced by AC overexpression still remains unclear. The enhanced formation of S1P, located downstream on AC activity and a potent anti-apoptotic agent, may account for the observed phenotypic change since SK inhibition reverses the migration phenotype¹⁹¹.

I.9.2.2 Role of AC in resistance to radiation therapy

Ceramide has been identified as both a necessary and sufficient mediator of radiation-induced cell death. Most studies indicate that defects in ceramide generation are related to increased resistance to radiation-induced apoptosis¹²⁰.

A recent study reported that radiation therapy caused upregulation of AC¹⁸⁹. This suggests a possible mechanism allowing cancer cells to establish radio-resistance. AC upregulation has shown to confer resistance to radiation in prostate cancer cells and genetic downregulation with siRNA or inhibition with LCL385, sensitized prostate cancer cells to radiation and significantly decreased tumor xenograft growth¹⁸⁹.

Although increased ceramide may be helpful in mediating apoptosis, AC upregulation upon radiation exposure was shown to enhance rapid hydrolysis of ceramide, which resulted in formation of sphingosine and S1P. The antagonistic effects of S1P on ceramide function results in minimizing the pro-apoptotic effect of ceramide with the paradoxical result of elevating the anti-apoptotic and angiogenic properties of S1P, which leads to enhanced tumor survival¹⁸⁶.

These overall findings and others suggest that the inhibition of AC activity may serve as useful target for cancer therapy, alone or on combination with other anti-oncogenic treatments.

II.OBJECTIVES

OBJECTIVES:

The general objectives of this work were:

1. To develop activity assays for AC and SPL and explore their possible applications as biomarkers, as well as in the identification of new enzyme inhibitors. This goal included the following specific aims:
 - a. To develop enzyme assays for SPL
 - b. To optimize a fluorogenic assay for AC and to use the optimized assay in the following:
 - i. In the diagnosis of FD;
 - ii. As a tool for the phenotypic characterization of cancer cells and
 - iii. In the high throughput screening (HTS) of libraries for the identification of AC inhibitors.
2. To investigate the role of AC in a model of prostate cancer and explore the therapeutic utility of AC inhibitors

III. RESULTS AND DISCUSSION

III.1 Development of enzyme assays for sphingosine-1-phosphate lyase

III.1.1. Determination of sphingosine-1-phosphate lyase activity by fluorimetry

The development of an assay to measure SPL activity using a fluorogenic sphinganine-1-phosphate analog as substrate is reported. In the novel substrate, RBM13, the C6-C18 chain of SaP is replaced by a coumarinic moiety. After SPL catalyzed cleavage, a coumarinic aldehyde is produced which then undergoes β -elimination at neutral-alkaline pH to release the fluorescent product, umbelliferone. The coumarinic unit is not fluorescent while it is still linked to the SaP backbone. This method allows the use of microtiter plates and is of utility for the screening of potential SPL inhibitors.

The synthesis of the substrate and the assay optimization were published in :

Bedia C., Camacho L., Casas J., Abad J. L., Delgado A., Van Veldhoven P. P., Fabrias G. **Synthesis of a fluorogenic analogue of sphingosine-1-phosphate and its use to determine sphingosine-1-phosphate lyase activity.** Chembiochem 2009; 10: 820-822

Impact Factor 2009: 3.824

My contribution to this work were the experiments depicted in Figure 2 of the article

Gemma Fabriàs Domingo

Thesis Director

III.1.2 Expression of recombinant SPL

Probably because of the low abundance and activity of SPL in cells, large amounts of protein were required in the fluorogenic assay. To solve this drawback, the *E. coli* TOP 10 strain was transformed with a construct (pVB001) provided by Prof. Paul Van Veldhoven. This plasmid encodes human *SGPL1* amino acids 59-568 preceded by a poly-histidine tag.

E. coli lysates of cells expressing SPL were separated by SDS-PAGE (20 µg protein/line) and analyzed by western blot for the presence of poly-His-tagged protein. In agreement with the reported results³², *SGPL1* expression was induced by arabinose, with good induction obtained with 0.02% and 0.2% arabinose for 2 h (Figure 19).

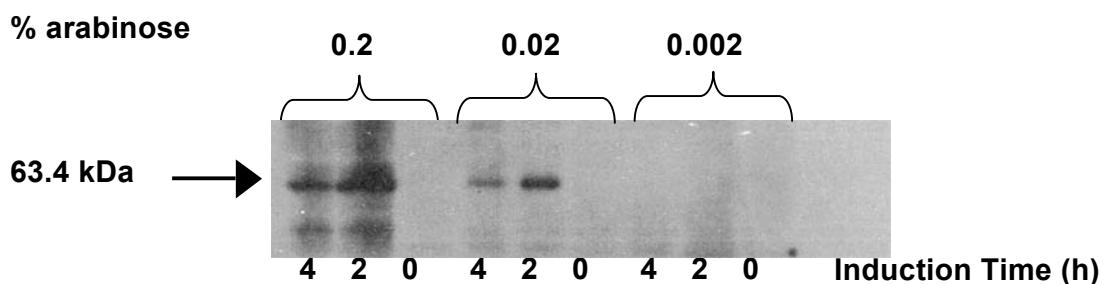


Figure 19. Western blot analysis of hSGPL1-transformed *E. coli* TOP 10

When the substrate was incubated with the transformed bacterial lysate, samples containing the encoding plasmid (pBV001) gave higher fluorescence levels than those transformed with an empty vector (Figure 20A)

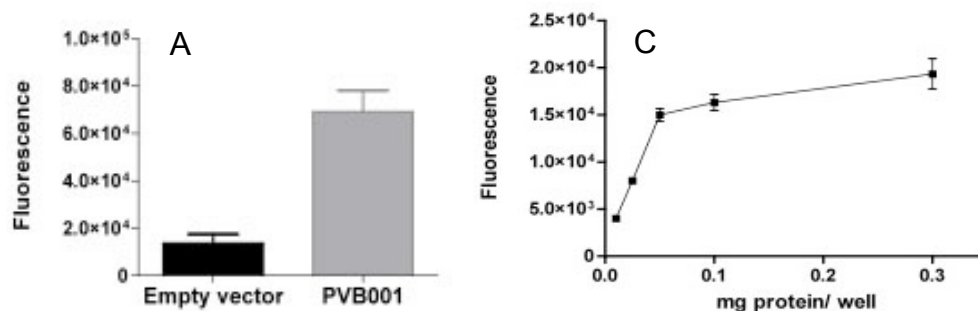


Figure 20. **A.** SPL activity in cells transformed with empty vector or the construct PVB001. **B.** Protein concentration-dependence. Assay conditions: $128 \mu\text{M}$ of substrate for 8h. Each data point represents the mean \pm SD of one experiment with triplicates

Using the lysates from *SGPL1* transformed *E. coli*, the amounts of protein necessary to achieve a good response were significantly reduced to 0.025-0,05 mg/well (Figure 20B). Therefore, bacterial supernatants containing less protein will be used in future library HTS programs for the discovery of SPL inhibitors.

III.1.3. Determination of sphingosine-1-phosphate lyase activity by gas chromatography coupled to mass spectrometry

As a result of the moderated affinity of SPL for the RBM13 substrate, the SPL fluorogenic assay is useful for the rapid identification of SPL inhibitors. However, kinetic characterization of inhibitors should be ideally carried out with a minimally modified alternative substrate. To this aim, we have developed an additional assay for SPL activity measurement, using C17-sphinganine-1-phosphate as substrate.

A draft of a manuscript in preparation follows in the next pages.

My contribution to this work consisted on the standardization of the chromatographic conditions and the training and supervision of Ester Reina during the experimental work of her Master Thesis.

Gemma Fabriàs Domingo

Thesis Director

Determination of sphingosine-1-phosphate lyase activity by gas chromatography coupled to mass spectrometry

Ester Reina, Luz Camacho, Josefina Casas, Paul van Veldhoven, Gemma Fabrias

Abstract

Sphingosine-1-phosphate lyase (SPL) serves central roles in development and chemotaxis, it prevents defects in reproductive structures and function, acts as a tumor suppressor, has a role in chemoresistance and it is also implicated in immunity. SPL has emerged as a novel therapeutic target in cancer and immunosuppression, and the identification of compounds able to modify SPL activity has attracted interest in a therapeutic context. In this article we report on a new assay for SPL activity using C17-sphinganine-1-phosphate as substrate. The released pentadecanal is easily measured by gas chromatography/mass spectrometry after derivatization into its (pentafluorophenyl)methyl oxime.

INTRODUCTION

The bioactive lipid sphingosine-1-phosphate and its saturated analog sphinganine-1-phosphate are catabolized to ethanolamine phosphate and hexadecanal or hexadecanal, respectively¹⁻³. This reaction is accomplished by the pyridoxal 5'-phosphate dependent enzyme sphingosine-1-phosphate lyase (SPL). This enzyme serves central roles in development⁴⁻⁶ and chemotaxis⁷, it prevents defects in reproductive structures and function⁸, acts as a tumor suppressor⁹⁻¹⁰, has a role in chemoresistance¹¹⁻¹⁴ and it is also implicated in immunity¹⁵. Therefore, SPL has emerged as a novel therapeutic target in cancer and immunosuppression¹⁶, and the identification of compounds able to modify SPL activity has attracted interest in a therapeutic context.

SPL activity can be determined using radioactive, fluorescent and fluorogenic substrates. The first one involves incubation of the enzyme with [4,5-³H] dihydrosphingosine-1-phosphate and, after extraction of lipids into an organic phase under acidic conditions followed

by thin-layer chromatography, the radioactive aldehyde is quantified by liquid-scintillation counting, autoradiography or phosphorimaging¹⁷. In the case of the fluorescent substrate, the resulting aldehyde is also extracted from the incubation mixture and quantified after separation by HPLC coupled to a fluorescent detector¹⁸. In a very recent assay, a non fluorescent coumarinic substrate is cleaved by SPL to release an aldehyde which undergoes a spontaneous β -elimination reaction to give umbelliferone¹⁹.

No separation of products is necessary and the assay can be performed in microtiter wells, which is an important improvement in high throughput screening of putative inhibitors. Nevertheless, given the high K_m of SPL for the fluorogenic substrate (152 μ M), kinetic characterization of inhibitors should be ideally carried out with a minimally modified alternative substrate.

In this article we report on a new assay for SPL using C17-sphinganine-1-phosphate. The released pentadecanal is easily measured by gas chromatography/mass spectrometry in selected-

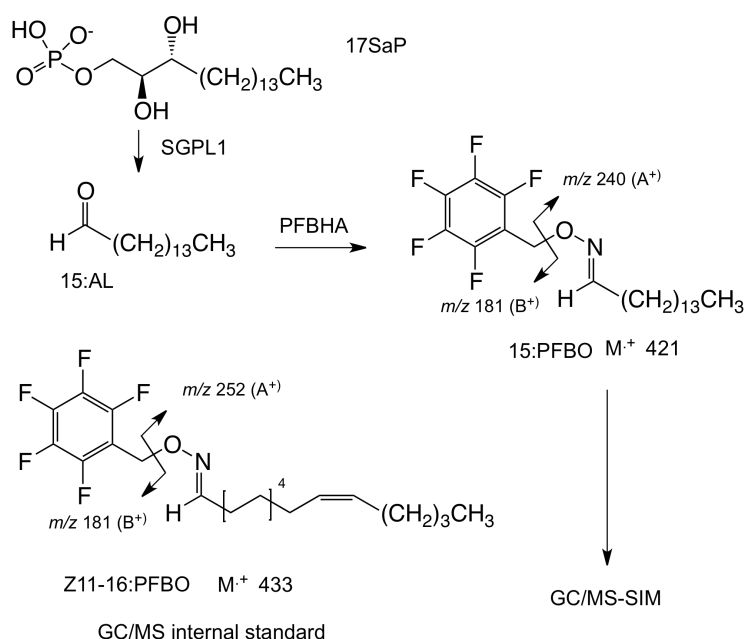


Fig. 1. SPL reaction and product derivatization to PFBO, showing the characteristic fragment ions of both analyte and internal standard

ion mode after derivatization with (pentafluorobenzyl)hydroxylamine hydrochloride (Fig. 1).

MATERIALS AND METHODS

Materials

The substrate C17-sphinganine-1-phosphate (17:SaP) was purchased from Avanti Polar Lipids. (Z)-11-hexadecenal (Z11-16:AL) and (pentafluorobenzyl)hydroxylamine hydrochloride (PFBHA) were from Sigma-Aldrich. Pentadecanal (15:AL) was synthesized as previously described²⁰.

Preparation of Calibration Curves

To prepare stock solutions, Z11-16:AL and 15:AL were dissolved in hexane at 10 mM and stored at 4°C. To construct the calibration curves, the stock solution of 15:AL was diluted 50-fold to obtain a concentration of 200 μ M, which was then submitted to serial dilutions (1/2) to

obtain a concentration range of 200-0.2 μ M. To 5 μ L of each dilution was added the internal standard, Z11-16:AL (5 μ L, 20 μ M final concentration), samples were evaporated under a careful stream of nitrogen to almost dryness and aldehydes were derivatized to their corresponding PFBO with 50 mM PFBHA HCl in 50 mM Tris-HCl buffer, pH 7.4 (100 μ L). The mixtures were incubated at 37°C for 15 min and extracted with one volume of hexane.

The solvent was evaporated under a careful stream of nitrogen. Residues were resolubilized in 10 μ L of hexane and stored at -20 °C until GC/MS analysis.

Cell culture

Wild type MEF215 cells were cultured in DMEM supplemented with 10 % FBS, at 37 °C and 0.5% CO₂.

Standard SPL assay

For a single sample, 40 μ L of 17:SaP stock solution (0.2 mM in ethanol, 40 μ M final concentration in the assay, 8 nmol) was added to an eppendorf tube and the solvent was removed under a stream of nitrogen. Inhibitors were added along with the substrate before solvent evaporation. To the residue is added 25 μ L of milliQ water and the mixture is sonicated for 1 min in an ultrasound bath. Cell pellets, obtained by trypsinization, are washed with PBS and then suspended in 0.5 M potassium phosphate buffer pH 7.4 (50 μ L per sample; 0.01-2 mg/ml of protein) and the mixture is sonicated for 10 min in ice-cold water in an ultrasound

bath. To 150 μL of 0.5 M potassium phosphate buffer pH 7.4 is added pyridoxal phosphate (2 μL , 12.5 mM), sodium orthovanadate (2 μL , 1.25 mM), EDTA (2 μL , 250 mM), sodium fluoride (2 μL , 1.25 mM) and dithiothreitol (2 μL , 100 mM). To the 25 μL substrate solution is added 125 μL of this solution and then the cell lysate (50 μl). After incubation for 1 h at 37 $^{\circ}\text{C}$, (Z)-11-hexadecenal (10 μL , 25 μM in dimethylsulfoxide, 250 pmol) and PFBHA (250 μL , 50 mM in Tris-HCl buffer pH 7.4, 12.5 μmol) are sequentially added and the mixture is incubated at 37 $^{\circ}\text{C}$ for 15 min after vigorous stirring. The PFBP are extracted with hexane (500 μL) and 400 μL of the organic solution is stored at -20 $^{\circ}\text{C}$ until analysis. Before injection, the solvent is carefully removed (nitrogen stream), 10 μL of hexane are added and 2 μL are injected into the GC/MS equipment for analysis.

Concentrations of the product, 15:AL, were calculated from the area ratios between both 15:PFBO and Z11-16:PFBO. Linearity of response was observed in the 0.3 to 100 μM range ($y=0.7572x+0.0271$, where y , concentration ratio; x , GC/MS ratio)

Gas chromatography/Mass spectrometry

Gas chromatography coupled to electron impact (70 eV) mass spectrometry was carried out using a Fisons gas chromatograph (8000 series) coupled to a Fisons MD-800 mass-selective detector. The system was equipped with a nonpolar Hewlett \pm Packard HP-1 capillary column (30 m x 0.20 mm i.d.), which was programmed from 100 $^{\circ}\text{C}$ to 340 $^{\circ}\text{C}$ at 7 $^{\circ}\text{C}/\text{min}$. Analyses were performed in the selected ion monitoring mode. Selected ions were those at m/z 181, 240, 252, 421 and 433. Dwell was set at 0.02 s and the mass span at 0.5.

Other analytical techniques

Protein concentrations were determined using the Bradford reagent (Bio-Rad), with bovine serum albumin as reference.

RESULTS AND DISCUSSION

The set up of a simple procedure to isolate the SPL reaction product was first attempted. Since both enzyme and derivatization reaction buffers are compatible, the PFBHA solution was directly added to the SPL reaction mixture after this was finished, previous addition of the internal standard, and the aqueous solution was extracted with hexane after the derivatization was complete. Importantly, since both Tris and *O*-substituted hydroxylamines react also with pyridoxal phosphate²¹, the PFBHA solution was also suitable to stop the lyase reaction. This was proven in an assay carried out in the presence of PFBHA, in which no aldehyde was produced (data not shown).

Since 17SaP was used as substrate, standard curves were prepared with 15:AL, using Z11-16:AL as internal standard. Fig. 2 shows a GC/MS chromatogram of a PFBHA-derivatized aldehyde standard solutions in SIM mode. This chromatogram shows two peaks at 25.8 min and 26.6 min, attributed to the PFBO of 15:AL and Z11-16:AL, respectively. In agreement with reported data, the mass spectrum of each compound shows the characteristic fragment ions arising from benzylic cleavage of PFBO. These ions include the base peak at m/z 181 and peaks at m/z 240 (15:PFBO) and 252 (Z11-16:PFBO). The molecular ions are also observed (15:PFBO, m/z 421; Z11-16:PFBO, m/z 433), although with very low abundance. The quantification was unequivocally achieved with the two fragment ions, the common one at m/z 181 and structure-specific ions at m/z 421 for 15:PFBO and 433 for Z11-16:PFBO.

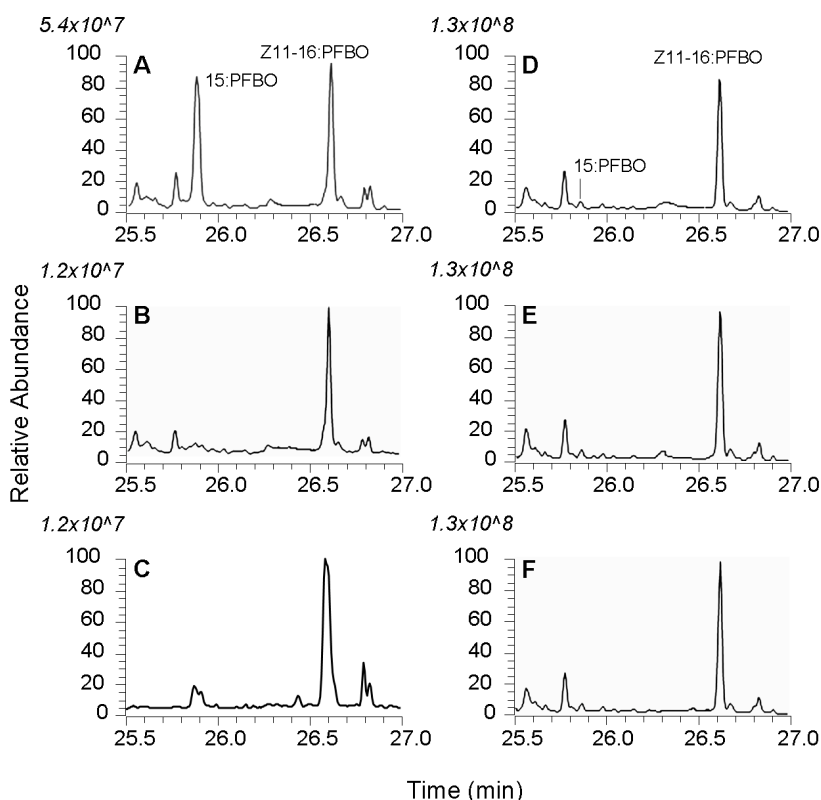


Fig. 2. GC-MS traces corresponding to the hexane extract of a SPL reaction mixture after treatment with PFBHA. The analysis was conducted under the selected ion monitoring mode. Selected ions are specified next to the traces and they correspond to: 181, oxime fragment B (base peak); 240, 15:PFBO fragment A; 252, Z11-16:PFBO fragment A; 421, molecular ion of 15:PFBO; 433, molecular ion of Z11-16:PFBO.

Compound abbreviations are: 15:PFBO, pentadecanal O-pentafluorobenzyl oxime; Z11-16:PFBO, (Z)-11-hexadecenal O-pentafluorobenzyl oxime. SGPL1 reaction and analytical conditions are detailed in the experimental section

The calibration curves were generated from the ratio of the peak area of 15:PFBO to the peak area of Z11-16:PFBO. A linear relationship between the analyte concentration and the ratio of the areas was observed in the examined range, with a regression equation $y=0.7572x+0.0271$ ($R=0.993$) and a detection limit below 100 nM (0.2 % of the substrate K_m), yielding an assay of higher sensitivity than that of the previously reported procedures.

We incubated the MEF215 cell lysates with C17:SaP under conditions similar to those employed previously for the fluorogenic assay¹⁹ and the reaction product was quantified by GC/MS analysis of its PFBO derivative. As shown in Fig. 3, the amounts of 15:AL formed in the SPL reaction varied with cell confluence, with higher activities occurring at 80-100% as compared to 40-60%.

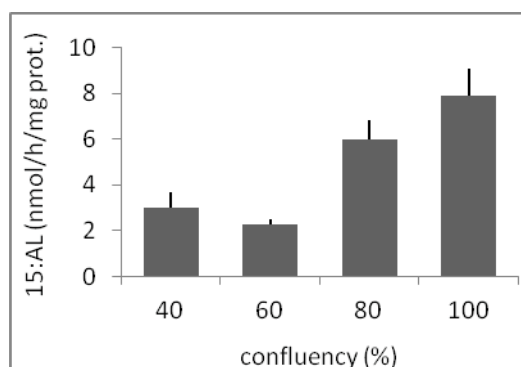


Fig. 3. Effect of cell confluence on SPL activity. Cells were seeded in 75mm plates at a density of 1.2×10^6 cells/ml. The assay was carried out with lysates from cells taken at different confluence levels. Protein amounts (μg) in the assay at each confluence were 36.5 (40%), 29.8 (60%), 18.3 (80%) and 15.2 μg (100%). The substrate concentration was 40 μM and the incubation time was 1 h. Each data point represents the mean \pm SD of one representative experiment with triplicates.

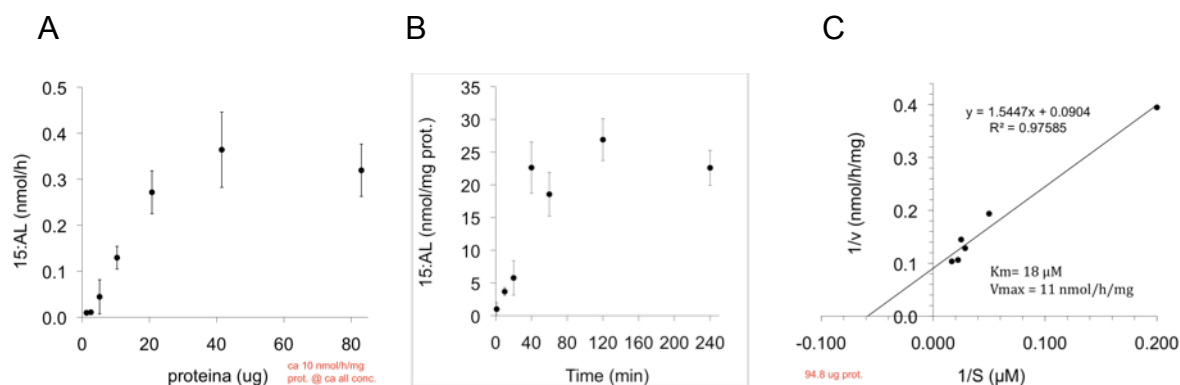


Fig. 4. Protein concentration (A) and time-dependence (B) of the SPL reaction using 17:SaP as substrate. In both cases, a 40 μM substrate concentration was used. In A, incubation time was 1 h and in B, protein amount was 20 μg . The reaction product was quantified by GC/MS after derivatization with PFBHA, using Z11-16:AL as internal standard. Each data point represents the mean \pm SD of one representative experiment with triplicates. C, Dependence of the SPL reaction rate on the substrate concentration. Different concentrations of 17SaP were incubated with 90 μg of protein for 1 h and the product was isolated and quantified by GC/MS. Lineweaver–Burk plots and the resulting kinetic parameters are shown. Each point corresponds to the mean \pm SD of three replicates. The data show a fit to the Michaelis–Menten equation ($y = 0.09 + 1.54x$; $R^2 = 0.98$) with $K_m = 18 \mu\text{M}$ and $V_{max} = 11 \text{ nmol/h.mg prot.}$

Likewise, enzyme activity increased with increasing the amounts of protein added (Fig. 4A). This increase was linear up to 20 μg of protein. On the other hand, the product formation augmented with the incubation time and the increase was linear over 40–60 min (Fig. 4B). Finally, the reaction rate was dependent on the substrate concentration (Fig. 4C), with $K_m = 18 \mu\text{M}$ and $V_{max} = 11 \text{ nmol/h.mg prot.}$ Thus, the catalytic efficiency of SPL for both the radiometric and 17SaP substrates is similar, which is expected given their almost identical structure. Routine experiments were performed with 20 μg of protein obtained from MEF215 cells at 80–100% confluence, at a 20 μM concentration of 17SaP and a 60 min incubation time. Under these conditions an about 8 % of substrate is cleaved yielding ion abundances that correlate linearly with the product concentration.

Finally, the assay was used in inhibition studies using the reported SPL inhibitor FTY720²². As shown in Figure 5, treatment of cell extracts with this compound reduced SPL activity to about

a 10% of control, which were incubated with vehicle (EtOH). This result is in accordance with previous articles reporting on the SPL inhibitory activity of FTY 720^{22,23}.

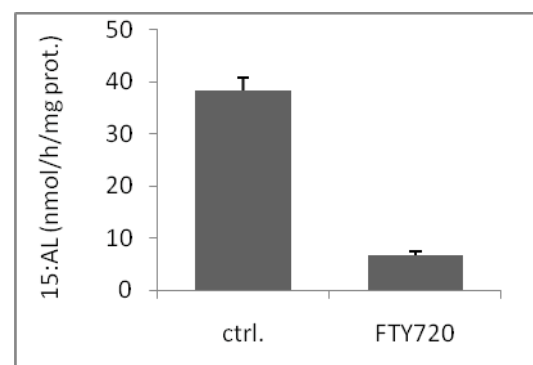


Fig. 5. Effect of FTY720 on SPL activity. The assay was carried out with lysates containing 14 μg of protein, which were incubated with 40 μM each of substrate and FTY720 (vehicle was added to controls). The incubation time was 1 h. Each data point represents the mean \pm SD of one representative experiment with triplicates.

In summary, a new assay to determine SPL activity has been developed. SPL inhibition has already been shown to modulate lymphocyte trafficking. Its potential to modulate other physiological endpoints such as inflammatory

responses, malignant growth and tissue homeostasis remain to be tested. To date, no specific small molecule inhibitors of SPL have been described. Generating specific inhibitors is an important goal that would facilitate the study of SPL activity and function and potentially offer a therapeutic strategy to treat certain pathological conditions by increasing circulating and/or tissue SLP levels. This assay offers an attractive alternative or complement to the previously reported procedures.

References

- [1] Van Veldhoven, P. P.; Mannaerts, G. P., *Adv. Lipid Res.* 1993, 26, 69-98.
- [2] Van Veldhoven, P. P.; Mannaerts, G. P., *J. Biol. Chem.* 1991, 266, 12502-7.
- [3] Ikeda, M.; Kihara, A.; Igarashi, Y., *Biochem. Biophys. Res. Commun.* 2004, 325, 338-43.
- [4] Li, G.; Foote, C.; Alexander, S.; Alexander, H., *Development* 2001, 128, 3473-83.
- [5] Herr, D. R.; Fyrst, H.; Phan, V.; Heinecke, K.; Georges, R.; Harris, G. L.; Saba, J. D., *Development* 2003, 130, 2443-53.
- [6] Kihara, A.; Ikeda, M.; Kariya, Y.; Lee, E. Y.; Lee, Y. M.; Igarashi, Y., *J. Biol. Chem.* 2003, 278, 14578-85.
- [7] Kumar, A.; Wessels, D.; Daniels, K. J.; Alexander, H.; Alexander, S.; Soll, D. R., *Cell Motil. Cytoskeleton* 2004, 59, 227-241.
- [8] Phan, V. H.; Herr, D. R.; Panton, D.; Fyrst, H.; Saba, J. D.; Harris, G. L., *Dev Biol* 2007.
- [9] Reiss, U.; Oskouian, B.; Zhou, J.; Gupta, V.; Sooriyakumaran, P.; Kelly, S.; Wang, E.; Merrill, A. H., Jr.; Saba, J. D., *J. Biol. Chem.* 2004, 279, 1281-1290.
- [10] Oskouian, B.; Sooriyakumaran, P.; Borowsky, A. D.; Crans, A.; Dillard-Telm, L.; Tam, Y. Y.; Bandhuvula, P.; Saba, J. D., *Proc. Natl. Acad. Sci. U. S. A.* 2006, 103, 17384-17389.
- [11] Min, J.; Stegner, A. L.; Alexander, H.; Alexander, S., *Eukaryot Cell* 2004, 3, 795-805.
- [12] Min, J.; Van Veldhoven, P. P.; Zhang, L.; Hanigan, M. H.; Alexander, H.; Alexander, S., *Mol Cancer Res.* 2005, 3, 287-96.
- [13] Li, G.; Alexander, H.; Schneider, N.; Alexander, S., *Microbiology* 2000, 146 (Pt 9), 2219-27.
- [14] Alexander, S.; Min, J.; Alexander, H., *Biochim Biophys Acta* 2005.
- [15] Schwab, S. R.; Pereira, J. P.; Matloubian, M.; Xu, Y.; Huang, Y.; Cyster, J. G., *Science* 2005, 309, 1735-9.
- [16] Bandhuvula, P.; Saba, J. D., *Trends Mol. Med.* 2007, 13, 210-217.
- [17] Van Veldhoven, P. P., *Methods Enzymol.* 2000, 311, 244-54.
- [18] Bandhuvula, P.; Fyrst, H.; Saba, J. D., *J. Lipid Res.* 2007, 48, 2769-2778.
- [19] Bedia, C.; Camacho, L.; Casas, J.; Abad, J. L.; Delgado, A.; Van Veldhoven, P. P.; Fabrias, G., *Chembiochem* 2009, 10, 820-2
- [20] Barr JR. , S. R., Yamaguchi K *J. Org. Chem.* 1989, 54, 2.
- [21] Leinweber, F.-J., *Mol Pharmacol* 1968, 4, 337-348.
- [22] Bandhuvula, P.; Tam, Y. Y.; Oskouian, B.; Saba, J. D. *J Biol Chem* 2005, 280, 33697-700.
- [23] Berdyshev, E.V., Goya, J., Gorshkova, I., Prestwich, G. D., Byun, H. S., Bittman, R., Natarajan, V. *Anal Biochem* 2011, 408, 12-8.

Concluding remarks to Section III.1

As mentioned in the Introduction, SPL expression and activity are downregulated in human colon cancer tissues compared with normal tissues¹⁹². Moreover, Colié *et al.*⁵⁴ have recently demonstrated that cells derived from *Sgpl1*^{-/-} mice have an increased growth ratio, colony formation in soft agar and tumor progression as compared to wild type cells, pointing to SPL as a tumor suppressor. Furthermore, SGPL1 is also downregulated in metastatic tumor tissues compared with primary tumors from the same patient⁵³. These overall reports highlight the importance of the study of SPL activity in different cancer cell types and tumors to determine if depletion of SPL activity and expression can be correlated with the malignancy grade of tumors. In this sense, SPL may emerge as a new biomarker and predictor of tumor malignancy and metastasis. For this purpose, the fluorogenic assay could allow the determination of SPL in patient biopsies having the advantages of being easily performed and not needing complicated or expensive infrastructure (HPLC or special radioactivity facilities).

On the other side, SPL blockage seems to be a good strategy for immunosuppression in transplantation and immune diseases. The recent crystallization and structural analysis³⁴ of SPL has incremented our knowledge of this enzyme and will allow the use of *in silico* and structure based design of new and specific SPL inhibitors. The fluorogenic assay developed in this work will allow the easy screening of compounds for SPL inhibitory activity, while the GC/MS assay will be an ideal complement for further kinetic characterization of hits.

III.2 Optimization and use of a fluorogenic enzyme assay for acid ceramidase

An unsolved drawback of the reported fluorogenic AC activity assay¹⁴¹ mentioned in the introduction was the existence of a suboptimal signal to background ratio. In order to improve this feature, optimization of the chemical steps was attempted. Additionally, the effect of changing the substrate *N*-acyl chain length over AC activity was also investigated, as well as selectivity in front of other CDases. The results obtained along these lines are presented and discussed in the following sections III.2.1 and III.2.2.

III.2.1. Optimization of the chemical steps

Specifically, one of the critical chemical steps of the assay, namely the aminodiol oxidation by sodium periodate (NaIO_4) (Figure 21), was studied in depth.

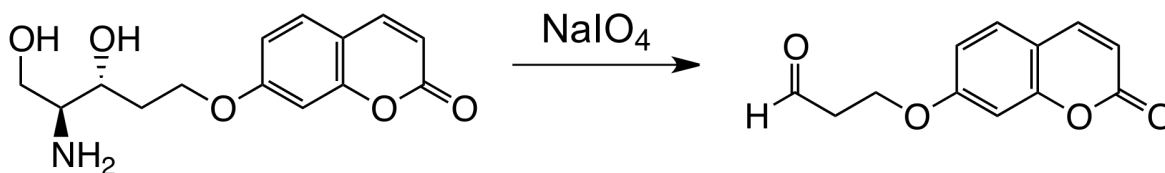


Figure 21. Oxidation reaction of the aminodiol (ADOL) to the aldehyde (ALD)

III.2.1.1 Aminodiol oxidation by sodium periodate (NaIO_4) in acid conditions

Although Reymond and coworkers¹⁹³, who first described the use of umbelliferone-based enzyme substrates, used NaIO_4 in phosphate buffer and BSA at pH 8,^{194,195} literature search showed that oxidation of carbohydrates with NaIO_4 is mainly carried out in acid conditions. Therefore, the oxidation of ADOL in acid solution was evaluated. To mimic the cell culture environment, the ADOL was dissolved in DMEM (without FBS). Serial dilutions of ADOL in DMEM were treated with a NaIO_4 solution 10 mg/mL in acetate buffer (100 mM, pH 4.5). After different incubation times, glycine buffer (200 mM, pH 10.6) was added and fluorescence was measured. The best results were attained at 30-60 min oxidation in acetate buffer and 1 h in glycine buffer.

Oxidation was fast in these conditions, but there was a large deviation between the umbelliferone concentration-response line and the fluorescence released from the same concentrations of ADOL (slope ratios 2.9), which suggested that oxidation occurred with low yield (Figure 22).

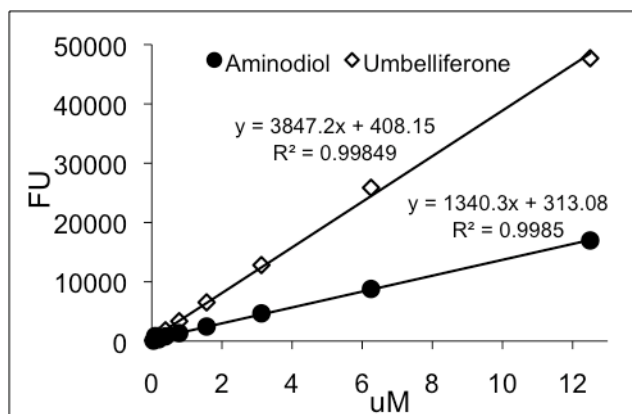


Figure 22. Oxidation of ADOL in acid conditions. ADOL solutions in DMEM at concentrations from 12.5 to 0.05 μM (100 μl /well) were treated with 25 μl of a NaIO_4 solution 10 mg/ml in acetate buffer (200 mM, pH 4.5). After 30 min, 100 μl of glycine buffer (200 mM, pH 10.6) was added and fluorescence was measured after 60 min. Serial dilutions of umbelliferone were also submitted to the same treatments.

These results indicated that NaIO_4 oxidation of ADOL in acid conditions was not appropriate. To confirm this issue, an experiment was performed to compare the reaction features in both acid and the reported basic conditions (but without BSA).

The results of this experiment are shown in Figure 23. Serial dilutions of RBM14, ADOL and umbelliferone were prepared in either acetate buffer (100 mM, pH 4.5) or DMEM, both in the presence and absence of FBS in the latter case. Then MeOH was added followed by addition of NaIO_4 in either acetate buffer or glycine buffer.

In the first case, glycine buffer was added 30 min after addition of the oxidant and the fluorescence produced was measured 60 min after addition of glycine. In these conditions, RBM14 gave fluorescence values barely above background, which confirmed the stability of the substrate under the assay conditions.

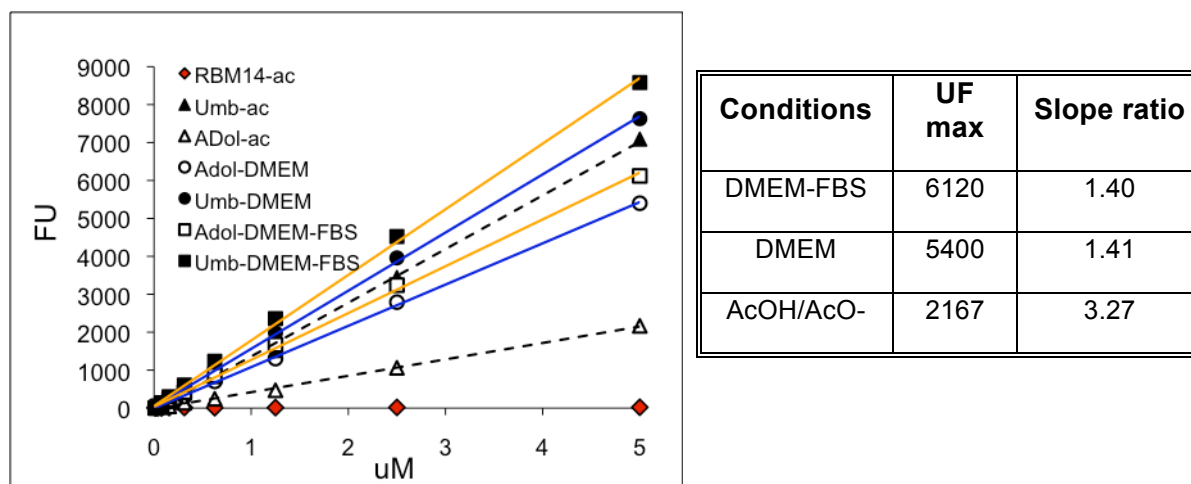


Figure 23. Effect of the oxidant in acid and basic conditions. Serial dilutions of RBM14 (red diamonds), ADOL (open symbols) and umbelliferone (solid symbols) from 5 to 0.001 μM were prepared in acetate buffer (50 μl /well) and DMEM (100 μl /well), either with or without FBS. 100 μl of a NaIO_4 solution 10 mg/ml in acetate buffer (dashed lines) or glycine buffer (blue lines for DMEM solutions and orange lines for DMEM-FBS solutions) were then added and the fluorescence was measured after 90 min. When the oxidant was provided in acetate buffer, glycine buffer was added 30 min after the oxidant and the fluorescence was measured after 60 min.

III.2.1.2 Oxidation in basic conditions with different amounts of NaIO_4

Another possibility for the low sensitivity could be an overoxidation of the aldehyde produced from ADOL leading the reaction to the acid formation, which would not eliminate to give umbelliferone. To check this point, ADOL was dissolved in DMEM (3 μM) and was treated with MeOH and then with a NaIO_4 solution of different concentrations in either phosphate buffer (100 mM, pH 8.0) or glycine buffer (200 mM, pH 10.6) and fluorescence was measured after different times.

As shown in Figure 24, the overall transformation was faster in glycine buffer than in phosphate buffer. Importantly, the NaIO_4 concentration affording the highest yield was 2.5 mg/ml, which gave a 60% more fluorescence counts than the 10 mg/ml solution previously used.

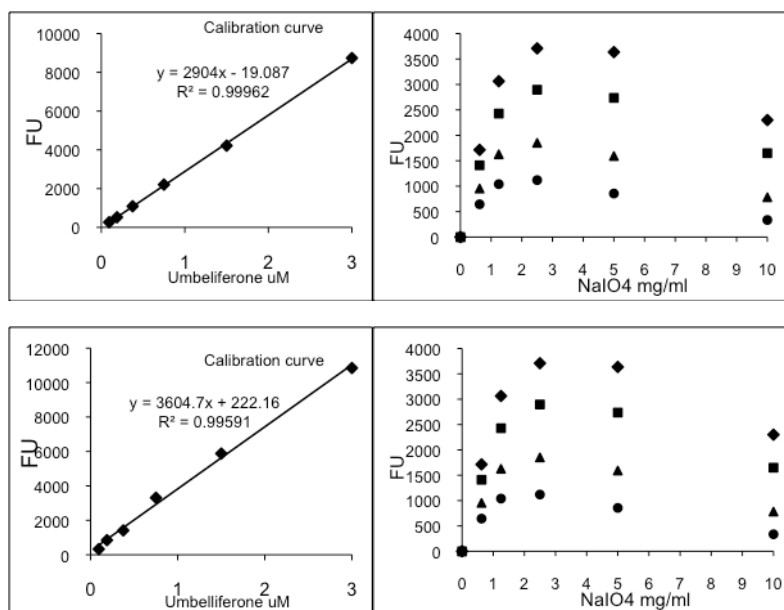


Figure 24. Effect of oxidant concentration. The ADOL dissolved in DMEM (100 μ l, 3 μ M) was treated with MeOH (100 μ l) and then with a NaIO₄ solution of different concentrations in: TOP: phosphate buffer (100 mM, pH 8.0); BOTTOM: glycine buffer (200 mM, pH 10.6) and fluorescence was measured after different times (diamond, 180 min; square, 90 min; triangle, 60 min; circle, 30 min). The calibration curve was performed with umbelliferone submitted to the same treatments.

Slightly different results were obtained when different volumes of oxidant 10 mg/ml were added. In this case, 50 μ l (equivalent to 100 μ l, 5 mg/ml) gave the best transformation, but it was worse than that obtained with 100 μ l of oxidant 5 mg/ml.

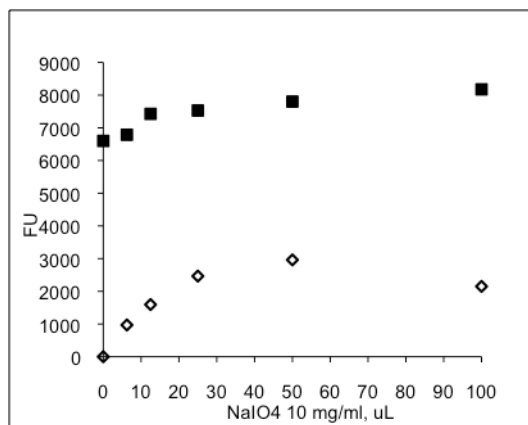


Figure 25 Effect of oxidant volume. The ADOL was dissolved in DMEM (100 μ l, 3 μ M) and was treated with MeOH (100 μ l) and then with different volumes of a NaIO₄ solution 10 mg/ml in phosphate buffer (100 mM, pH 8.0) and fluorescence was measured after 120 min (diamonds). The same solutions without oxidant were considered as blanks. Umbelliferone dissolved in DMEM (100 μ l 3 μ M) submitted to the same treatments, but with buffer without oxidant was also measured (squares).

In the same conditions, 3 μ M umbelliferone gave more than two-fold fluorescence counts than 3 μ M ADOL, whereas in the experiment of Figure 23, fluorescence ratio was 1.4. Since in that experiment oxidant was also added to umbelliferone, one possibility was that umbelliferone decomposes in part in the presence of NaIO₄. On the other hand, 50 μ l of methanol were added in experiment of Figure 23, whereas 100 μ l were added in those of Figure 24-25. Therefore, the volume of methanol added per well could also affect the reaction parameters.

RESULTS

To check both possibilities, two experiments were carried out in parallel: in one of them, 3 μM ADOL and 3 μM umbelliferone were mixed with different volumes of methanol before addition of the oxidant (Figure 26A); in the other, different concentrations of umbelliferone were treated with a constant volume of methanol (100 μL) and then with different concentrations of NaIO_4 (Figure 26B and 26C). Although the effects were very slight, 25 μL of methanol and 2.5-1.25 mg/ml of NaIO_4 gave the highest fluorescence counts.

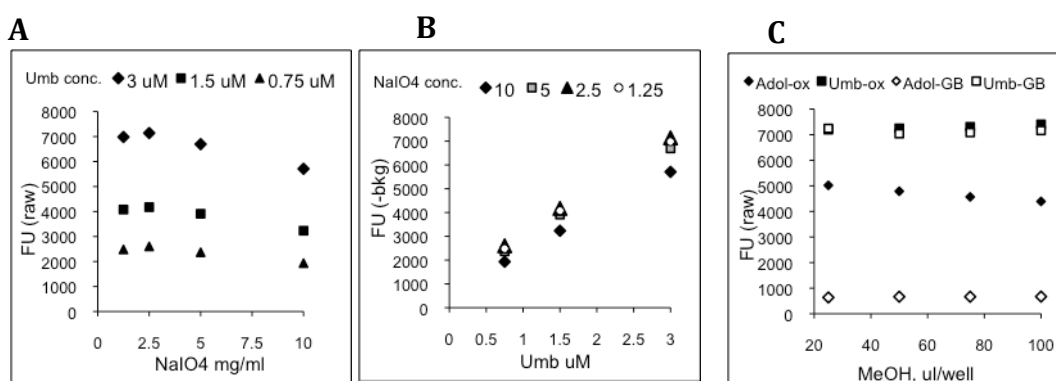


Figure 26. Effect of methanol and NaIO_4 on umbelliferone signal. ADOL and umbelliferone were dissolved in DMEM (100 μL , 3 μM) and treated with: (A) different volumes of methanol and then with 100 μL of NaIO_4 2.5 mg/ml in glycine buffer (100 μL of glycine buffer in blanks); (B) different concentrations of umbelliferone and 100 μL of MeOH; (C) 100 μL of methanol and different concentrations of NaIO_4 (100 μL /well)

In the light of these results, concentration-response lines were constructed for both ADOL and umbelliferone in the optimal conditions: solutions in DMEM, 25 μL /well of methanol, 100 μL /well of NaIO_4 2.5 mg/ml in glycine buffer, reading after 60-90 min. As shown in Figure 27, the slope ratio between the two lines was around 2 even in the optimized conditions. No further optimization was attempted.

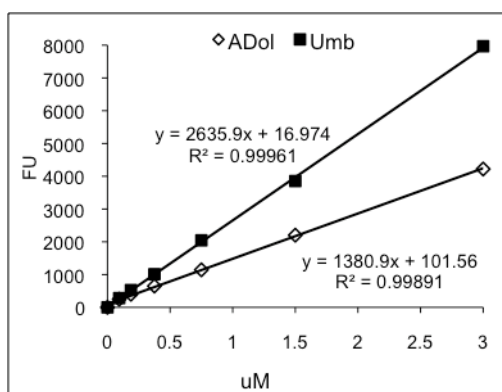
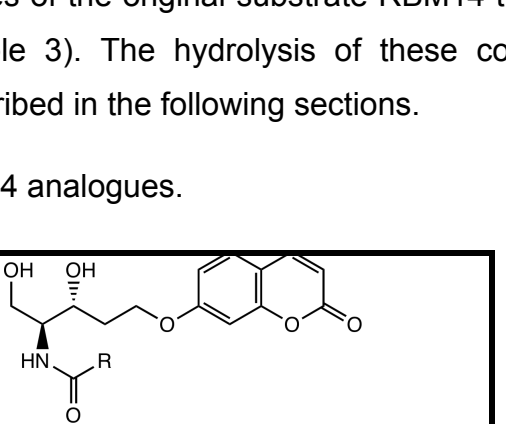


Figure 27 Concentration-response lines. Serial dilutions of ADOL and umbelliferone in DMEM (100 μL /well) were treated with 25 μL of methanol and then with 100 μL of NaIO_4 2.5 mg/mL in glycine buffer and fluorescence was measured after 90 min.

III.2.2 Determination of the AC activity-dependence on the substrate *N*-acyl chain length

Although the oxidation step was improved, further optimization was attempted by changing the substrate *N*-acyl moiety. According to the literature, AC recognizes C6 to C16 Cer as substrate; however, AC shows highest activity with C12 Cer. Therefore, changing the substrate *N*-acyl chain could afford better substrates of AC than the original C16 derivative. To assess this possibility, Dr. José Luis Abad synthesized several analogues of the original substrate RBM14 that differed in the fatty acid chain length (Table 3). The hydrolysis of these compounds by the different ceramidases is described in the following sections.

Table 3. RBM14 analogues.

		
R	Substrate	logP ^a
C ₃ H ₇	RBM14C4	0.97
C ₇ H ₁₅	RBM14C8	2.64
C ₉ H ₁₉	RBM14C10	3.48
C ₁₁ H ₂₃	RBM14C12	4.31
C ₁₃ H ₂₇	RBM14C14	5.15
C ₁₅ H ₃₁	RBM14	5.98
C ₂₃ H ₃₁	RBM14C24	

^aCalculated with the ChemBioDraw Ultra program, which gives values of logP of 4.27 and 6.18 for C2 and C6 ceramide, respectively.

III.2.2.1 Activity of AC over the RBM14 analogues both in intact cells and cell lysates

These experiments were carried out in the previously used¹⁴¹ Moh pAS cell line transduced to overexpress functional AC and the parental Moh cells, corresponding to a Farber disease patient, which exhibit almost undetectable AC activity. These cells only exhibit neutral and alkaline CDase activity, allowing us to discern between the hydrolysis caused by AC and other CDases.

As expected, in Moh cells the released fluorescence from all substrates was significantly lower than in Moh pAS 10X cells, indicating that AC was the enzyme responsible for the hydrolysis of the RBM14 analogues. In agreement with previously reported data on AC substrate specificity¹³⁵, the best substrates in the Moh pAS 10X cells were the C10, C12 and C14 RBM14 analogues, both *in vitro* and in intact cells (Figure 28). Importantly, the three compounds were hydrolyzed significantly more efficiently than the original C16 compound (RBM14) in the two experimental setups. Interestingly, RBM14C12 was a better substrate in cell lysates than RBM14C10 and RBM14C14, which gave similar fluorescence levels. However, the best substrates in intact cells were in the order RBM14C14 > RBM14C12 > RBM14C10. This difference can be explained in terms of cell permeability. Considering the partition coefficient for *n*-octanol/water (logP) as an indirect measure to estimate cell permeability, the values for the three compounds RBM14C14, RBM14C12 and RBM14C10 are, respectively, 5.15 > 4.31 > 3.48 (Table 3), which follows the same order than that of their hydrolysis. In agreement, LC/MS analyses demonstrated that amounts of RBM14C14 found in lipid extracts were about 5 times higher than those of the C12 and the C16 analogs (the C10 derivative was not analyzed) (see Section III.2.4.3). Additionally, it is also possible that the originally fed substrate undergoes deacylation/reacylation⁷⁴ in whole cells (see Section III.2.4.3) so that a mixture of differently acylated RBM14 analogues rather than a single amide is hydrolyzed by AC in cultured cells. Then, the actual AC substrate preference in cells would be biased by the deacylation/reacylation rates. In contrast, single amides are hydrolyzed in cell lysates, in which the deacylation/reacylation reactions do not occur in the experimental conditions of the assay.

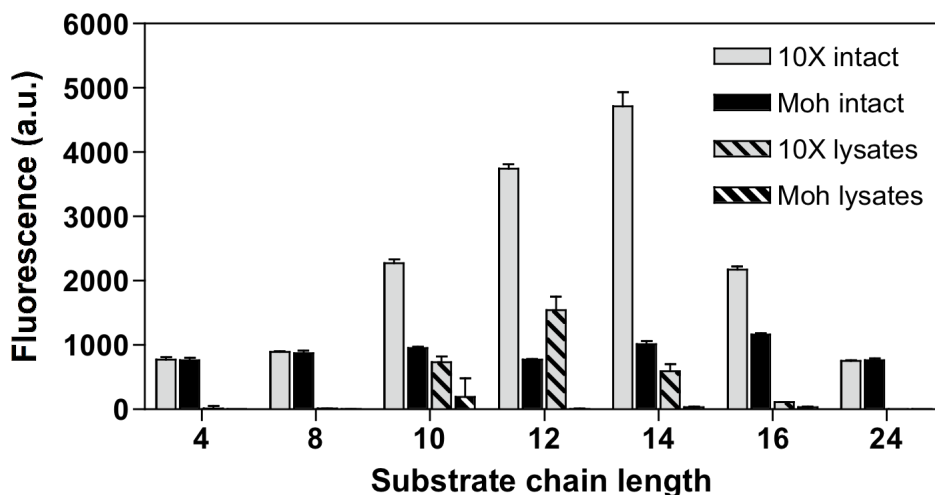


Figure 28. Hydrolysis of coumarinic substrates (40 μ M) in intact Moh pAS 10X and Moh cells (20,000 cells/well), and cell lysates. *In vitro* experiments were done at pH 4.5 (100 mM acetate buffer). Results were normalized by protein quantity (3.5 mg/mL). Data are represented as the mean of three replicates \pm SD.

In summary, these overall results indicated that RBM14C12 was the best AC substrate *in vitro*, while RBM14C14 was the best in whole cells.

III.2.2.2 Hydrolysis of RBM14 analogues by other CDases in intact cells

Since experimental evidence suggests that the five reported CDases have different substrate specificities⁷⁸, we wondered if one or more of the RBM14 analogues would be also substrates for neutral or alkaline CDases. Neutral and alkaline CDases are expressed at very low levels in fibroblasts. Therefore, Moh pAS cells were transfected to overexpress NC, ACER1, ACER2 or ACER3. The use of Moh pAS cells allowed us to avoid the interference of AC in the experiments. Transfection conditions are detailed in the methods section. The fluorogenic assay was performed under the same conditions as above, but using the suitable buffer solution to achieve the required pH. As shown in Figure 29, none of the RBM14 analogues was hydrolyzed by ACER1, ACER2 or ACER3 in intact cells. The success of transfection⁷⁸ was confirmed by activity assay (ACER1), Western blot (ACER2) and fluorescence microscopy (ACER3) (see Materials and Methods). Although a number of publications claim that these enzymes prefer long chain Cers as substrates⁷⁸, the lack of solubility of long chain Cers in aqueous media has precluded the study of their metabolization when added exogenously to intact cells. Conversely, the hydrophilicity conferred by the coumarin unit to the RBM14 analogues allows to determine the metabolic fate of a wide range of amides of different *N*-acyl chain lengths.

In contrast to the three ACERs, compounds RBM14C8 to RBM14C16 were hydrolyzed by NC being RBM14C10 the best substrate in intact cells. Remarkably, RBM14C8 appeared to be NC specific, since it was only hydrolyzed by cells overexpressing NC. These results are in contrast to the previously reported for mouse NC¹⁹⁶, which appears to prefer Cer's of long acyl chains, C16 or C18. Whether RBM14C8 is transacylated in these cells to longer *N*-acyl derivatives is still not known and will be investigated in the near future.

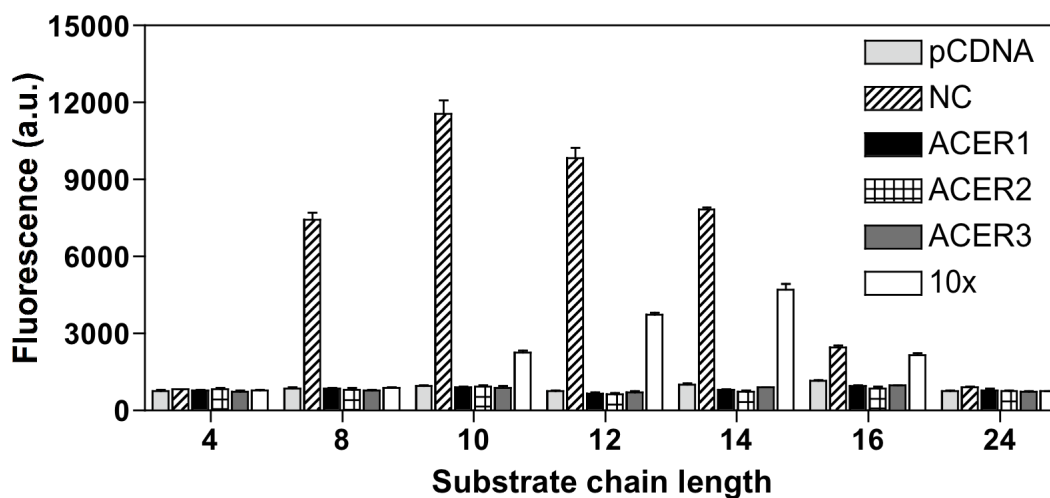


Figure 29. Hydrolysis of coumarinic substrates in intact Moh pAS 10X cells and Moh cells transfected to overexpress NC, ACER1, ACER2 or ACER3. Data are represented as the mean of three replicates \pm SD.

Overall, while substrate hydrolysis by AC in intact cells followed the order C14 > C12 > C10 ~ C16 (Figs. 28 and 29), NC substrate preference was C10 > C12 > C8 ~ C14. From the results depicted in Figure 29, AC appears to have a lower activity than NC. However, it must be pointed out that cells overexpressing either enzyme do not necessarily produce the same amounts of ceramidase and the observed differences may just indicate different enzyme expression levels. In this regard, it should be stressed out that promoters and transfection systems are different in both cases. The AC gene inserted to the same vector used to clone NC is now available and will be used for comparison in future experiments.

1.2.2.3 *In vitro* hydrolysis of RBM14 analogues by CDases

In order to confirm that the fluorogenic substrate hydrolysis profiles occurs as a function of pH, the compounds were tested *in vitro* with cell lysates derived from transfected cells at neutral or alkaline pH (for acid pH, see section III.2.2.1). In agreement with the lack of conversion of the substrates by the alkaline ceramidases ACER1, ACER2 and ACER3, no activity was found on any substrate *in vitro* at pH 9.0 in lysates from cells transfected with each ACER (data not shown). However, as shown in Figure 30, cell lysates derived from NC overexpressing cells hydrolyzed the RBM14 substrates. Best hydrolyses occurred at the enzyme optimal pH (7.5), although residual enzyme activity was also detected at both acid and basic pH. Although the highest activity was toward RBM14C10, the analogues with C8, C12 and C14 were also hydrolyzed efficiently.

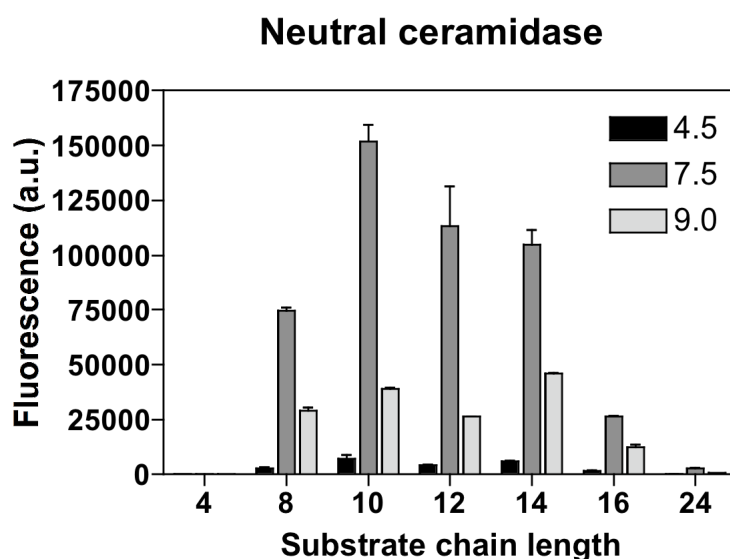


Figure 30. *in vitro* hydrolysis of RBM14 analogues. Cell lysates derived from Moh cells transfected with pcDNA5/TO-NC were measured for ceramidase activity at pH 4.5 (100 mM acetate buffer), pH 7.4 (25 mM PB or pH 9.0 (100 mM glycine/NaOH buffer) using RBM14 analogues (40 μ M) as substrates. Results are normalized by protein quantity. Data represent the mean and SD of three values. Moh cells transfected with empty pcDNA5/TO plasmid showed no activity on any substrate (not shown).

Altogether these results partially agreed with already published works describing that ACER1 has little or no activity on ceramides with *N*-acyl chain length of less than C18, but opposite to our results, it catalyzes the hydrolysis of C24:1⁷⁹. Moreover, ACER2 also hydrolyzes efficiently C24:1 Cer⁸⁰. And finally, ACER3 prefers long chain unsaturated ceramides C18:1, C20:4 Cer and phytoceramides⁸⁶.

Additionally, these results suggested that NC activity might interact with the correct determination of AC activity. However, normal NC expression in almost all tissues is very low, and it is not likely that it will interfere in AC activity assays in not transfected cells.

As mentioned above RBM14C8 has shown to be a specific substrate for NC, which opens the interesting possibility of its use in a high-throughput assay for NC, both in cell screening and in the development of NC inhibitors

III.2.2.4 Dose-dependence of RBM14 hydrolysis by CDases.

Moh pAS 10X cells were incubated with different concentrations of the several RBM14 substrates. As shown in Figure 31, the fluorescence produced by the C10 to C16 analogs increased with their concentration up to 20 μM . Amongst the four substrates, the response values followed the order $\text{C14} > \text{C12} > \text{C10} > \text{C16}$. The C4 and C8 analogs were poor substrates at all concentrations tested.

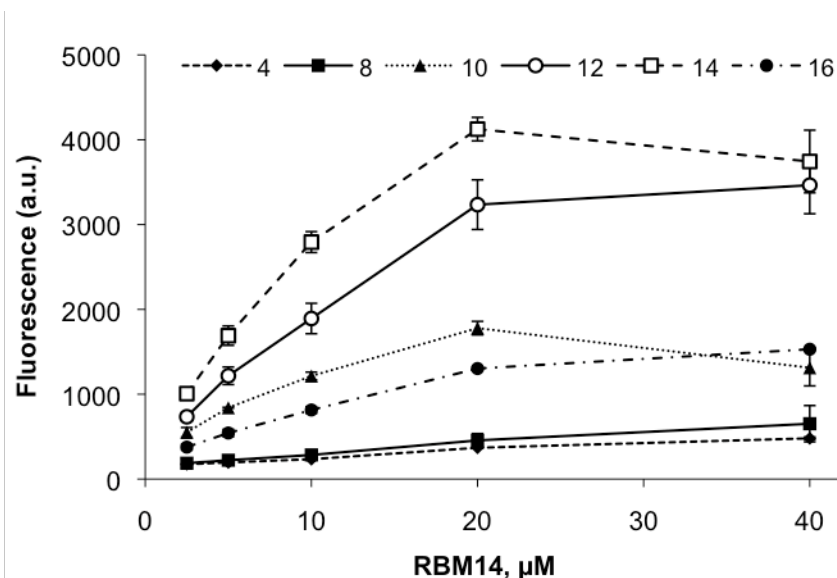


Figure 31. Dose dependence of RBM14 hydrolysis in intact Moh pAS 10X cells incubated with different concentrations of RBM14 analogues under the standard assay conditions Data represent the mean and SD of three values.

III.2.3 Application to the diagnosis of FD

After the detailed study described in the previous sections, the optimized fluorogenic assay using RBM14C12 as substrate was applied as a tool for the diagnosis of Farber disease. This work was carried out in collaboration with Dr. Thierry Levade (Toulouse, France)

More detailed information is given in the recently published article¹⁹⁷:

Bedia, C., Camacho, L., Abad, J.L., Fabrias, G. & Levade, T. **A simple fluorogenic method for determination of acid ceramidase activity and diagnosis of Farber disease.** *J Lipid Res* 2010, 51, 3542-3547

Impact factor: 4.92

My contribution to this work was the experiment of Figure 1B.

This work has given rise to the patent application P201031008 (Priority date 29/06/2010)

Gemma Fabriàs Domingo

Thesis Director

III.2.4 Application to screening of AC activity in cancer cells

Over the last two decades alterations in sphingolipid metabolism in several cancer types have been described, particularly decreased amounts of Cer in human colon cancers, gliomas and ovarian cancer⁷⁷. This pointed out the important role of Cer in cancer biology and also the crucial role of CDases, the main enzymes in charge of Cer degradation. Thus, hydrolysis of the RBM14 analogues was assessed in several cancer cell lines, in order to identify putative differences that might become of diagnostic or prognostic relevance. This work was conducted in the frame of an ongoing collaboration with Dr. Timothy Thomson (IMBB, CSIC, Barcelona). The assays were performed in both intact cells and cell lysates. In the latter case, the experiments were carried out only in acid and neutral pH, as previous studies had shown that the RBM14 substrates were not transformed by alkaline CDases.

III.2.4.1 Hydrolysis of RBM14 analogues in intact cancer cells

Selected cell types were the estrogen receptor alpha-negative, highly invasive, fibroblast-like MDA-MB-231 breast cancer cell line; the human neuroblastoma IMR-32 cell line and two clones of each of the human colon cancer HCT116 and prostate cancer PC3 lines. For the HCT116 cells, a p53 deficient clone (HCT116-379) and the wild type clone (HCT116-40 16) were available, while for the PC3 cell line, accessible clones included the PC3/Mc (highly metastatic but poorly invasive) and PC3/S (non metastatic but highly invasive). The assay was performed under the standard conditions as detailed in the Methods Section. For the assay in intact cells, cells were plated 3 hr before the assay to avoid misleading results due to differences in growth rates between cell lines.

The results obtained are summarized in Figure 32. HCT116 40 16 and PC3/Mc cells were the most active at hydrolyzing RBM14C12 to C16. These results are in agreement with the literature¹⁰⁰, since high AC activity has been described in prostate cancer, and colon cancer has been reported to exhibit more than a 50% decrease in the cellular content of ceramide when compared with normal colon mucosa¹¹⁹, which appeared to result from increased CDase expression and activity.

Interestingly, the HCT116 379 clone hydrolyzed the coumarinic substrates with 3-4 fold lower activity as compared to wild type HCT116-40 16 cells, suggesting a putative role of p53 in regulation of AC at different possible levels (transcription, expression, etc.). In this context, Hara et al.¹⁹⁸ reported that in human glioma cells without functional p53, gamma-radiation triggers ceramide generation and apoptosis, whereas endogenous p53 eliminates the ceramide signal through upregulation of AC, resulting in glioma cells resistant to gamma-radiation induced cell death.

Moreover, treatment with either an AC inhibitor or siRNA renders cells with functional p53 sensitive to gamma-radiation, underscoring the interest of AC inhibitors as adjuvants in cancer therapies. In a more recent paper, Morselli et al.¹⁹⁹ reported that cytoplasmic p53 induces apoptosis and inhibits autophagy. With the same HCT116 cell lines used here, these authors found that twice as much cells with punctate cytoplasmic LC3-GFP distribution occurred in p53^{-/-} than in p53^{WT} cells, indicating higher autophagy in the former than in the latter. These reports suggested a possible link between AC activity and autophagy inhibition by cytoplasmic p53.

Likewise, the prostate cancer clone PC3/S was about 2-4 times less active than the PC3/Mc clone at hydrolyzing the coumarinic substrates. Finally, neither MDA-MB-231 or IMR32 cells showed remarkable CDase activity as compared with the other lines. Unfortunately, corresponding pairs with differential specific phenotype features for comparison were not available at the time of these experiments.

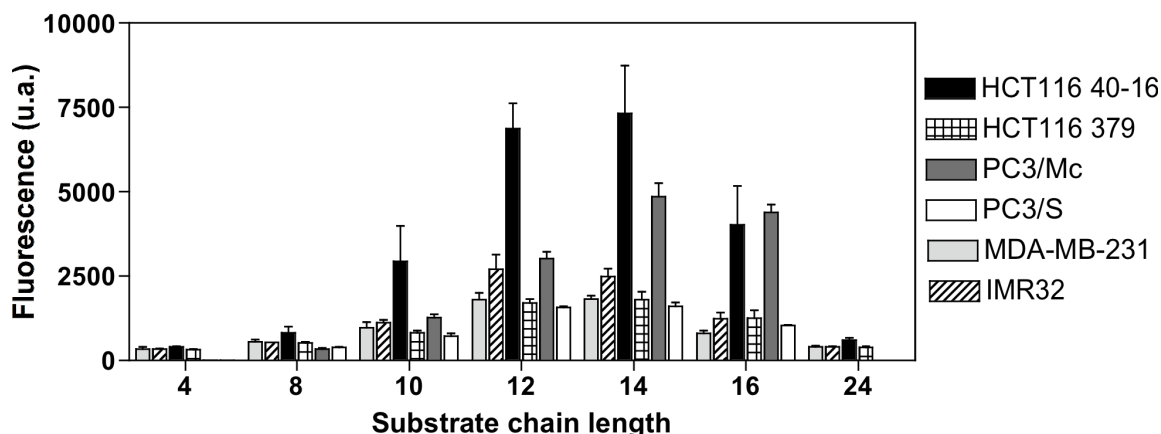


Figure 32. Hydrolysis of coumarinic substrates by intact cancer cells. Results were normalized by cell number. Data represent the mean of three values \pm SD.

III.2.4.2 *In vitro* hydrolysis of RBM14 analogues by cancer cells lysates

The results obtained in intact cells led us to choose the pairs HCT116-40-16/HCT116 379 and PC3/S/PC3/Mc for further studies. First, the hydrolytic fate of RBM14 compounds was determined in cell lysates to confirm that the increased ceramidase activity was due to AC. The results of hydrolysis of the coumarinic substrates under acid conditions *in vitro* are shown in Figure 33A. Similarly to the results obtained in intact cells, the fluorescence released by HCT116 40-16 and PC3/Mc lysates was higher than that from HCT116 379 and PC3/S, respectively, suggesting that AC is less active or expressed at lower levels in these last cell types.

Under neutral conditions, high fluorescence levels were observed in lysates from the four cell lines. This likely reflects the residual AC activity occurring at neutral pH. Although NC activity could also account for the signal produced at pH 7.5, the lack of fluorescence from RBM14C8 (compare to Fig. 30) does not support this possibility.

In agreement with the results obtained in intact cells (Figure 33B), HCT116 40-16 and PC3/Mc cell lines exhibited significantly higher CDase activity than the respective clones HCT116 379 and PC3/S at both pH's (Figure 33)

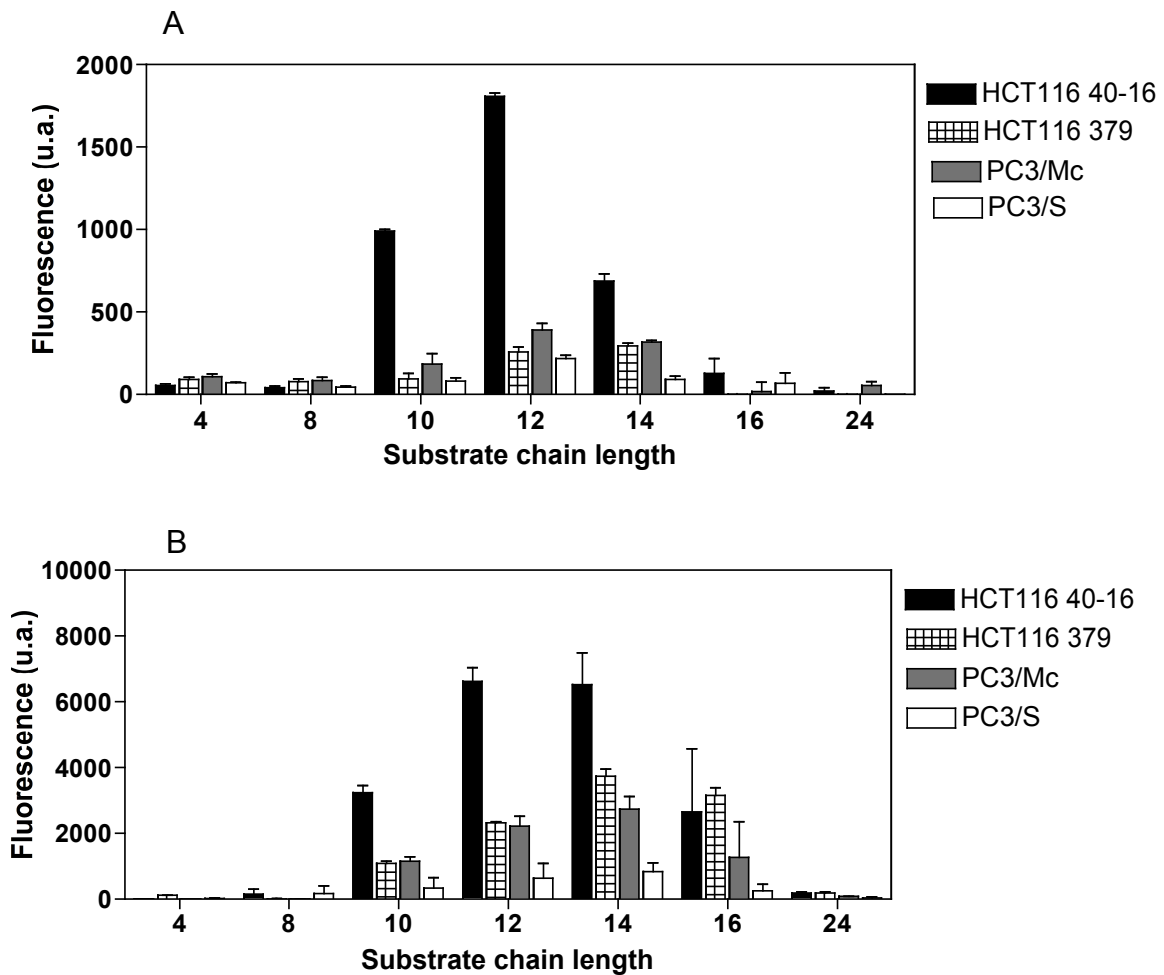


Figure 33. *In vitro* hydrolysis of coumarinic substrates by cancer cell lysates in A) acid conditions (100 mM acetate buffer pH 4.5) and B) neutral conditions (25 mM PB pH 7.4) Results are normalized by protein quantity. Data are represented by the mean of three values \pm SD.

III.2.3.3 Metabolism of RBM14 and its analogues

The metabolic fate of the best CDase RBM14 substrates (RBM14C12, RBM14C14 and RBM14C16) was also investigated in the several cell lines in order to obtain a better picture of the compounds intracellular uptake and their incorporation into the sphingolipid metabolic routes, which was assumed would depend on the cell type. To this aim, 1×10^6 cells were incubated for 3 h with the several coumarinic analogues at 40 μ M. Lipids were then extracted and analyzed by UPLC/TOF as described in the Methods Section.

Seven cancer cell lines besides the FD fibroblasts Moh pAS and Moh pAS 10X were analyzed. The results are summarized in Figure 34. The cell line showing the highest amounts of each of the three administered compound was the Moh (Figure 34 A, B, and C). This result was expected given the lack of AC activity of this cell line, which is derived from a FD patient. The compound exhibiting the highest incorporation was RBM14C14 in all cell lines (Figures 34 A, B and C). This can result from both high uptake and low metabolization, as the percentage of RBM14C14 detected as such was in the range 80-95% of the total coumarinic metabolites (Figure 34D).

Compound RBM14C16 was also poorly metabolized, except for both HCT116 clones. In this case, it is worth noting the formation of C24 and C24:1 transacylation products, derived from *N*-deacylation/reacylation of the substrate, as the main metabolites in HCT116 4016. This suggests the occurrence of CerS2 and/or CerS4 in these cells and that the aminodiol released upon CDase hydrolysis may be a substrate of these CerS's.

The substrate undergoing the highest metabolization was RBM14C12, which decreases to a 50% of the total metabolites in the case of SKN, IMR-32, MDA-MB231 and HCT116 40 16. Although the high CDase activity accounts for the high metabolization of RBM14C12 in HCT116 40 16, this is not the case for the other three cell lines, which did not show remarkably high CDase activity (see III.2.4.1 and III.2.4.2). However, as shown in Figure 34 E, the main metabolites in these cells were those arising from *N*-deacylation/reacylation.

The high percentage of the C18 transacylation product in the SKN and IMR-32 cell lines points to the occurrence of CerS1 and/or CerS4 in these cells and that the aminodiol released upon CDase hydrolysis may be a substrate of these CerS's. Interestingly, no RBM14C16 is formed from either RBM14C12 or RBM14C14 in any cell line examined. Moreover, no RBM14C12 and RBM14C14 are produced from any of the substrates. This suggests that CerS5 and/or CerS6 are not present in any of the cell lines examined. However, all of them contain C16-ceramides in high amounts, which is against the lack of CerS5/CerS6. A more likely explanation is that the coumarinic aminodiol is not a good substrate of these CerS's.

The detection of deacylation/reacylation products, which in some cell types reach high levels (i. e. SKN and IMR-32), urges caution in drawing wrong conclusions, since low fluorescence values will be obtained in cells with high AC activities if reacylation rates are high. The use of a general CerS inhibitor (i. e. Fumonisin B1) in AC screening in intact cells may be advisable in these studies.

Finally, the low percentage of both SM and GlcCer (less than 10%) suggests that the RBM14 compounds are poor substrates of sphingomyelin synthases and glucosylceramide synthase.

In summary, RBM14C12 is the most rapidly metabolized substrate in almost all cell types studied. The main metabolites were the *N*-deacylation/reacylation products, which accounted for around 10 to 30% of the total intracellular substrate. These results indicate that the aminodiol formed upon CDase activity over the RBM14 substrates is a substrate of some CerS's. Which is the affinity of this aminodiol for the 6 different CerS enzymes will be investigated in the near future.

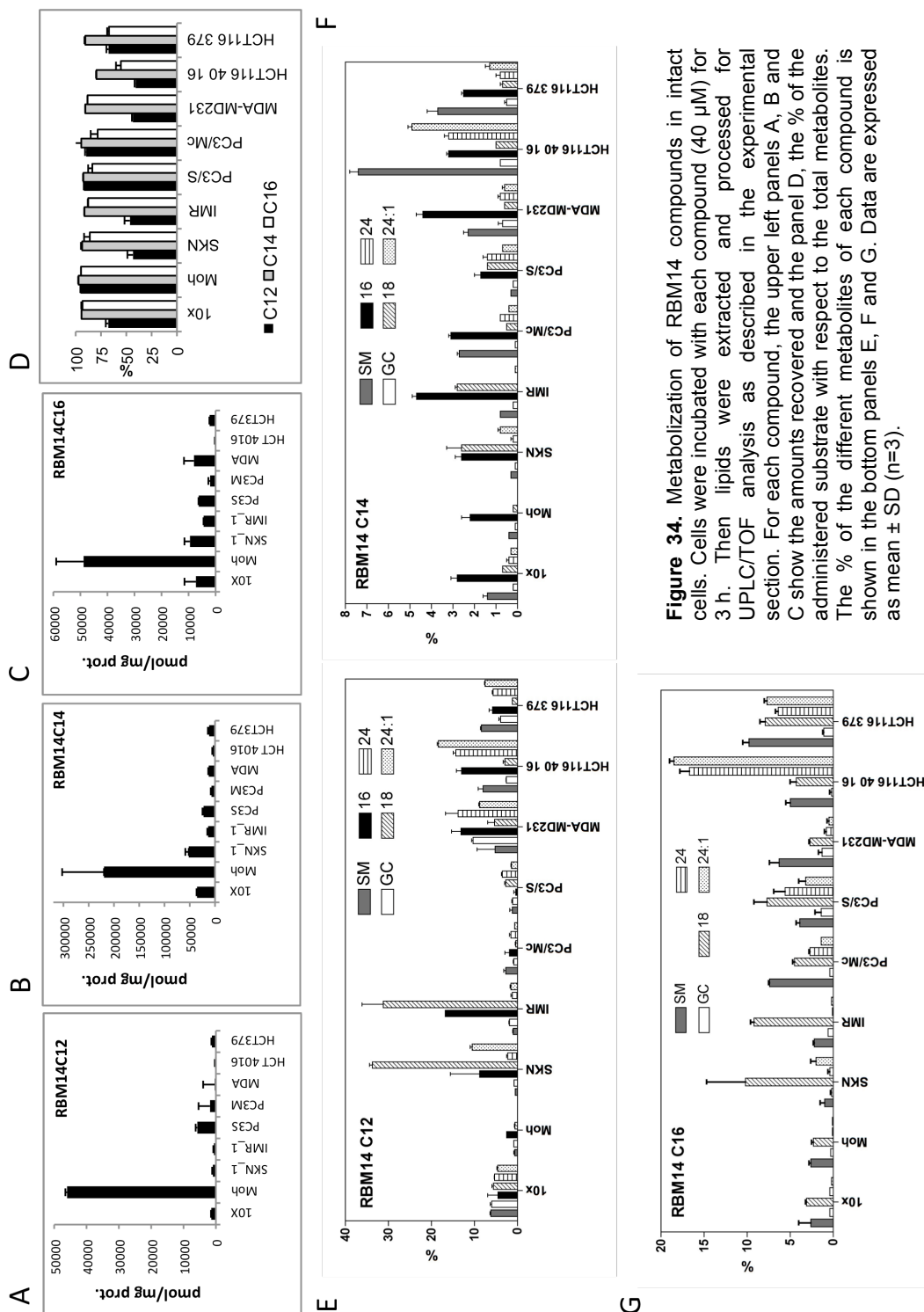


Figure 34. Metabolization of RBM14 compounds in intact cells. Cells were incubated with each compound (40 μ M) for 3 h. Then lipids were extracted and processed for UPLC/TOF analysis as described in the experimental section. For each compound, the upper left panels A, B and C show the amounts recovered and the panel D, the % of the administered substrate with respect to the total metabolites. The % of the different metabolites of each compound is shown in the bottom panels E, F and G. Data are expressed as mean \pm SD (n=3).

III.2.5 Application to screening, identification and characterization of AC inhibitors

Specific inhibition of AC leads to enhanced pro-apoptotic signaling through ceramide accumulation, and prevents conversion of ceramide to sphingosine, with a subsequent decrease of S1P. Therefore, AC has emerged as a therapeutic target for synergistic treatment of cancer with chemotherapeutics, particularly in those cases of drug resistance¹⁰¹.

In this context, the search for potent and specific AC inhibitors is of importance. The fluorogenic AC activity assay has allowed us to screen large series of compounds for their effect as AC inhibitors. The studies carried out with some of the most active inhibitors are described in the following sections. As detailed below, one family of compounds (RBM2-1) was used in a preliminary study conducted in the HCT116-40 16 cell line (Section III.2.5.1). This study, which is still ongoing, will be continued with the HCT116 p53 (-/-) mutant with the aim of exploring the possible relationships between AC, p53 and autophagy. Another family (RBM1) was used in a model of prostate cancer (Section III.2.5.2)

III.2.5.1 Compounds RBM2-1

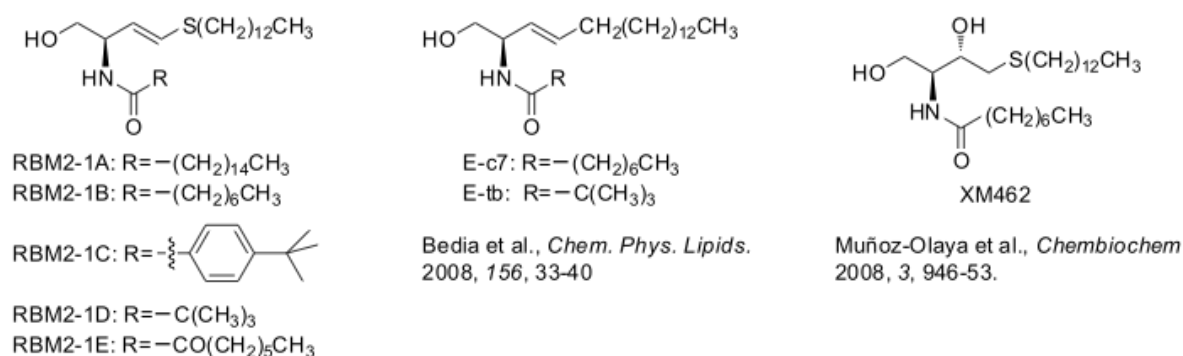


Figure 35. Chemical structures of compounds RBM2-1 and other previously published inhibitors of AC (E-c7 and E-tb) and DHCD (XM462).

Compounds RBM2-1 were unexpectedly obtained by María Garrido while attempting to synthesize XM462 analogues as part of her Ph. D. thesis²⁰⁰. As shown in Figure 35, these are reminiscent of the previously reported AC inhibitors E-c7 and E-tb¹¹⁸. Therefore, RBM2-1 compounds were first tested as AC inhibitors both *in vitro* and in intact cells, using the Moh pAS 10X cell line.

The most active AC inhibitors were RBM2-1B, RBM2-1C and RBM2-1D, the activity of which was higher in intact cells than in cell lysates (Figure 36 A). Dose-response curves afforded *in vitro* IC₅₀ values of 77, 315, and 51 μM for compounds RBM2-1B, RBM2-1C and RBM2-1D, respectively. The effect of compounds on NC was also determined in both intact and lysed Moh pAS cells transfected to overexpress NC (CerC12NBD was used as substrate). As previously found with structurally similar compounds E-c7 and E-tb¹¹⁸, none of the compounds RBM2-1 modified NC activity as compared to controls (Figure 36 B) either *in vitro* or in intact cells. In light of these results, further studies are ongoing with the most potent inhibitors, RBM2-1B and RBM2-1D using the HCT116 40 16 colon carcinoma cell line.

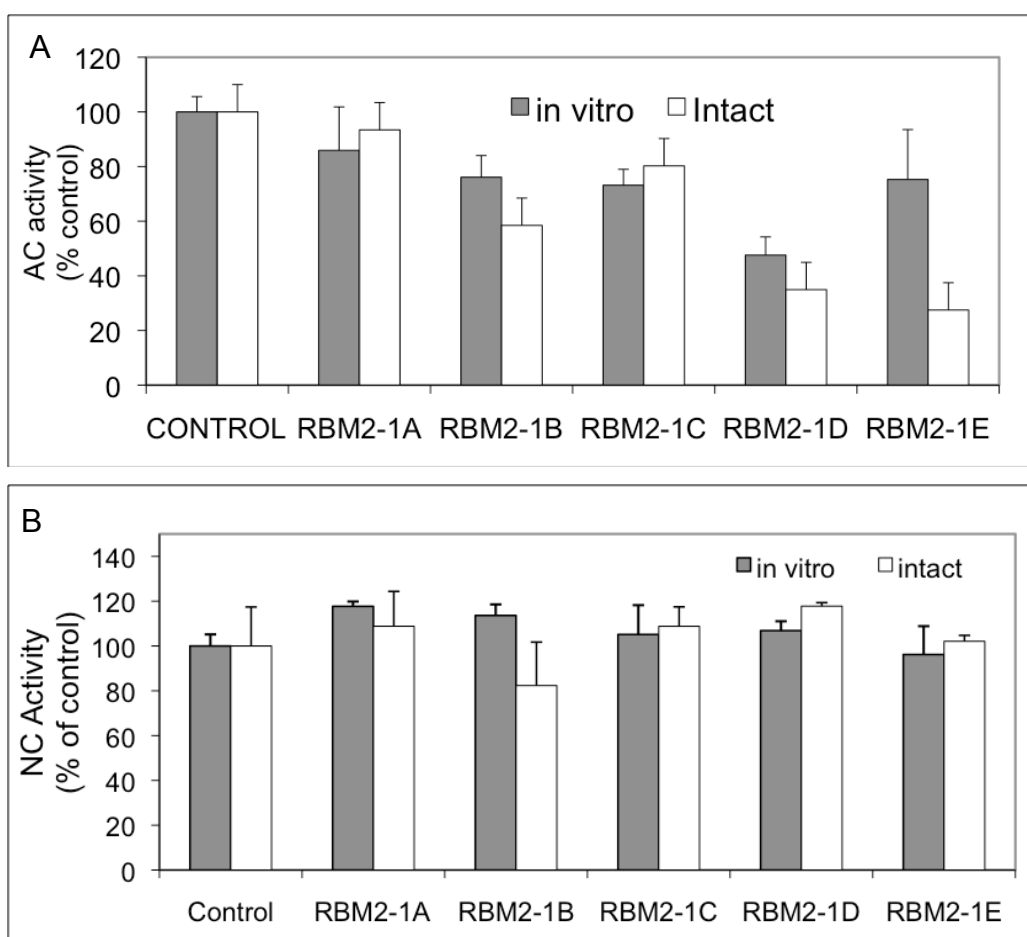


Figure 36. Activity of compounds as AC (A) and NC (B) inhibitors. AC activities were determined with a fluorogenic substrate (16 μM) and NC was measured using CerC12NBD as substrate (5 μM). Compounds were tested at 16 μM (AC; S/I = 1) or 50 μM (NC; S/I = 0.1) and the experiments were performed as detailed in the experimental section. In all panels, data correspond to the mean % of control (±S.D). Results are normalized to amount of protein (*in vitro*) or number of cells (intact), which was similar in all cases. Control corresponds to Moh cells (A) or Moh transfected with the empty vector

III.2.5.1.1 Effect of RBM2-1B and RBM2-1D on the sphingolipidome

The effect of RBM2-1B and RBM2-1D on the sphingolipidome of HCT116 40 16 colon carcinoma cells was investigated. Since both compounds inhibited AC, whose activity was found to be high in this cell line (see sections III.2.4.1 and III.2.4.2), increased levels of ceramides were expected in cells after treatments. However, as shown in Figure 37, this was not the case. Unexpectedly, RBM2-1B and RBM2-1D produced increases in dihydroceramides, which were statistically significant in all the several *N*-acyl species (Figure 37). These increases were accompanied with significant increases in both DHSM's and GlcDHCer's (Figure 37B), and a significant reduction in the most abundant C16 and C24-GlcCer's, C24-Cer and C16-SM (Figure 37). These results strongly suggested that besides inhibiting AC, both RBM2-1B and RBM2-1D were also DHCD inhibitors. This assumption was confirmed in activity measurements in the presence and absence of each compound, RBM2-1B and RBM2-1D, which inhibited DHCD with IC₅₀ values of 18 μM and 100 μM, respectively (Fabio Simbari, Ph. D. Thesis).

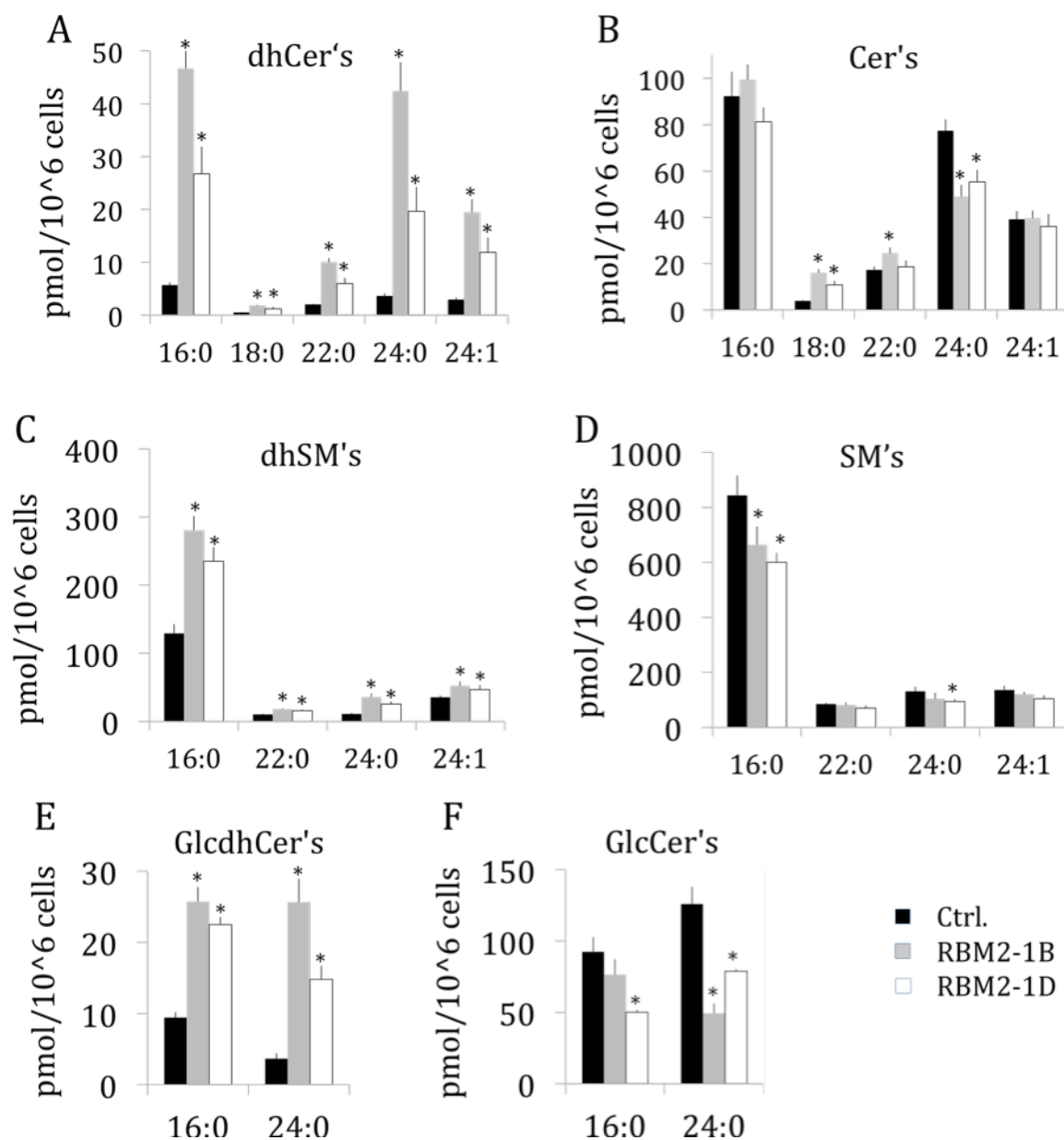


Figure 37. Effect of compounds RBM2-1B and RBM2-1D on the sphingolipidome. HCT116 40 16 cells were incubated with the compounds (20 μ M) for 14 h and then lipids were extracted and analyzed as detailed in the experimental section. Data correspond to the mean \pm S.D of one representative experiment with triplicates. Asterisk indicates statistically significant difference from the control mean ($p \leq 0.05$; unpaired two-tail t -test).

Despite that no ceramide increased upon treatments with either RBM2-1B or RBM2-1D, both compounds were cytotoxic to HCT116 40 16 cells (Table 4). Their LD₅₀ values were about 3 times lower than that of the weaker AC inhibitor RBM2-1C. Further experiments are ongoing to decipher the type of cell death and the mechanisms involved.

Table 4. Cytotoxicity of compounds.^a

Compound	HCT116
RBM2-1B	28
RBM2-1C	81
RBM2-1D	30

^aCells were seeded at a density of 10⁵ cell/mL in 96-well plates (100 µL/well). Fresh media and compounds were added after 24 h and the number of viable cells was determined with the MTT test 24 h after treatments. Data correspond to the CC₅₀ values (µM) obtained by regression analysis of the dose-response curves constructed with data from two experiments with triplicates.

As mentioned before, a number of AC inhibitors are currently known, including several C2-substituted aminoethanol amides reported by our group¹¹⁸ (Figure 35). In contrast, only a few DHCD inhibitors have been published, which include fenretinide²⁰¹, celecoxib²⁰², resveratrol²⁰³, and the dihydroceramide analogs GT11^{204,205} and XM462²⁰⁶ (Figure 35). The latter is a dihydroceramide analog with a sulfur atom replacing the natural C5 methylene unit. Compounds RBM2-1 can thus be regarded as hybrid structures containing the most relevant structural features of the above AC and DHCD inhibitors. Biological studies have shown that the three compounds inhibit both enzymes, AC and DHCD, although their selectivity is modulated by the *N*-acyl substituent. Thus, while the *p*-*tert*-butylphenylamide is a very poor inhibitor of both AC and DHCD, the pivaloylamide is a better inhibitor of AC and the linear octanoyl group confers preferential activity over DHCD.

Compound RBM2-1D was the most potent AC inhibitor of the three analogs. The activity of RBM2-1D on AC is similar *in vitro*, but lower in intact cells, than that of E-tb¹¹⁸. The higher metabolization of RBM2-1D (34% conversion into the C1-O-phosphocholine metabolite as compared to E-tb (16% conversion into the C1-O-phosphocholine metabolite)¹¹⁸ may account in part for this difference.

Antoon et al.²⁰⁷ reported that *N*-pivaloylsphingosine inhibits the viability and clonogenic survival in several breast cancer cell lines. Similar activities were reported by the same authors for a ceramide analog with the pivaloylamide unit²⁰⁸. Although the effect of these compounds on AC activity was not determined, we found that both *N*-pivaloylsphingosine and *N*-pivaloylsphinganine produce a 50% and 40% inhibition of AC activity, respectively, as measured in intact MOH pAS 10X cells with the fluorogenic substrate in the usual conditions followed in our laboratories (Carmen Bedia, unpublished). Therefore, it is possible that inhibition of this enzyme and the subsequent increase in ceramides is responsible for the effects observed by Antoon et al.²⁰⁷. These overall results reinforce the importance of the *tert*-butyl group for AC inhibition.

Compound RBM21B was the most active DHCD inhibitor, although its activity is lower than that of XM462. This difference can be explained assuming a higher affinity of the latter for the enzyme by virtue of its C4-OH group, which is not present in RBM2-1B. On the other hand, since XM462 could arise in cells from metabolic hydration of RBM2-1B, this possibility was investigated and ruled out in the sphingolipidome analyses, as no traces of XM462 or its metabolites were detected in extracts from cells treated with RBM2-1B (data not shown). Likewise, no evidence of dehydration of XM462 to RBM2-1B was obtained in the LC-MS analyses of lipids extracted from cells incubated with XM462 (data not shown). It is worth noting that compound E-c7 induced an accumulation of ceramides, but not dihydroceramides, in A549 cells treated with the compound for 24 h¹¹⁸. This effect indicates that, unlike RBM2-1B, compound E-c7 does not inhibit *Des1* in a similar concentration range, reinforcing the importance of the sulfur atom at C5 for *Des1* inhibition.

The observed effect of the compounds on the sphingolipidome was in agreement with the overall data. Thus both RBM2-1B and RBM2-1D increased dihydroceramide levels, although RBM2-1B produced a significantly higher increase than RBM2-1D ($p \leq 0.017$ see Figure 37B), accordingly with its higher potency as DHCD inhibitor. This result is in contrast with the previously reported effect of E-tb¹¹⁸, which increased ceramides but not dihydroceramides in treated A549 cells.

Analysis of long chain bases by UPLC/TOF gave inconsistent results derived from the low sensitivity of this technique for these compounds, which are only detected when present at high levels. A more sensitive procedure to measure both long chain bases (sphingosine and sphinganine) and their phosphates (sphingosine-1-phosphate and sphinganine-1-phosphate) is currently available in our laboratories and it should allow us to clarify the effect of RBM2-1B and D on the production of these lysosphingolipids. In this context, sphinganine has been reported to increase and kill cancer cells in fenretinide treatments. This increase results from concomitant inhibition of DHCD and induction of dihydroceramidase *ASAH3L* by the drug. Similarly, the cytotoxic activity of RBM2-1B and RBM2-1C may be due to increases in sphinganine levels. This base would arise from *ASAH3L*-catalyzed hydrolysis of DHCer's, which increases in cells upon treatment with either compound. Confirmation of this hypothesis awaits reliable measurements of long chain bases and their phosphates, as well as the determination of *ASAH3L* expression and activity after treatment with RBM2-1B and RBM2-1D.

The three compounds, RBM2-1B, RBM2-1C and RBM2-1D, were toxic to the HCT116 40 16 cell line, and RBM2-1C, which exhibited the poorest activity on sphingolipid metabolism, was also the least toxic compound. This supports that cell death induced by these molecules is mediated, at least in part, by altered sphingolipid metabolism. The role of ceramides as sphingolipid mediators of apoptotic cell death has been extensively documented. Whether apoptosis is involved in cell death produced by RBM2-1B and RBM2-1D is still unknown and will be investigated. Since it has been reported that dihydroceramide accumulation induces autophagy in a number of cell lines^{201,203,206}, the effect of RBM2-1B and RBM2-1D on autophagy in HCT116 cells will also be examined using XM462 and starvation as positive controls.

In the context of autophagy, it should be taken into account that Merrill and co-workers²⁰⁹ showed that silencing the *ASAH1* gene in breast cancer MCF7 cells reduced the autophagy induced by fenretinide treatment. In agreement, Turner et al²¹⁰, have recently shown that DU145 and PPC1 prostate cancer cell lines overexpressing AC have increased levels of autophagy.

Therefore, although the experimental evidence are still scarce, DHCD and AC seem to play opposite roles on autophagy. As a consequence, the dual activity of RBM2-1B and RBM2-1D as AC and DHCD inhibitors may render cells unable to undergo autophagy leading them to apoptotic or necrotic cell death. Additional experiments will be conducted to clarify these points.

III.2.5.2 Compounds RBM1

Compounds RBM1 were synthesized by Dr. José Luis Abad. Their structures are not shown due to intellectual property protection reasons. All compounds were tested in intact Moh pAS 10X cells as well as in cell lysates at pH 4.5. The assays were carried out under the standard assay conditions using RBM14C12 as substrate (40 μ M) and 40 μ M of inhibitors. As shown in Figure 36, the best inhibitors in intact cells were compounds RBM1-12, 13, 18 and SABRAC, with a percentage of inhibition ranging from 40 to 70 %. While RBM1-12, 13, and SABRAC maintained the inhibitory activity in the *in vitro* assay, RBM1-18 had no inhibitory activity in cell lysates (Figure 38).

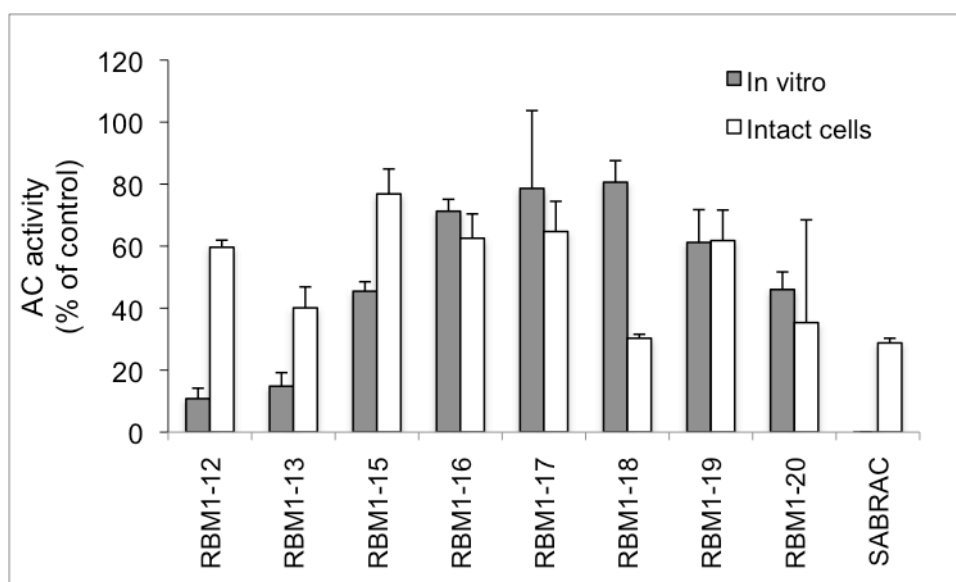


Figure 38. Activity of compounds RBM1 as AC inhibitors. AC activities were determined with the fluorogenic substrate RBM14C12 (40 μ M). Compounds were tested at 40 μ M and the experiments were performed as detailed in the experimental section. Data correspond to the mean % of control (\pm S.D) of three replicates. Results are normalized to the amount of protein (*in vitro*) or number of cells (intact), which was similar in all cases.

III.2.5.1.1 RBM1 compounds over NC activity *in vitro*

Compounds RBM1-12, 13 and SABRAC were tested as NC inhibitors. In these experiments, the fluorogenic RBM14 compounds were not available and the standard CerC12NBD was used as substrate. As shown in Figure 39, none of the compounds inhibited NC.

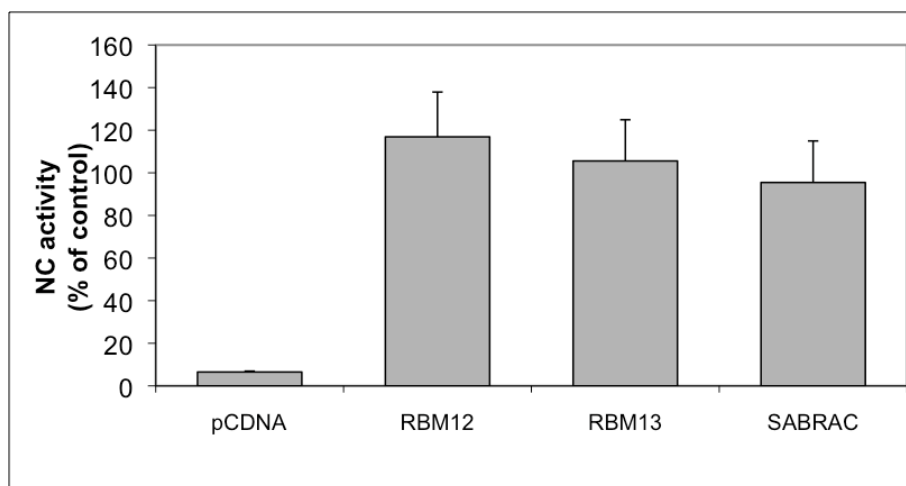


Figure 39. Activity of compounds RBM1-12, RBM1-13 and SABRAC as NC inhibitors. Activities were determined with lysates from Moh cells transfected with pcDNA5/TO-NC and using CerC12NBD as substrate (5 μ M). Compounds were tested at 40 μ M and the experiments were performed as detailed in the experimental section. Data correspond to the mean % of control (\pm S.D) three replicates. Results are normalized to amount of protein, which was similar in all cases. pCDNA corresponds to Moh cells transfected with the empty vector.

III.2.5.1.2 Dose response of RBM1 compounds over AC activity

The best RBM1 inhibitors both *in vitro* and in intact cells were selected to determine the IC₅₀. As shown in Table 5, SABRAC was the best inhibitor, with an IC₅₀ value in the low nM range, followed by RBM1-12 (IC₅₀ < 1 μM). Compound RBM1-13 was the weaker inhibitor.

Table 5. Potency of compounds as AC inhibitors^a

Compound	IC ₅₀
RBM1-12	0.3 μM
RBM1-13	60 μM
SABRAC	0.05 μM

^aIC₅₀ values were determined by analysis of the dose-response curves obtained in Moh pAS 10X cell lysates. The experiments were conducted as detailed in the experimental section in triplicate. RBM14C12 was used as substrate at 40 μM

The use of these three compounds in a model of prostate cancer is presented in the following Section (III.3)

III.3 Study of the contribution of the acid ceramidase to the invasiveness of prostate cancer cells

Thomson and co-workers generated two distinct clonal populations from the PC-3 prostate cancer cell line. PC-3/S cells were isolated *in vitro* by single-cell colony isolation from luciferase-expressing PC-3 cells²¹¹. A second single cell progeny, hereafter designated PC-3/Mc, was isolated from luciferase expressing PC-3/M cells, a PC-3 subline that had been selected *in vivo* for its high metastatic potential²¹². The two clonal populations display very different phenotypes and metastatic potentials (Celià-Terrasa et al. submitted). Briefly, PC-3/Mc cells grow rapidly, are barely invasive and highly clonogenic *in vitro*. Moreover, they form large tumors by intramuscular grafting and are very metastatic after intravenous injection in NOD-SCID mice. In contrast, PC-3/S cells grow slowly, are highly invasive and show limited clonogenicity; they do not produce tumors readily after intramuscular grafting and do not metastase after intravenous injection in NOD-SCID mice. Thus, the *in vitro* invasive capabilities of PC-3/Mc and PC-3/S cells are inversely correlated with their clonogenic and proliferative potentials.

This suggests a dichotomy in these cells between two fundamental processes that determine the capacity of tumor cells to metastasize, selfrenewal potential and invasive capacity.

Since the overexpression of AC in diverse cancer tissues, including three human PC cell lines (DU145, LNCaP and PC-3), has been reported¹⁰⁰, we decided to investigate whether AC plays a role in the phenotypic differences exhibited by the PC-3/S and PC-3/Mc cell lines.

As mentioned in section III.2.4, PC-3/Mc cells exhibited a significantly higher AC activity than PC-3/S cells. Elevated AC enzymatic activity significantly decreases cellular ceramide levels and increases proliferation under nutrient-depleted conditions in cell culture, augments tumorigenicity *in vivo*, and enhances migration rates through collagen-coated Boyden chambers¹⁸⁷. Diverse studies using B13 and other ceramide analogues revealed that administration of AC inhibitors or siRNA reverses the aggressive behavior¹⁰³. Furthermore, AC inhibition also sensitizes cancer cells to radio and chemotherapy¹⁹⁰.

From this prior information, we aimed at investigating whether blocking AC in the PC-3/Mc clone modified its phenotype to make it more similar to that of the PC-3/S clone in terms of invasiveness, clonogenicity and metastatic potential. AC activity blockade was accomplished by both RNA interference (RNAi) and chemical means, using the AC inhibitors RBM1-12, RBM-13 and SABRAC (see section III.3.2).

III.3.1 Genetic inhibition of the *ASAH1* gene

Following the detailed methodology described in experimental methods, a stable *ASAH1* knockdown PC3/Mc cell line was generated. Briefly, PC3/Mc cells were transduced with 5 different viral constructions encoding for 5 different shRNAs. Figure 40 A shows the *ASAH1* mRNA expression levels obtained for each shRNA expressing PC3/Mc cell line. Sequences 399, 400 and 402 were effective at decreasing *ASAH1* mRNA expression with variable efficiency, from 90 to 60 %. shRNAs 399 and 402 produced the best inhibition levels. Additionally, evaluation of AC activity (Figure 40 B) confirmed that in cells bearing plasmids 399 and 402 *ASAH1* expression was properly inhibited. This finding was finally confirmed by Western blotting. As shown in Figure 40 C, AC was almost undetectable in 399 and 402 *ASAH1* knockdown cells.

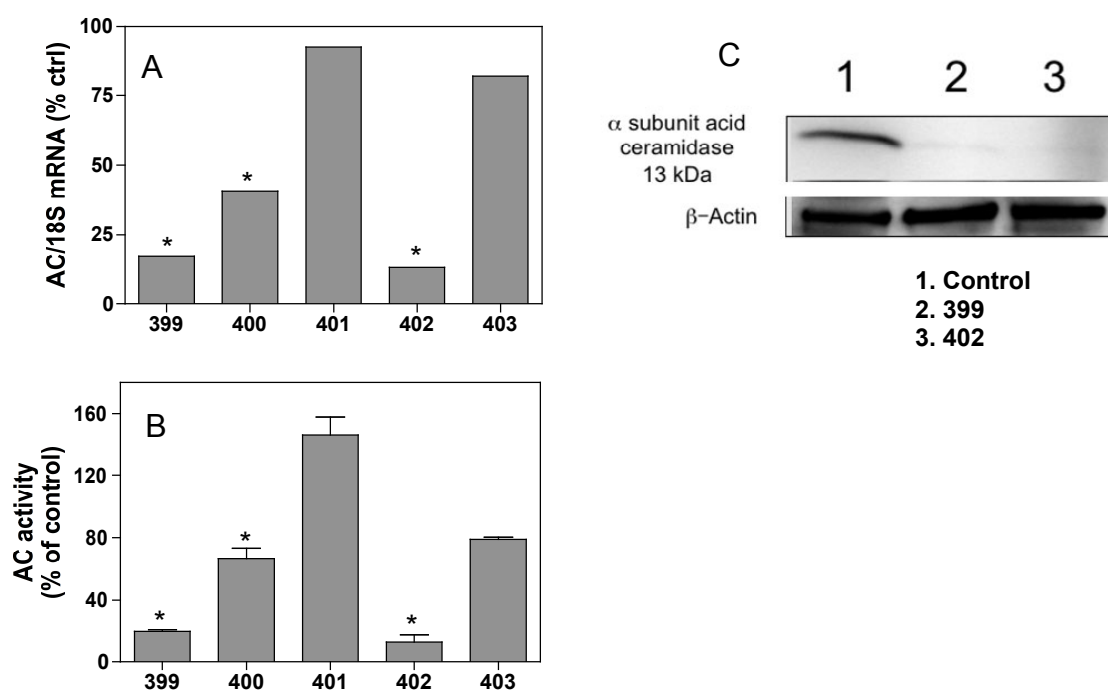


Figure 40. *ASAH1* knockdown analysis. A) *ASAH1* mRNA expression levels evaluated by qPCR. Data are represented as the mean % of control of three replicates \pm S.D. Results were normalized to 18S mRNA. B) AC activity determined by the fluorogenic assay with cell lysates under standard AC conditions. Data correspond to the mean % of control (\pm S.D) of three replicates. C) Western blotting for AC. 20 μ g of protein were loaded for each sample. Means are significantly different from controls at: *, $p \leq 0.05$; (unpaired two-tail *t*-test). Acting signal was used as a reference for protein loading.

III.3.1.1 Sphingolipid profile of PC3/Mc_ASAH1 knockdown cells

The sphingolipid content of *ASAH1* knockdown cells (clones 399 and 402) was analyzed by UPLC-TOF. As shown in Figure 41, both *ASAH1* knockdown clones accumulated Cers, DHCers, SMs, DHSMs and GlcCers as a result of the impairment in Cer metabolism. Unexpectedly, sphingosine was increased in both knockdown clones, suggesting the upregulation of other CDases upon AC blockade.

The contribution of these data to cell behavior will be discussed in the following sections.

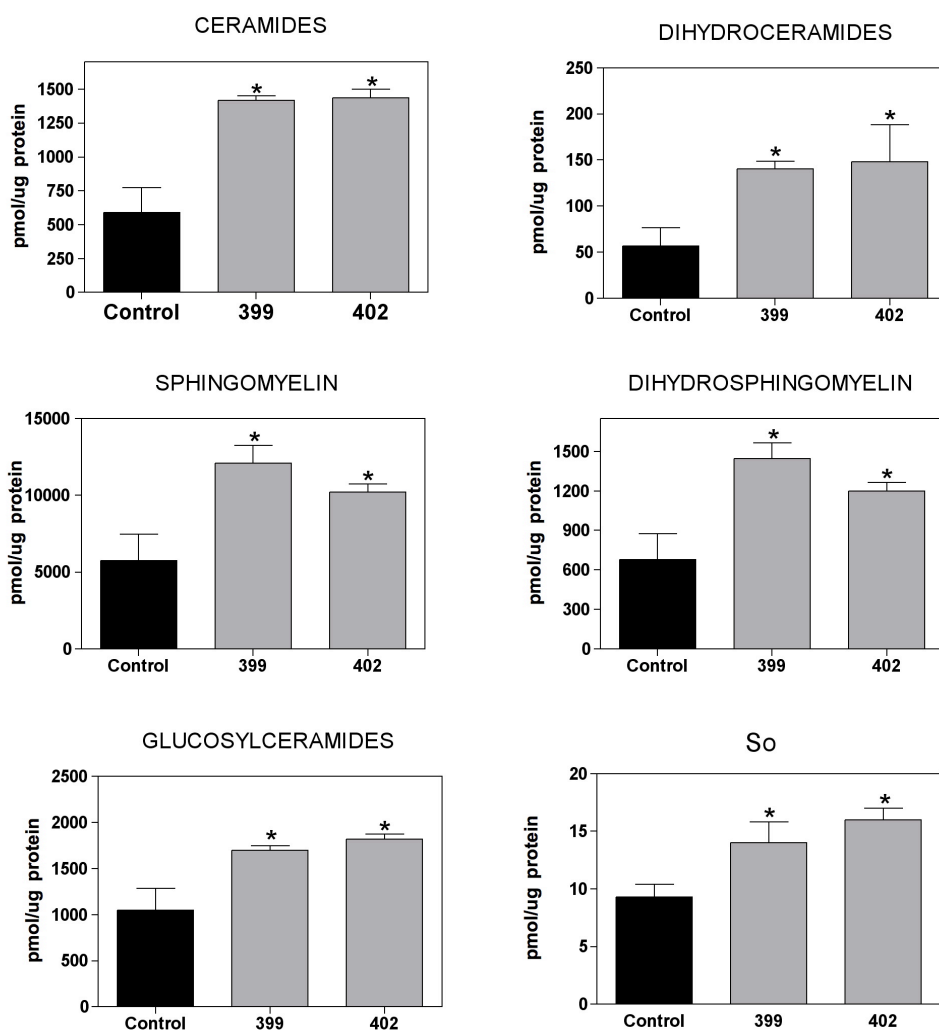


Figure 41. Sphingolipid content of PC3/Mc_ASAH1 knockdown cells. Determinations were done by UPLC/TOF. Results were standardized by protein quantity and are shown as the mean of three values \pm SD. * $p \leq 0.05$.

III.3.1.2 Effects of *ASAH1* silencing on cell growth

The growth of normal cells is arrested when they come in contact with each other, a process known as contact inhibition. Contact inhibition is lost during tumorigenesis, resulting in uncontrolled cell growth²¹³. In order to investigate if *ASAH1* knockdown allowed cells to regain this capacity, the growth rate at two different FBS concentrations was determined.

As is shown in Figure 42, when cells were cultured with 10% FBS there was no difference in growth rates between *ASAH1* knockdown cells (399 and 402) and control cells when initial cell number was higher than 1000 per well. Conversely, when cells were seeded at an initial concentration of 500 cells per well, there was a significant decrease in growth. Furthermore, under low growth factors conditions (0.5% FBS) the rate of growth was clearly decreased in knockdown cells as compared with normal cells (Figure 42).

The decrease was more drastic when 1000 or 500 initial cells were plated. These findings agree with reported data showing that the elevation of ceramide, which occurs in silenced *ASAH1* cells, interrupts normal cell growth, leading to antiproliferative outcomes, such as terminal differentiation, cell cycle arrest, and apoptosis²¹⁴.

The fact that *ASAH1* knockdown arrest at densities significantly lower than control cells also suggests that AC may be involved in contact inhibition. Finally, that the critical densities for growth arrest are more clearly attained by *ASAH1* knockdown cells when they are starved of growth factors (0.5% FBS) also suggests that AC is required for proper response to extrinsic growth factors.

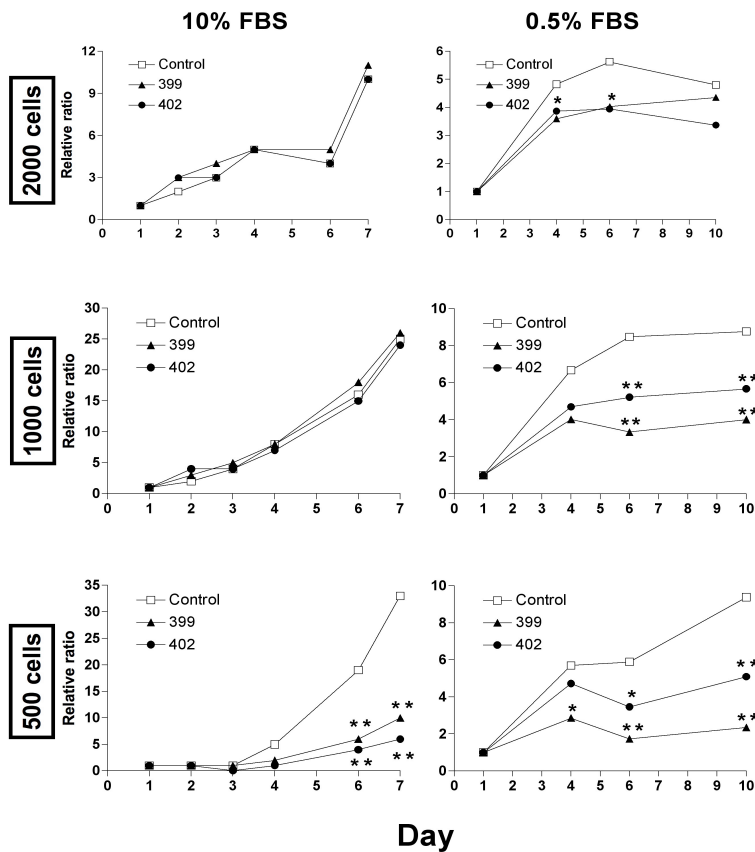


Figure 42. Growth rate was determined by MTT assay. Left, *ASAH1* knockdown cells cultured in 10% FBS; Right, *ASAH1* knockdown cells cultured in 0.5% FBS. Results are represented as mean ± SD (n=3). * p ≤ 0.05, ** p ≤ 0.001.

III.3.1.3 Effects of *ASAH1* silencing on the cell cycle

After observing that silencing of the *ASAH1* gene increases the dependence of cells on growth factors, the effect on cell cycle was determined and compared to control cells. As shown in Figure 43, flow cytometry analyses evidenced that both control and *ASAH1* knockdown clones had similar cell populations at each phase of the cell cycle. Therefore, genetic blockade of *ASAH1* expression does not seem to affect the cell cycle, at least under the conditions of nutrient and growth factors of the assay (0.5% FBS, incubation 48h).

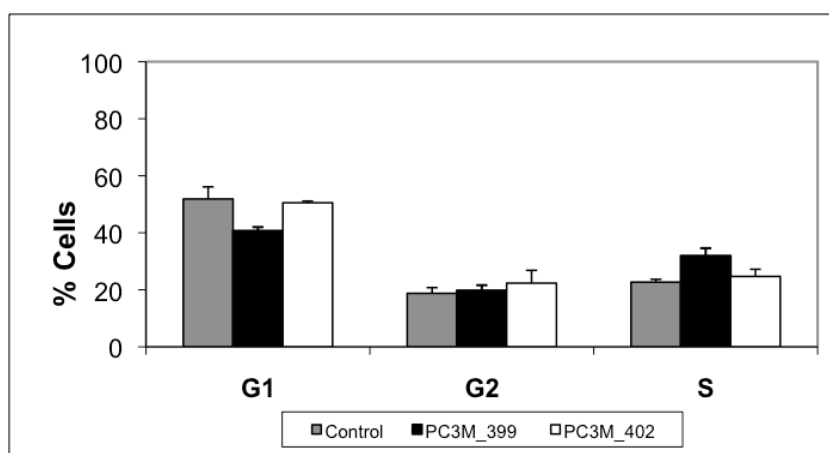


Figure 43. Cell cycle analysis of control and *ASAH1* knockdown cells (402 and 399). Results are represented as the mean of three values \pm SD.

III.3.1.4 Effects of *ASAH1* silencing on invasiveness

In order to invade tissues and form distant metastases, tumor cells formed in tissues contained by a basement membrane must cross that barrier before penetrating the underlying stroma. Cells do this by producing proteases that degrade the extracellular matrix. To assess the *in vitro* invasiveness of PC3/Mc_ *ASAH1* knockdown cells, a matrigel-based invasion assay was used. As shown in Figure 44, the capacity of knockdown cells to invade appeared to be increased when compared with controls. These results disagree with a report according to which prostate cancer cells overexpressing AC exhibited increased invasiveness¹⁰³. The reasons for this discrepancy are thus far unknown, although it may be due to the different cell lines used in both studies (PC3-derived in this thesis and DU145 and PCC1 in the reported article¹⁰³).

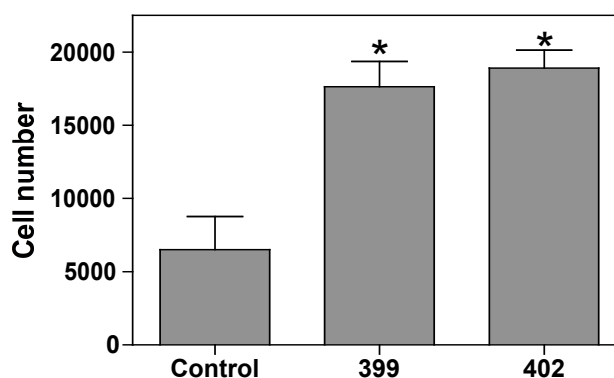


Figure 44. *In vitro* invasiveness of PC3/Mc_ *ASAH1* knockdown cells compared with control PC3/Mc cells. Data are represented as the mean of three replicates \pm SD. * $p \leq 0.05$

III.3.1.5 Effects of *ASAH1* silencing on 3D growth and tumor formation

The ability of tumor cells to form colonies in soft agar is closely related to their capacity to produce metastases. PC3/Mc cells gave rise to numerous colonies while *ASAH1* knockdown cells showed a dramatically diminished capacity of colony formation (Figure 45 A). These results are in accordance with a previous report by Mahdy *et al.*¹⁹⁰ in which the authors described that AC silencing by siRNA in combination with ionizing radiation significantly reduced clonogenicity compared to unspecific siRNA-treated PPC-1 cells. Here we demonstrate that *ASAH1* silencing is enough to diminish clonogenicity independently of radiation in PC3/Mc cells.

In agreement with the results of the growth rate experiments (see section III.3.1.2), *ASAH1* knockdown cells injected in NOD-SCID male mice produced significantly smaller tumors when compared with PC3/Mc control cells independently of the initial cell numbers injected (Figure 45 B). These results are in agreement with data showing that cells expressing higher AC levels displayed augmented tumorigenicity *in vivo*.^{103,190} and underscore the significance of AC as a target for prostate cancer therapy.

The exact mechanism of decreased tumorigenicity induced by *ASAH1* knockdown in this work has not been investigated, but apoptosis induced by increased levels of ceramide and So does probably play a role. The apoptogenic activity of ceramide has been extensively addressed in the introduction to this thesis. Regarding So, it has been reported that So induces apoptosis in hippocampal neurons and astrocytes²¹⁵ and may mediate apoptosis induced by phorbol myristate acetate in human promyelocytic leukemia HL-60 cells²¹⁶ by down-regulation of Bcl-2²¹⁷. Moreover, treatment of human prostatic carcinoma DU-145 cells with So, but not ceramide, induced apoptosis by suppression of Bcl-X(L)²¹⁷.

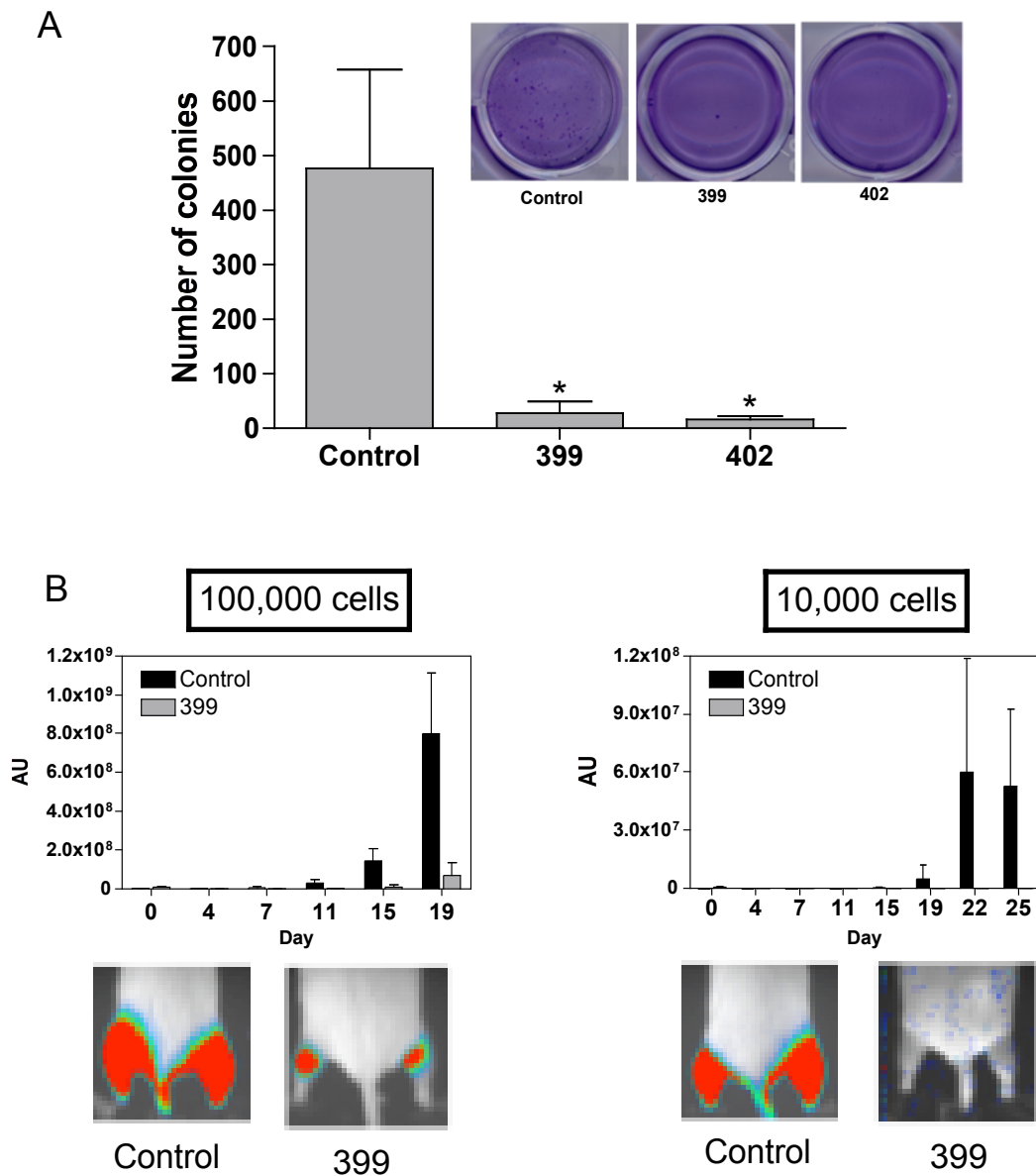


Figure 45. A) Control and PC3/Mc_ASAH1 knockdown cells (399 and 402) were cultured on soft agar and colonies were stained with crystal violet after incubation for 3 weeks. Data are represented as the mean of three replicates \pm SD. B) PC3/Mc control and PC3/Mc_ASAH1 knockdown cells were injected intramuscularly into each limb of NOD-SCID mice (6 per group) and tumor growth was monitored by luminiscence release 5 minutes after intraperitoneal injection of luciferine. Data are represented as the mean of twelve replicates (one tumor for each limb) \pm SD. * $p \leq 0.05$

III.3.1.6 Effects of *ASAH1* silencing on lung colonization

In order to know if the capacity to form tumors in lungs was affected in PC3/Mc_*ASAH1* knockdown cells, NOD-SCID mice were injected through the dorsal caudal vein with 5×10^5 PC3/Mc_ or PC3/Mc_*ASAH1* knockdown cells (clone 399). As shown in the Kaplan-Maier plot of Figure 46 (the number of mice that remain free of lung colonization at each time point) there is a delay in lung tumor development in mice bearing *ASAH1* knockdown cells as compared to control PC3/Mc cells.

These results are of great relevance, since the delayed colonization of distant organs decreases the probability of metastatic progression of cancer. It should be mentioned that these *ASAH1* knockdown cells exhibited both an increased invasive capability and a decreased clonogenicity *in vitro*. However, they produced less lung metastases than controls when injected in animals.

These results are in agreement with the characteristic features found for these cells (Celià-Terrassa et al., submitted), which support the reported inverse correlation between local invasiveness and the ability of cells to colonize distant organs found in some other models of neoplasia²¹⁸. Such inverse correlation suggests that in some types of cancer, these two critical features of the metastatic process are dissociated and possibly expressed by separate tumor cell subpopulations²¹⁹.

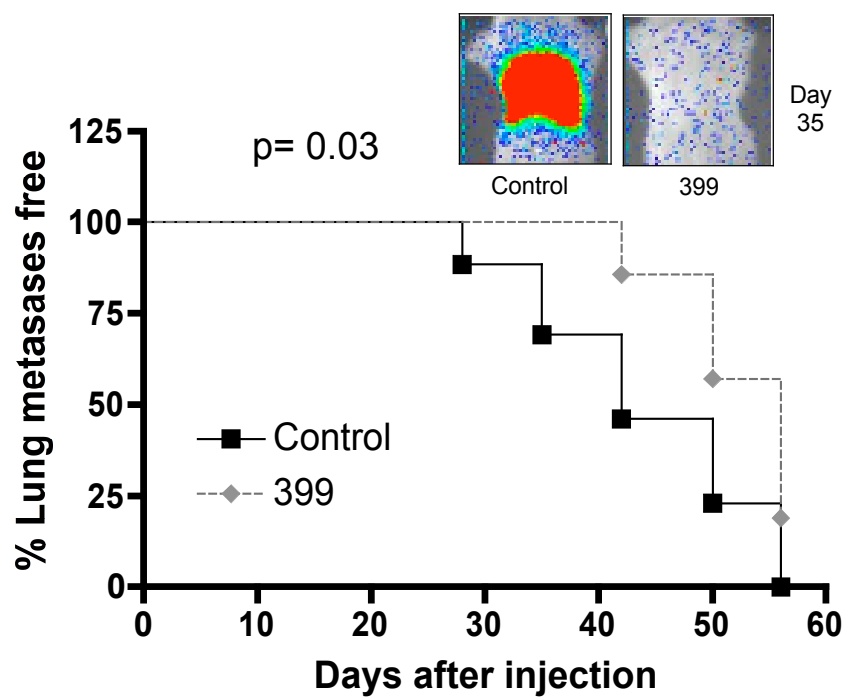


Figure 46. Kaplan-Meier representation of lung colonization in NOD-SCID mice injected i.v. with 5×10^5 PC3/Mc cells or PC3/Mc_ASAH1 knockdown (clone 399). Data are represented as the percentage of mice without tumors ($n = 6$ for each group). p value was determined with Prism GraphPad Software.

III. 3.2 Chemical inhibition of AC in PC3/Mc cells

After studying the effect of blocking AC activity by genetic methods, the effect of chemical inhibition was determined. This study was carried out with compounds RBM1-12, RBM1-13 and SABRAC, described in section III.2.5.2. PC3/Mc cells were incubated with increasing doses of inhibitors for 48 hours, then cells were lysed and AC activity was measured as described using RBM14C12 as substrate. As shown in Figure 47, inhibition of AC by RBM1-12 and SABRAC was dose-dependent (RBM1-12: $1 \mu\text{M} < \text{IC}_{50} < 5 \mu\text{M}$; SABRAC: $\text{IC}_{50} < 1 \mu\text{M}$). Intriguingly, RBM1-13, which had shown to be a good AC inhibitor in Moh pAS 10X intact cells and cell lysates (see Figure 38), did not have any inhibitory effect in PC3/Mc cells. In fact, RBM1-13 apparently augmented somehow AC activity. The reason for this difference between cell lines is still unknown, although differential metabolization of the compounds in both cell lines may contribute to the discrepancy.

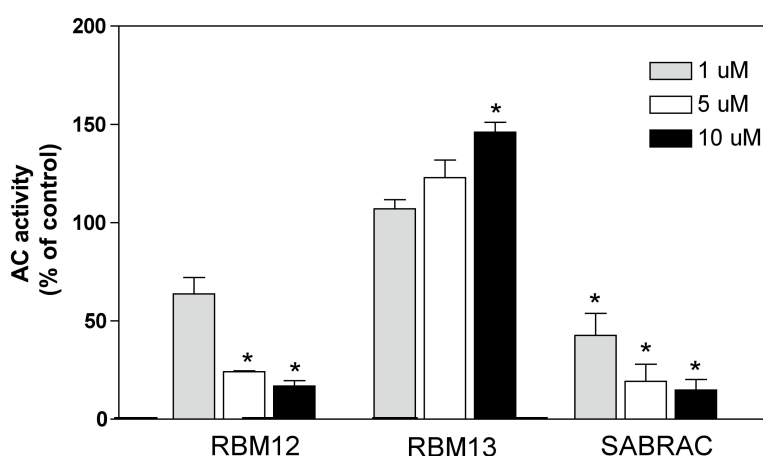


Figure 47. Dose-dependent inhibition of AC in PC3/Mc cells treated with RBM1-12, 13 and SABRAC. Results were normalized by protein quantity. Results are shown as the mean of three values \pm SD. * $p \leq 0.05$.

The cytotoxicity of these compounds was evaluated by the MTT cell viability assay after incubating cells with inhibitors for 72 h. The most toxic compound was RBM1-12 (CC_{50} $13.7 \mu\text{M}$), followed by RBM1-13 (CC_{50} $37 \mu\text{M}$) and SABRAC ($\text{CC}_{50} > 100 \mu\text{M}$).

III.3.2.1 Sphingolipid profiles of PC3/Mc cells treated with AC inhibitors

Sphingolipid profiles of PC3/Mc cells were evaluated after 48 h of incubation with RBM1-12, RBM1-13 or SABRAC at two different concentrations, 1 and 5 μM . As shown in Figure 48, both SABRAC and RBM1-12 induced an increase of Cer's and DHCer's (marginal DHCer's increase with 1 μM RBM1-12). In contrast, amounts of both Cer's and DHCer's found in cells treated with RBM1-13 were similar to those of controls. These results are in accordance with those found on AC activity, which was inhibited by RBM1-12 and SABRAC, but not by RBM1-13. Complex sphingolipids such as SM, dhSM or GlcCer were not modified by any compound (Figure 48). This is in contrast with the results found in *ASAH1* knockdown cells, (Figure 41), which showed accumulated GlcCer, SM or DHSM. This discrepancy can be explained considering that *ASAH1* knockdown cells are constitutively deficient in AC and the accumulated Cers have been directed to metabolic pathways leading to complex sphingolipids. However, the increase in Cer's occurring during only 48 h of treatment with inhibitors may not be high or prolonged enough to produce an increment in complex downstream metabolites. Finally, in agreement with their activity as AC inhibitors, both RBM1-12 and SABRAC produce a decrease in the amounts of sphingosine. In contrast, an unexpected raise in sphingosine levels was observed in *ASAH1* knockdown cells (see Figure 41). As discussed in section III.3.1.1, it is reasonable to propose that constitutive AC blockade brings about the upregulation of other ceramidases in order to eliminate the deleterious ceramide excess. Under the experimental conditions followed, chemical inhibition may be too transient, or may not be as drastic as, to promote changes in the transcription or expression of other ceramidases.

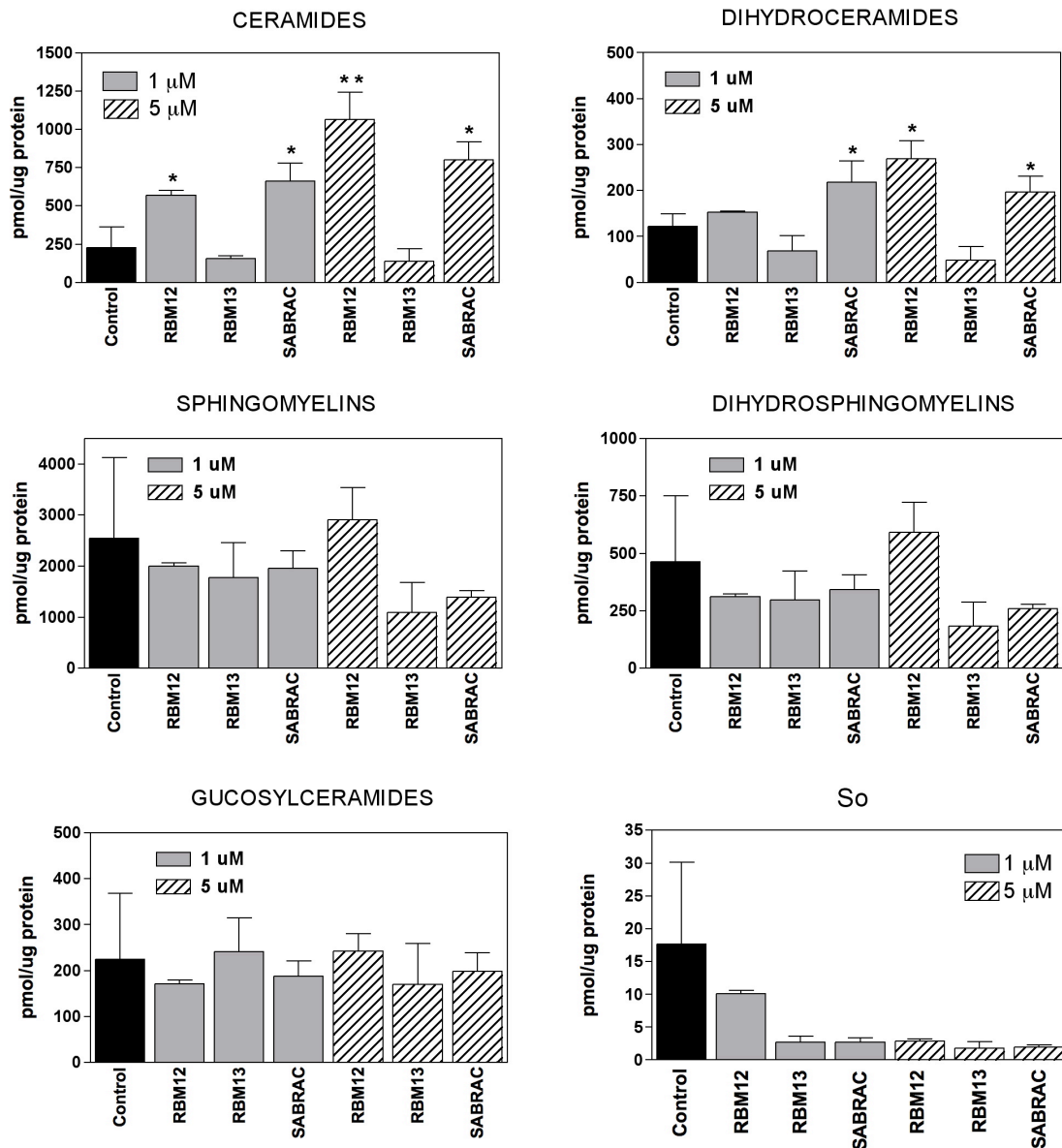


Figure 48 Sphingolipid content of PC3/Mc cells treated with 1 or 5 μM of RBM1-12, RBM1-13 or SABRAC during 48 h. Results were standardized by protein quantity and are shown as mean ± SD of triplicates. *p ≤ 0.05.

III.3.2.2 Effects of AC inhibitors on cell growth

In these experiments, PC3/Mc cells were cultured with 10% FBS in the presence of 5 μ M of RBM1-12, RBM1-13 or SABRAC. Despite the lack of inhibitory activity of RBM1-13 on AC, this compound was included in further experiments in order to correlate the observed phenotypic effects with AC inhibition. As shown in Figure 49, a significant decrease in growth was observed with the 3 inhibitors independently of the initial cell number. Compound RBM1-13 was the least active at decreasing cell growth and it had no effect when 500 cells were plated. Moreover, from the careful examination of the growth curves with 1000 and 2000 initial cells, it seems that the effects of RBM1-13 on cell growth began from day 3, indicating that perhaps this compounds has a delayed effect. This possibility would explain the results of previous experiments in which the incubation periods were no longer than 3 days.

The effect of inhibitors on cell cycle and their putative pro-apoptotic activity will be determined in future experiments in order to better characterize their activity at the cellular level.

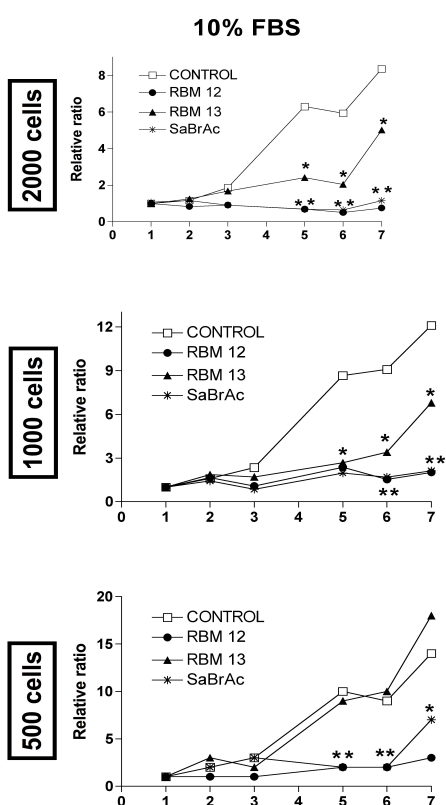


Figure 49. Effects of RBM1-12, RBM1-13 and SABRAC on cell growth. PC3/Mc cells were incubated in the absence (control) or presence of the compounds (5 μ M) in media with 10 % FBS. Cells were quantified by MTT assay after different times from 1 to 7 days. Results are represented as mean \pm SD (n=3). * p \leq 0.05, ** p \leq 0.001

III.3.2.3 Effects of AC inhibitors on invasiveness

The effect of AC inhibitors on invasiveness was evaluated with the same method used with *ASAH1* knockdown cells. PC3/Mc cells were incubated with inhibitors 48 h before the invasiveness assay.

Results are shown in Figure 50. The capacity of PC3/Mc cells to invade decreased significantly by treatment with RBM1-12 and SABRAC, as compared with control cells. Interestingly, RBM1-13 did not significantly reduce the invasive capacity of the cells, which provides additional support for a role of AC in this phenotypic feature of cancer cells. These results agree with literature reports according to which Cer accumulation diminishes invasiveness¹⁰³. However, they are in conflict with those found by *ASAH1* silencing. In that case, genetic blockade of AC increased the number of cells that migrated through the matrigel membrane as compared to controls. A possible explanation may lay in the differential production of sphingosine-1-phosphate. As commented on in the Introduction to this Thesis, sphingosine-1-phosphate stimulates cell migration. Unfortunately, a method for the accurate and reliable measurement of sphingosine-1-phosphate has been available in our laboratories only recently and we do not know whether the knockdown cells produce higher S1P amounts than the PC3/Mc cells treated with the AC inhibitors. Nevertheless, levels of So, the S1P immediate precursor, are increased in knockdown cells and decreased in PC3/Mc cells treated with AC inhibitors. The determination of S1P in both scenarios will be carried out to confirm that the different invasion capacity of *ASAH1* knockdown cells and PC3/Mc cells treated with AC inhibitors is due to different production of S1P.

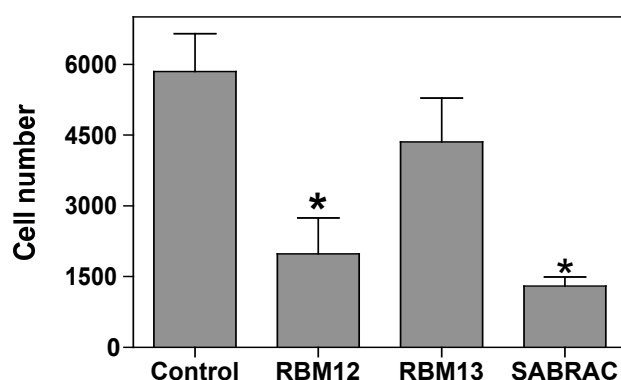


Figure 50. Effects of RBM1-12, RBM1-13 and SABRAC on the *in vitro* invasiveness of PC3/Mc cells. Cells were treated with AC inhibitors at 5 μ M during 48 h, and then seeded on the transwell plate. Data are represented as the mean of three replicates \pm SD. * $p \leq 0.05$.

III.3.2.4 Effects of AC inhibitors on 3D growth

To continue with the comparison of the effects of genetic and chemical inhibition of AC on PC3/Mc cell phenotypic features, PC3/Mc cells were allowed to grow in soft agar in the presence of RBM1-12, RBM1-13 or SABRAC at 1 and 5 μ M. As shown in Figure 51, cells treated with 1 μ M of either compound were not affected in their capacity to form 3D colonies. However, RBM1-12 and SABRAC at 5 μ M almost completely abolished anchorage-independent growth of PC-3/Mc cells, in agreement with the results obtained with *ASAH1* knockdown cells. Importantly, RBM1-13 had no effect on colony formation, thus affording an additional proof of the role of AC on clonogenicity, a surrogate of metastatic potential.

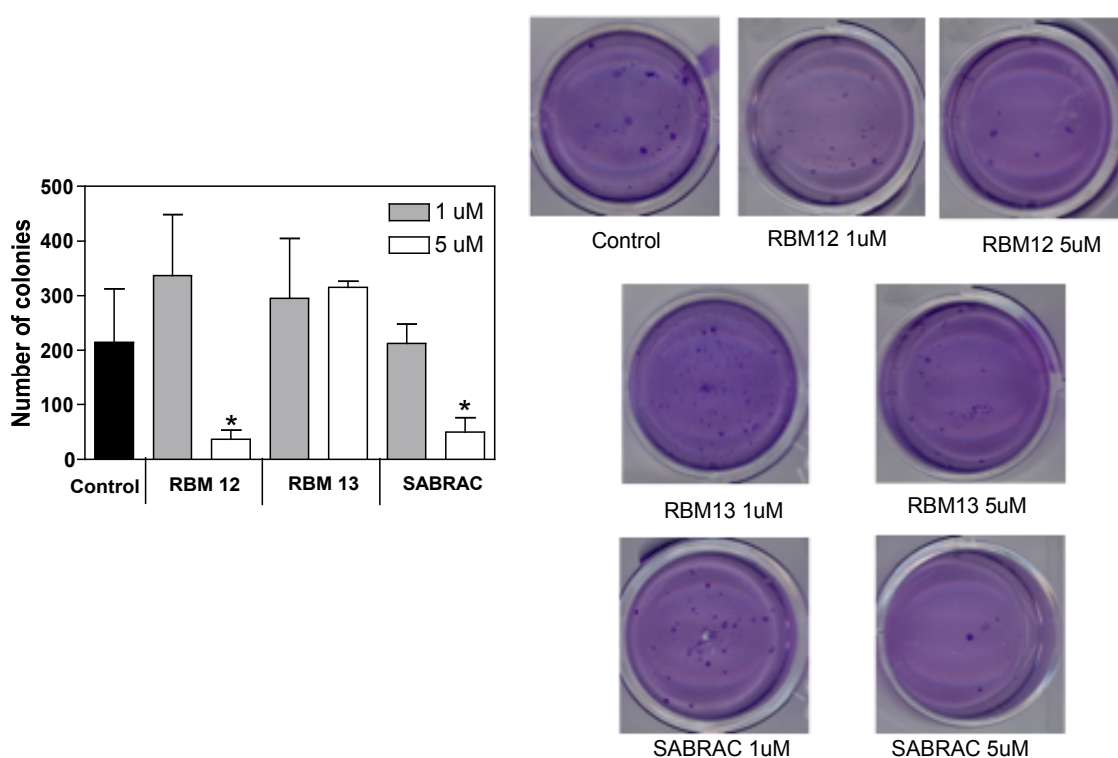


Figure 51. PC3/Mc cells were cultured on soft agar in the presence or absence of test compounds (1 and 5 μ M) and colonies were stained with crystal violet after 3 weeks. Data are represented as the mean of three replicates \pm SD. * $p \leq 0.05$.

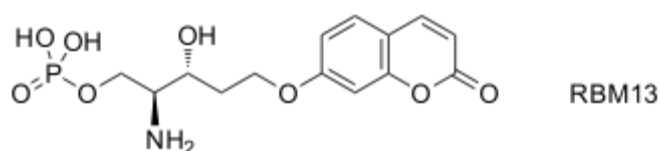
III.3.2.5 Toxicity of SABRAC

As a step prior to the determination of the compounds effect on *in vivo* tumorigenesis and lung colonization in NOD-SCID mice, the toxicity of the selected inhibitor, SABRAC, was determined. Both acute (single dose/24 h) and chronic (repeated administrations twice a week/5 weeks) toxicities were determined in male CD1 mice by intraperitoneal route. The acute LD₅₀ was 200 mg/kg. For the chronic treatment, a dose of 75 mg/kg was selected. Only one mouse died out of 6. Therefore, a treatment regime of 75 mg/kg/twice a week was selected for the experiments in NOD-SCID mice, which will begin shortly.

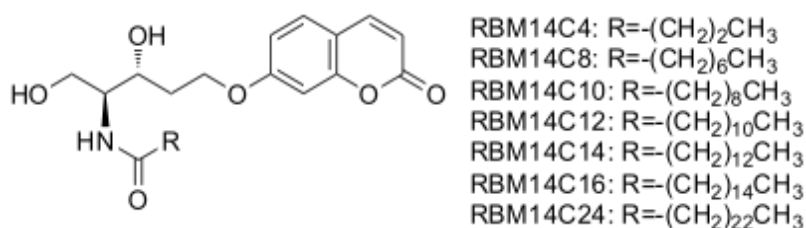
IV.CONCLUSIONS

CONCLUSIONS:

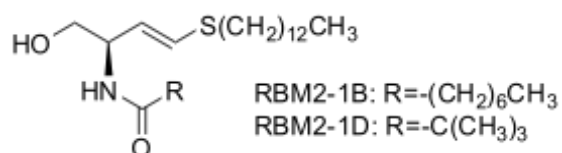
1. Compound RBM13 is a substrate of sphingosine-1-phosphate lyase. Although its affinity for the enzyme is low ($K_m = 152 \mu\text{M}$), its use in combination with a bacterial extract enriched in SPL affords a convenient system for the identification of SPL inhibitors in HTS of chemical libraries. Importantly, Triton X100, normally used in other SPL assays, must be avoided in this one, as it interferes with fluorescence reading.



2. Quantification of pentadecanal by gas chromatography coupled to mass spectrometry after conversion into *O*-((pentafluorophenyl)methyl)oxime is a sensitive procedure to measure SPL activity using the C17 analog of sphinganine-1-phosphate as substrate. The reaction is linear up to 60 min and 20 μg of protein. Kinetic constants are $K_m=18 \mu\text{M}$ and $V_{\text{max}}=11 \text{ nmol/h/mg}$.
3. Compounds RBM14 from C10 to C16 are hydrolyzed by AC and NC, but not by the alkaline ceramidases ACER1, ACER2 and ACER3. Conversely, RBM14C4 is not a substrate of either AC or NC and RBM14C8 is hydrolyzed exclusively by NC. While substrate hydrolysis by AC follows the order C14 > C12 > C10 ~ C16, NC substrate preference was C10 > C12 > C8 ~ C14.



4. RBM14C12 is an excellent tool for diagnosis of Farber disease.
5. The p53 deficient colon carcinoma HCT116-379 cell line is less active at hydrolyzing the RBM14 substrates than wild type HCT116 cells. The prostate cancer PC3/S (non metastatic but highly invasive) is less active at hydrolyzing the RBM14 substrates than the PC3/Mc (highly metastatic but poorly invasive). These differences occur both in intact cells and in lysates at acid pH, which indicates lower AC activity in HCT116 p53(-/-) and PC3/S than in their paired cell lines.
6. The RBM14 compounds are poorly metabolized by enzymes of sphingolipid metabolic pathways other than NC and AC. Interestingly, the observation of transacylated derivatives suggests that the aminodiol released by CDase activities is a substrate of some ceramide synthases. The occurrence of different reacylated RBM14 derivatives may indicate the existence of specific CerS's in each cell type.
7. Compounds RBM2-1B and RBM2-1D, which only differ in the amide acyl group, are dual inhibitors of both AC and DHCD and produce an accumulation of dihydroceramides in cells. RBM2-1B, with an octanamide unit, is a better inhibitor of DHCD than of AC, while pivaloylamide RBM2-1D is a better inhibitor of AC than of DHCD. Therefore, for a common long chain base, enzyme selectivity can be modulated by varying the *N*-acyl group.



8. Despite that no ceramide increased upon treatments with either RBM2-1B or RBM2-1D, both compounds were cytotoxic to HCT116-40 16 cells. Whether cytotoxicity is linked to sphingolipid metabolism is still unknown, but we suggest that sphinganine could be the cytotoxic agent.
9. Both genetic and chemical blockade of AC produce an accumulation of ceramides and dihydroceramides, but while sphingosine decreased upon chemical inhibition, it raised unexpectedly in *ASAH1* knockdown cells. This result suggests an upregulation of other CDases as a response to the constitutive AC blockade, which is more drastic than transient chemical inhibition.
10. Both genetic and chemical blockade of AC reduce cell growth and clonogenicity of PC3/Mc cells. However, silencing the *ASAH1* gene increases, while chemical inhibition of AC decreases, migration. This can be explained assuming that AC knockdown cells, which produce higher amounts of sphingosine than PC3/Mc cells submitted to treatment with AC chemical inhibitors, produce also more S1P, which is a reported inducer of cell migration. This hypothesis awaits confirmation until S1P is determined.
11. RBM1-13 inhibit AC in Moh pAS 10X cells, but not in PC3/Mc cells. The reason for this difference is still unknown.
12. In NOD-SCID mice, *ASAH1* knockdown cells produced significantly smaller tumors than PC3/Mc control cells and have a reduced capability to develop metastatic lung tumors.
13. SABRAC is the most potent AC inhibitor reported to date. Its low toxicity in mice warrants the future development of SABRAC as a drug for cancer treatment.

V. GENERAL MATERIALS AND METHODS

V.1 Materials

Table 6. Materials

Sigma Aldrich	Sodium cholate (Z)-11-hexadecenal (pentafluorophenyl)methyl)hydroxylamine hydrochloride Umbelliferone EDTA PMSF KOH Pyridoxal phosphate NaF DTT Na ₃ VO ₄ Triton-X100 NaIO ₄ DMEM (both high and low glucose) Aprotinin and leupeptin N-dodecanoylsphingosine N-dodecanoylglucosylsphingosine N-dodecanoylsphingosylphosphorylcholine
Avanti Polar Lipids	C17-sphinganine-1-phosphate (17:SaP) C18-sphingosine-1-phosphate (SoP) Cer C24:1
Synthesized in our laboratories	Cer C12 NBD Pentadecanal Aminodiol ADOL
INVITROGEN- GIBCO	Lipofectamine 2000 PBS 10X FBS Penicilline/streptomycine
PAA	RPMI1640 Trypsin-EDTA

V.2 Buffers

All buffers and solutions were prepared with water purified by a Milli-Q system (Millipore)

Table 7. Buffers

Buffer	Composition
Glycine/NaOH 200 mM pH 10.6	25 mL 0.4 M glycine and 2.75 mL of 0.4 M NaOH; adjust pH to 10.6 and volume to 100 mL
Sodium acetate 100 mM pH 4.5	30.5 mL of 0.2 M acetic acid and 19.5 mL of 0.2 M sodium acetate; adjust pH to 4.5 and volume to 100 mL
Tris-HCl 25 mM pH 7.5	303 mg/80 mL of water of Tris-base; adjust pH to 7.5 with conc. HCl and volume to 100 mL
PB 25 mM	0.78 g of NaH ₂ PO ₄ ·H ₂ O and 5.2 g of Na ₂ HPO ₄ ·7H ₂ O, dissolve in 800 mL of water and adjust pH to 7.4, add water to complete 1L.
TBS (1X)	20 mM Tris and 0.5 M NaCl; adjust pH to 7.6
PBS (1X)	Diluted from a 10X GIBCO Stock
Running (1X)	25 mM Tris, 380 mM glycine and 0.1% SDS
Transfer (1X)	25 mM Tris, 192 mM glycine and 20% MeOH
Sodium borate 50 mM	1.9 g/100 mL of water of sodium borate

V.3 Plasmids

Table 8. Constructions used in this thesis

Plasmid name	vector	gene	protein	Source
pcDNA5/TO-ASA2	pcDNA5/TO	ASA2	NC	Dr. C. Bedia
pcDNA5/TO-ASA3	pcDNA5/TO	ASA3	ACER1	Dr. C. Bedia
pcDNA4/TO/LacZ-ASA3L	pcDNA4/TO7LacZ	ASA3L	ACER2	Dr. C Mao
pEGFP-aPHC	pEGFP	aPHC	ACER3	Dr. C Mao
pBV001	pBADHisC	SG1PL	SPL	Dr. P Van Veldhoven

Plasmid name	Sequence	Source
000399	CCGGGCACCAATGCTA AAGGTTATACTCGA	SIGMA
000400	CCGGGCTGTTACTGAT ATACCTTTACTCGA	SIGMA
000401	CCGGGAAAGGAATCAT TGGATGTATCTCGA	SIGMA
000402	CCGGGCCTGCAAAGAT GTGTCTGAACTCGA	SIGMA
000403	CCGGGCTGTTATTGAC AGCGATATACTCGA	SIGMA
pLK0.ps	Control plasmid	Dr. T. Thomson
pVSV-G	Plasmid containing gag, pol and rev genes	Dr. T. Thomson
pCMV8.9	Plasmid expressing envelope	Dr. T. Thomson

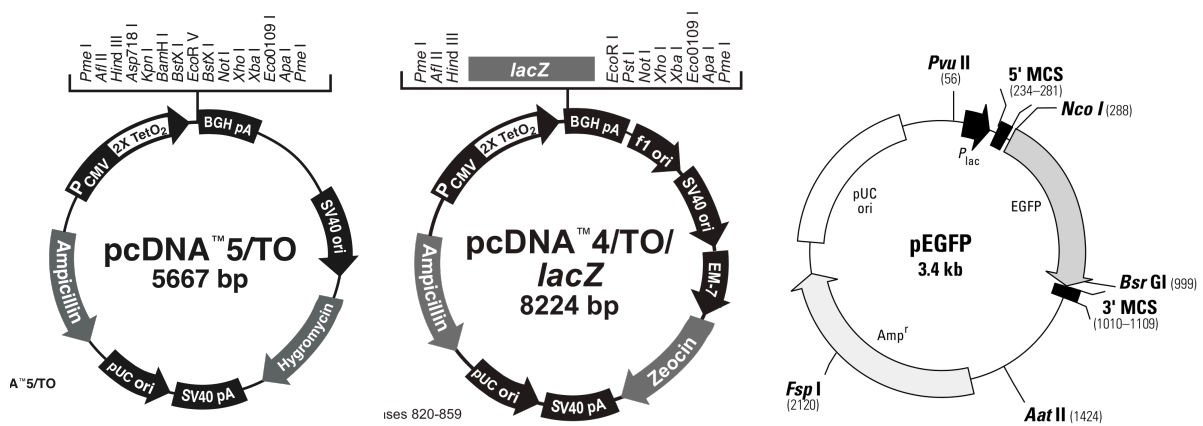


Figure 52. Plasmids

V.4 Antibodies

Table 9. Antibodies for WB used in this thesis.

PRIMARY ANTIBODIES	Source	Dilution (WB)	Dilution buffer	Conditions
Anti-His	Amersham Biosciences	1:3000	3% dry milk in PBST	4°C/overnight
Anti-actin	Abcam	1:3000	5% BSA in PBST	25 °C/1 h
Anti AC	BD Transduction Laboratories	1:250	3% dry milk in PBST	4°C/overnight
Anti-ACER2	SIGMA	1:250	3% dry milk in PBST	4°C/overnight
SECONDARY ANTIBODIES				
HRP conjugated mouse anti-IgG	Amersham Biosciences	1:5000	3% dry milk in PBST	25 °C/1 h
HRP conjugated mouse anti-IgG	Amersham Biosciences	1:5000	3% dry milk in PBST	25 °C/1 h

V.5 Biochemistry and molecular biology

V.5.1 Enzyme activity assays

V.5.1.1 Ceramidase activities

A) Fluorogenic assay

Cell lysates

Cells were collected by trypsinization, the pellet was washed twice with PBS, and it was resuspended in 0.25 M sucrose (100 μ L/1x10⁶ cells). Cells were lysed by ultrasonication in an ultrasonic bath (10 min/ice cold water). In a 96 well plate (NUNC MicroWell®) were added 75 μ L/well of either of the following buffers: 100 mM sodium acetate buffer pH 4.5 for AC, 25 mM PB pH 7.4 for NC or 200 mM glycine/NaOH buffer pH 9 for ACERs. To the buffer had been added the required volume of a 4 mM stock solution of the RBM14 substrate in EtOH to obtain a 40 μ M final concentration (1% final concentration of EtOH). To these 75 μ L/well of substrate solution was added 25 μ L of cell lysate (20 μ g protein/well for AC and 100 μ g protein/well for NC). For testing inhibitors, compounds were added with the substrate solubilized in EtOH at the desired concentrations, and the same volume of EtOH alone was used in controls. The mixture was incubated for 3 hr at 37°C, and then was added 25 μ L of MeOH, followed by 100 μ L of NaIO₄ 2.5 mg/mL dissolved in 200 mM glycine/NaOH buffer pH 10.6. After 1 hr at 37°C, another 100 μ L of 200 mM glycine/NaOH buffer pH 10.6 was added and fluorescence was read at excitation/emission wavelengths of 355/460 nm using a SpectraMax Microplate Reader (Molecular Devices).

Intact cells

The day before the assay, 2x10⁴ cells per well were seeded in a 96 well plate (NUNC MicroWell®). Cells were incubated for 24h at 37°C, 5% CO₂. Medium was replaced by 100 μ L of fresh medium to which the required volume of a 4 mM stock solution of the RBM14 substrate in EtOH had been added to obtain a 40 μ M final concentration (1% final concentration of EtOH).

For testing inhibitors, compounds were added solubilized in EtOH at different concentrations, and EtOH alone was used as control. The plate was incubated for 3h at 37°C, 5% CO₂ and the assay was continued as described above for cell lysates.

B) Hydrolysis of Cer C12 NBD

Cell lysates

NC activity was determined as described¹³⁰ using *N*-[12-[(7-nitro-2-1,3-benzoxadiazol-4-yl)amino]lauroyl]-*D*-erythro-sphingosine (CerC12NBD) as substrate and Moh pAS cells transfected with pcDNA5/TO-*Asah2*. Twenty-four hours before transfection, cells were plated at a density of 2.5×10^5 cells in 35 mm well plates (NUNC). Then cells were transfected with pcDNA5/TO (*empty* vector) or pcDNA5/TO-*Asah2* with lipofectamine 2000 (INVITROGEN) (10 μ L, 0.4 μ g DNA /mL). Twenty-four hours after transfection cells were collected by trypsinization and washed twice with PBS. The cell pellets were suspended in 1 mM Tris-HCl, 0.1 mM EDTA, pH 7.5 (100 μ L, 5-6 mg protein/mL), lysed by sonication (10 min in ice cold water, ultrasonic bath), and 20 μ l were incubated at 37°C for 1 h with 20 μ l of 5 μ M CerC12NBD in reaction buffer (25 mM Tris-HCl, pH 7.5, 1% sodium cholate) with or without the test compounds (40 μ M final concentration). The reaction was terminated by the addition of methanol (1 mL) and 50 μ L were injected into the HPLC-FD system.

Intact cells

To determine NC activity with CerC12NBD in intact cells, 24 h before transfection, 2.5×10^5 cells per well were plated in 6 well-plates (COSTAR) (35 mm²). Then cells were transfected with pcDNA5/TO (*empty* vector) or pcDNA5/TO-*Asah2* with lipofectamine 2000 (10 μ L, 0.4 μ g DNA /mL). Twenty-four hours after transfection cells were treated with the test compounds added in EtOH (50 μ M final concentration, 1% EtOH concentration) or vehicle for 4 h. Cells were collected and NC activity was determined as described above for cell lysates.

C) Quantification of So by NDA derivatization

Moh cells were transfected with the plasmid pcDNA5/TO-ASA3. Twenty-four hours before transfection, cells were plated at a density of 2.5×10^5 cells in 35 mm well plates (COSTAR). Then cells were transfected with pcDNA5/TO (*empty* vector) or pcDNA5/TO-*Asah2* with lipofectamine 2000 (INVITROGEN) (10 μ L, 0.4 μ g DNA /mL).

Twenty-four hours after transfection cells were collected by trypsinization and washed twice with PBS. The cell pellets were suspended in 25 mM Tris-HCl, pH 9.0 (100 μ L, 5-6 mg protein/mL), lysed by sonication (10 min in ice cold water, ultrasonic bath), and 40 μ L of cellular lysates were incubated with Cer C18:1 substrate (50 μ M) in 40 mL assay buffer (Tris 25 mM pH 9.0 0.1% Nonidet P-40) at 37°C for 1 hr. The reactions were stopped with the mixture chloroform/methanol, and 10 μ L of a solution of Phytosphingosine C-18 (20 μ M) was added as internal standard.

Extraction

25 μ L of the cell lysates were mixed with 150 μ L of chloroform:methanol (1:2, v/v) and sonicated for 5 min. 100 μ L each of 1M NaCl and additional chloroform and 10 μ L of 3N NaOH were added. After thorough vortex containing sphingoid base 1-phosphates was transferred to a new tube. The lower organic phase was re-extracted and the organic phases combined. 300 μ L of additional chloroform and 20 μ L of HCl (concentrated) were then added to the combined aqueous phases and mixed well. After centrifugation (13,000 x g) for 2 min, the lower organic phase was transferred to another tube and dried under N₂ stream, and resuspended in 50 μ L of ethanol, and used for So analysis.

Derivatization with NDA

50 μ L of the re-suspended lipid extraction solution was added to 100 μ L of the NDA derivatization reaction mixture (containing 50 mM borate buffer, NDA 5mM in MeOH and NaCN 5 mM). After 10 min incubation at 50°C the reaction mixture was diluted 1:3 with ethanol and centrifuged (13000 x g) for 5 min. The sphingoid base derivatives were separated by HPLC injecting 30 μ L of each sample.

Sphingoid bases were detected by HPLC as described in section V.9.3

V.5.1.2 Sphingosine-1-phosphate lyase activity

A) Fluorogenic assay

Cells were collected by trypsinization and washed twice with PBS at 4°C and then resuspended in 0.5 M phosphate buffer pH 7.4 (1 mL/15x10⁶ cells). The buffer contained freshly added PMSF, aprotinin and leupeptin at final concentrations of 1 mM, 10 µg/ml and 10 µg/ml, respectively. Cell pellets were sonicated for 10 min on ice cold water (ultrasonic bath). On a 96 well plate (NUNC) were added 75 µL of cell lysate and 100 µL of the reaction mixture, which consisted of 25 mM NaF, 25 mM sodium orthovanadate, 0.5 mM EDTA, 0.25 mM pyridoxal phosphate and 200 µM RBM13. The latter was added from a 1.3 mM stock solution in PBS. The mixture was incubated for 6 hr at 37°C. Fifty µL of MeOH and 100 µL of 200 mM Glycine-NaOH buffer pH 10.6 were sequentially added. The plate was incubated for 1 hr at 37 °C and fluorescence was determined at excitation/emission wavelengths of 355/460 nm using a SpectraMax Microplate Reader (Molecular Devices).

B) GC/MS assay

For a single sample, 40 µL of 17:SaP stock solution (0.2 mM in ethanol, 40 µM final concentration in the assay, 8 nmol) was added to an eppendorf tube and the solvent was removed under a stream of nitrogen. To the residue was added 25 µL of milliQ water and the mixture was sonicated for 1 min in an ultrasonic bath. Cell pellets, obtained by trypsinization, were washed with PBS and then suspended in 0.5 M potassium phosphate buffer pH 7.4 (50 µl per sample; 0.01-2 mg/ml of protein) and the mixture was sonicated for 10 min in ice-cold water in an ultrasound bath. To 150 µL of 0.5 M potassium phosphate buffer pH 7.4 was added pyridoxal phosphate (2 µL, 12.5 mM), sodium orthovanadate (2 µL, 1.25 mM), EDTA (2 µL, 250 mM), sodium fluoride (2 µL, 1.25 mM) and dithiothreitol (2 µL, 100 mM). To the 25 µL substrate solution was added 125 µL of this solution and then the cell lysate (50 µl). After incubation for 1 h at 37 °C, (Z)-11-hexadecenal (10 µL, 25 µM in dimethylsulfoxide, 250 pmol) and PFBHA (250 µL, 50 mM in Tris-HCl buffer pH 7.4, 12.5 µmol) were sequentially added and the mixture was incubated at 37 °C for 15 min after vigorous stirring. The PFBP were extracted with hexane (500 µL) and 400 µL of the organic solution was stored at -20 °C until analysis. Before

injection, the solvent was carefully removed (nitrogen stream), 10 μ L of hexane were added and 2 μ L were injected into the GC/MS equipment for analysis.

V.5.2 Lipid extraction and processing

A cell pellet containing approximately 1×10^6 cells, was resuspended in 500 μ L of MeOH and internal standards (N-dodecanoylsphingosine, N-dodecanoylglucosylsphingosine and N-dodecanoylsphingosylphosphorylcholine, 0.2 nmol each) were added. The mixture was transferred to a glass vial and 0.25 ml of chloroform were then added followed by 0.1 ml of water. The mixture was sonicated in a bath sonicator until the pellets appeared dispersed and then extraction was continued overnight at 48 °C.

Tubes were cooled to room temperature and 75 μ L of 1 M KOH in methanol was added, samples were sonicated and incubated for 2 h at 37 °C. This methanolysis step removes most of the interfering glycerolipids, in particular phosphatidylcholines, which can mask sphingomyelins. After methanolysis, 3 μ L of glacial acetic acid were added to bring the pH near neutral. Finally the solvent was evaporated under a nitrogen stream, and the extracts were stored at – 20 °C until their analysis, which is routinely carried out within a week after preparation.

V.5.3 Protein quantification

A) Bradford

For protein quantification, 20 μ L of protein extract or standard was mixed with 80 μ L of ready-to-use Bradford Reagent (Bio-Rad). The mixture was incubated 10 min at room temperature and absorbance measured at 595 nm using a SpectraMax Microplate Reader (Molecular Devices). A standard curve of BSA (60-10 μ g/mL) was used to determine the concentration of samples.

B) Micro BCA

Protein quantification for western blot was made with Micro BCA Protein Assay Kit (Thermo Scientific) according to the manufacturer's instructions. A curve of albumin standards (2-0.01 mg/mL) was used to calculate the unknown concentrations. Working solution was prepared by mixing 25 parts of Micro BCA

Reagent A and 24 parts Reagent B with 1 part of Reagent C. In a 96 well plate, 20 μ L of each standard or unknown sample were mixed with 100 μ L of working solution, the plate was covered using sealing tape and incubated at 37°C for 30 min. The absorbance was measured at 562 nm on a SpectraMax Microplate Reader (Molecular Devices).

The average 562 nm absorbance reading of the Blank standard replicates was subtracted from the 562 nm reading of all other individual standard and unknown sample replicates.

V.5.4 Western blot analysis

After being washed with ice-cold PBS, cells were lysed in a lysis buffer, which consisted of 10 mM Tris-HCl, pH 7.4, containing 100 mM NaCl, 1 mM EDTA, 1 mM EGTA, 1 mM NaF, 20 mM $\text{Na}_4\text{P}_2\text{O}_7$, 2 mM Na_3VO_4 , 1% Triton-X 100, 10% glycerol, 0.1% SDS, 0.5% deoxycholate, 1 mM PMSF, and a protease inhibitor cocktail (aprotinine and leupeptine 1mg/mL). The cell lysates were then centrifuged at 10,000 g for 15 min at 4°C, and the resulting supernatant was assayed for protein concentrations using Micro BCA protein assay reagent kit. Proteins (20–30 μ g) were separated on SDS-polyacrylamide gels (Bio-Rad laboratories) and were transferred onto nitrocellulose membrane blots (Bio-Rad Laboratories). After blocking with 5% nonfat milk in PBS containing 0.1% Tween 20 (PBST) for 1 h at room temperature, the membrane blots were incubated with a primary antibody for 1 h. After three washes with PBST, the blots were incubated with a goat anti-rabbit IgG or anti-mouse IgG antibody conjugated with a HRP.

Immunodetection

Once proteins were transferred to the membrane, it was incubated during 30 min at room temperature with 10% dry milk in PBST (10 mM Na_2HPO_4 , 2 mM KH_2PO_4 , 140 mM NaCl, 3 mM KCl and 0.1% (v/v) Tween 20). After blocking, the membrane was washed three times with PBST and then was incubated with the primary antibody at the suitable dilution in the appropriate buffer and conditions (See table 9). Then the membrane was submitted to three washes with PBST for 5 min. When necessary, incubation with the secondary antibody was carried out (Table 9).

Finally, the membrane was submitted to 3 more washes with PBST and detection was accomplished with ECL Western Blotting Detection Kit (Amersham Biosciences) according with the manufacturer's instructions.

V.5.5 Plasmid amplification

E. coli DH5 α competent cells (SIGMA) were transformed with the required plasmid, and plated on LB ampicillin (100 mg/ml) or kanamycine (50 μ g/mL) plates. Several colonies were picked and grown overnight in 100 ml of liquid LB-ampicillin medium. The plasmid DNA was isolated from these cultures using the alkaline lysis procedure Midi or MaxiPrep (Qiagen), accordingly with the manufacturer specifications. Plasmid DNA concentration was determined by OD_{260/280} measurement on a Perkin Elmer Lambda 3B UV/VIS spectrophotometer. The presence of the insert was confirmed by PCR, restriction enzyme analysis and finally sequence analysis.

V.5.5.1 SPL expression in *E. coli*

Sequenced plasmids were transformed into an *E. coli* TOP 10 expression strain. Transformed bacterial strains were grown in LB ampicillin medium overnight at 37° C to saturating cell density and diluted 1:50 the next morning for expression in 500 mL of culture medium (LB-ampicillin). Growth at 37 °C was monitored by optical density at 600 nm (OD₆₀₀). When OD₆₀₀ reached a value of 0.5 to 0.6, expression was induced with 0.2% arabinose. After induction the cells were kept at 37 °C for another 4 h and either used immediately or were harvested by centrifugation and pellets stored at -80° C.

V.5.6 Total RNA isolation and RT-PCR

Total RNA was extracted using the RNAsy Kit (Quiagen) as was described in the manufacturer's instructions. The RNA obtained was dissolved in RNase free water and stored at -80°C. The quality of the RNA was analyzed using the NanoDrop 2000 spectrophotometer (Thermo Scientific).

The cDNA was generated from 100 ng of total RNA using the One Step RT-PCR kit (Qiagen).

Components	Volume	Final concentration
Buffer 5X	10 μ L	1x
dNTP mix	2 mL	400 μ M of dNTPs
Random primers	3 μ L	0.6 μ M
Enzyme mix	2 μ L	5-10 U / reaction
RNA template	variable	1 μ g
water	variable	until 50 μ L

RT-PCR conditions

25°C 10 min
37°C 120 min
85°C 5seg
4°C

V.5. 7 Real-time PCR (qPCR).

Complementary DNAs were synthesized with the High-Capacity cDNA Reverse Transcription Kit (Applied Biosystems, Carlsbad, CA). Real-time quantitative PCR assays were performed on a LightCycler 480 instrument (Roche Diagnostics) and analyzed with the LightCycler 480 Software release 1.5.0. The amplification levels of RN18S1 and HMBS were used as an internal reference to estimate the relative levels of specific transcripts, and relative quantization was determined by the $\Delta\Delta C_p$ method. All determinations were done in triplicate.

μ

V.8 Cell biology

V.8.1 Cell lines.

Cell line	Origin	Medium	
Moh pAS	Farber disease fibroblasts	DMEM High glucose	Kindly given by Dr. Jeffrey A. Medin, Ontario Cancer Institute, Canada
Moh pAS 10x	Farber disease fibroblasts transduced to express ASAH1		Kindly given by Dr. Jeffrey A. Medin, Ontario Cancer Institute, Canada
MEF 215A	Fibroblasts derived from wildtype mouse embryonic fibroblasts SPL(+/+)		Kindly given by Prof. Thierry Levade INSERM France
HEK 293 T	Human embryonic kidney		
MDA-MB-231	Estrogen receptor alpha-negative, highly invasive, fibroblast-like breast cancer cell line		Kindly given by Prof. Paul van Veldhoven Katholieke Universiteit Leuven
HCT 116 (40-16)	Human colon carcinoma +/+ p53		Kindly given by Dr. Timothy Thomson IBMB, CSIC
HCT 116 (379.2)	Human colon carcinoma -/- p53		
IMR-32	Malignant glioma	DMEM Low glucose	Kindly given by Dr. Timothy Thomson IBMB, CSIC
PC3/Mc	Prostate cancer highly metastatic non invasive clone.	RPMI 1640	
PC3S	Prostate cancer non metastatic, highly invasive clone		
SK-N-SH	Human neuroblastoma		

All cell lines were growth at 37°C, 5% CO₂ and 95 % humidity.

V.8.2 Transient transfection of fibroblasts

Twenty-four hours before transfection, cells were plated at a density of 25×10^4 cells in 35 mm well plates. The next day, cells were transfected with the specific constructs and the empty vectors using lipofectamine 2000 (Invitrogen) according to the manufacture's instructions. Twenty-four hours after transfection cells were either used in following treatments or collected by trypsinization.

In the first case, the medium was replaced with fresh medium before further experimentation; in the second case, cells were washed twice with PBS after trypsinization, centrifuged and the pellets were used as required in further experiments

In transfections with NC and the three ACER's, the success of transfection was confirmed by: NC, activity assay with CerC12NBD in intact cells as described in section V.5.1.1 B; ACER1, activity assay by measurement of sphingosine as described in; ACER2, Western blot with anti-ACER2 and ACER3, fluorescence microscopy of GFP, which is co-expressed with ACER3.

V.8.3 Cell viability assay (MTT)

MTT assay is a colorimetric assay based on 3-(4,5-Dimethylthiazol-2-yl)-2,5-diphenyltetrazolium bromide (MTT), a yellow compound that is reduced to formazan by respiratory chain enzymes in the mitochondria of living cells, giving a purple color; the assay is therefore a measure of mitochondrial activity. Cells were treated with inhibitors, chemotherapeutic agents or solvents as controls, and were analyzed after 24, 48 or 72 hours after the addition of the compound. MTT was added to cultured cells at a final concentration of 0.5 mg/mL of culture medium. Cells were incubated at 37°C for 3 hours to allow the formation of formazan precipitates; culture medium was removed and formazan was solubilized with 100 μ L of dimethyl sulfoxide (DMSO). After 1 hour, the absorbance of the formazan solution was measured at 570 nm using a SpectraMax Microplate Reader (Molecular Devices).

V.5.4. Production and transduction of retroviral particles for establishing stable knockdown cells.

The retrovirus packaging cell line PG13 was co-transfected with constructs 000399 to 000403 and pVSV-G, pCMV 8.9 using Fugene HD (Roche). Supernatants were collected for the following 48 h, filtered through 0.22 μ m methylcellulose filters (Millipore) and concentrated by ultracentrifugation at 27,000 rpm for 90 minutes on 20% sucrose density gradients. Viral particles were resuspended with RPMI1640 and added to PC-3/Mc cells together with 8 μ g/mL polybrene (Sigma). Plates were

centrifuged at 1,800 rpm for 60 minutes followed by incubation at 37 °C for 24 h. Selection for cells with integrated sequences was carried out for 3 days in medium supplemented with 5 µg/mL of puromycin (Biomol).

V.8.5 Cell cycle analysis.

Cells were seeded in 6-well plates (Costar), detached with Trypsin/EDTA/1% BSA, washed twice and resuspended in PBS, followed by dropwise addition of 70% ethanol and fixation at 4 °C for 2 hours. Subsequently, cells were washed twice with PBS/50 mM EDTA/1% BSA, incubated with 1 mg/mL RNase A (Sigma) at 37°C for 1 hour and 0.1 mg/mL propidium iodide (Sigma). DNA content was determined in a Cytomics FC500 instrument (Coulter, Hialeah, FL), and cell cycle distribution analyzed with the Multicycle program coupled to the instrument. All determinations were done in triplicate.

V.8.6 Anchorage-independent growth assays (3D growth assays).

For soft agar colony formation assays, 0.5% agar in complete culture medium was placed at the bottom of 12-well plates, allowed to solidify and overlaid with a suspension of 3×10^3 cells in 0.3% agar in complete medium. After solidification, wells were fed with complete medium twice a week. After 3 weeks, they were fixed with 0.5% glutaraldehyde, stained with 0.025% crystal violet and visualized under a Leica magnifying glass (Wetzler, Germany) coupled to an Olympus digital camera (Olympus, Hamburg, Germany). Colonies ≥ 0.2 mm diameter were scored with ImageJ 1.43u (NIH, USA) software. Each experimental condition was performed in triplicate.

V.8.7 *In vitro* invasiveness assays.

Transwell chambers (Costar) with 8-µm diameter pore membranes were coated with growth factor-reduced Matrigel (BD Biosciences) at 410 µg/mL and human umbilical cord hyaluronic acid (Sigma) at 100 µg/cm². Cells (1.5×10^5 cells per well in 24-well plates) were serum-deprived for 24 h, detached, resuspended in RPMI/1% BSA/0.5% FBS and then seeded onto the pre-coated Transwell inserts, with the lower chamber containing RPMI supplemented with 0.5% FBS. After 24 hours, cells having migrated to the lower chamber well were collected by detachment with trypsin-EDTA, washed with PBS, and counted in a Coulter Multisizer II instrument (Coulter Electronics, Luton, UK). Each experimental

condition was performed in triplicate.

V.8.8 *In vivo* tumor formation.

For localized growth, cells (1×10^3 to 1×10^5) were injected in a volume of 50 μ L of RPMI 1640 (without FBS) intramuscularly in each hind limb. Tumor growth was monitored by luminometry on a ORCA-2BT instrument (Hamamatsu Photonics, Hamamatsu, Japan), 5 min after intraperitoneal injection of luciferine (100 mg/Kg in 150 μ L). Tumors were allowed to grow up to 1.5 cm in diameter, at which point animals were euthanized. For lung colony formation, 5×10^5 cells in 150 μ L RPMI 1640 were injected through the dorsal caudal vein of anesthetized 6-week-old male NOD-SCID mice. Mice were imaged immediately after injection and thereafter, tumor development was monitored by weekly imaging on an IVIS-200 instrument (Xenogen-Caliper Life Sciences, Hopkinton, MA) after intraperitoneal injection of 1.5 mg luciferine (15 mg/mL in PBS). For bioluminescence plots, photon flux was calculated relative to background values from luciferin-injected mice with no tumor cells, and normalized to the value obtained immediately after xenografting. Lesions were localized by *ex vivo* bioluminescence imaging and resected under sterile conditions. Some of the lesions were fixed with formalin and processed for histological analysis. Statistics: in lung colonization and bone metastasis free survival analysis, lesions that had an increased photon flux value above day 0 were counted as events.

V.8.9 Toxicity of SABRAC in mice

Acute toxicity

A dose escalation study was made to determinate the acute toxicity of SABRAC, male CD-1 mice received a single intraperitoneal (i.p.) dose of SABRAC, 24h later survival was assessed. There were three groups of 4 mice treated with 75, 150 or 200 mg/kg, and one group (4 mice) with vehicle (MeOH 30%, 40% Cremophor[®] and 30% PBS).

Chronic toxicity

Based in the acute toxicity results, in which 75mg/kg didn't have any toxic effect this dose was selected for chronic experiments. Male CD-1 mice received a i.p. dose of SABRAC twice a week, treatments were given for 5 weeks. There was one

group of 6 mice treated SABRAC and one group (6 mice) with vehicle (MeOH 30%, 40% Cremophor[®] and 30% PBS).

V.9 Instrumental Analysis

V.9.1 Sphingolipids analysis by UPLC/MS

The liquid chromatography-mass spectrometry equipment consisted of a Waters Acquity UPLC system connected to a Waters LCT Premier orthogonal accelerated time of flight mass spectrometer (Waters, Millford, MA), operated in positive electrospray ionization mode. Full scan spectra from 50 to 1500 Da were acquired and individual spectra were summed to produce data points each 0.2s. Mass accuracy and reproducibility were maintained by using an independent reference spray by the LockSpray interference. The analytical column was a 100 mm × 2.1 mm i.d., 1.7 μ m C8 Acquity UPLC BEH (Waters). The two mobile phases were phase A: water with 0.01% TFA; phase B: Acetonitrile 0.01% TFA. A linear gradient was programmed-0.0 min: 80% B; 3 min: 90% B; 6 min: 90% B; 15 min: 99% B; 18 min: 99% B; 20 min: 80% B. The flow rate was 0.3 mL/min. The column was held at 30°C. Quantification was carried out using the extracted ion chromatogram of each compound, using 50 MDa windows. The linear dynamic range was determined by injecting standard mixtures. Positive identification of compounds was based on the accurate mass measurement with an error <5 ppm and its LC retention time, compared to that of a standard ($\pm 2\%$).

V.9.2 Gas chromatography/Mass spectrometry

Gas chromatography coupled to electron impact (70 eV) mass spectrometry was carried out using a Fisons gas chromatograph (8000 series) coupled to a Fisons MD-800 mass-selective detector. The system was equipped with a nonpolar Hewlett \pm Packard HP-1 capillary column (30 m x 0.20 mm i.d.), which was programmed from 100 °C to 340 °C at 7 °C/min. Analyses were performed in the selected ion monitoring mode. Selected ions were those at m/z 181, 240, 252, 421 and 433. Dwell was set at 0.02 s and the mass span at 0.5 amu.

V.9.3 HPLC/fluorescence detection

These analyses were carried out with an Alliance Waters 2695 HPLC system coupled to a Waters 2475 Multi λ fluorescence detector (Waters, Milford USA), and equipped with an Atlantis T3 C18 (50 mm x 4.6 mm) column (Waters, Milford USA). The mobile phase was composed of a mixture of acetonitrile/H₂O (80:20) (NBD products) or MeOH/H₂O (97:3) (NDA derivatives). All solvents contained a 0.1 % of trifluoroacetic acid. The flow rate was 1 mL/min. Fluorescent compounds were monitored at excitation / emission wavelengths of 420 / 483 nm, respectively. Peak quantification was carried out using the Empower Pro 2.0 (2005-2008 Waters) software.

V.10 Statistical analysis

Significance was determined by the two-tailed unpaired *t*-test using the Graph Pad Prism 4.0 software.

VI. REFERENCES

REFERENCES

1. Sabourdy, F., *et al.* Functions of sphingolipid metabolism in mammals--lessons from genetic defects. *Biochim Biophys Acta* **1781**, 145-183 (2008).
2. Merrill, A.H. Sphingolipids. in *Biochemistry of lipids, lipoproteins and membranes* (ed. Vance, D.E.) 364-396 (Elsevier, Atlanta GA, 2008).
3. Gangoiti, P., *et al.* Control of metabolism and signaling of simple bioactive sphingolipids: Implications in disease. *Prog Lipid Res* **49**, 316-334 (2010).
4. Merrill, A.H., Jr. De novo sphingolipid biosynthesis: a necessary, but dangerous, pathway. *J Biol Chem* **277**, 25843-25846 (2002).
5. Zheng, W., *et al.* Ceramides and other bioactive sphingolipid backbones in health and disease: lipidomic analysis, metabolism and roles in membrane structure, dynamics, signaling and autophagy. *Biochim Biophys Acta* **1758**, 1864-1884 (2006).
6. Luberto, C. & Hannun, Y.A. Sphingomyelin synthase, a potential regulator of intracellular levels of ceramide and diacylglycerol during SV40 transformation. Does sphingomyelin synthase account for the putative phosphatidylcholine-specific phospholipase C? *J Biol Chem* **273**, 14550-14559 (1998).
7. Gomez-Munoz, A. Ceramide-1-phosphate: a novel regulator of cell activation. *FEBS Lett* **562**, 5-10 (2004).
8. Gomez-Munoz, A. Ceramide 1-phosphate/ceramide, a switch between life and death. *Biochim Biophys Acta* **1758**, 2049-2056 (2006).
9. Merrill, A.H., Jr. & Jones, D.D. An update of the enzymology and regulation of sphingomyelin metabolism. *Biochim Biophys Acta* **1044**, 1-12 (1990).
10. Kitatani, K., Idkowiak-Baldys, J. & Hannun, Y.A. The sphingolipid salvage pathway in ceramide metabolism and signaling. *Cell Signal* **20**, 1010-1018 (2008).
11. Spiegel, S., English, D. & Milstien, S. Sphingosine 1-phosphate signaling: providing cells with a sense of direction. *Trends Cell Biol* **12**, 236-242 (2002).
12. Pyne, S., Lee, S.C., Long, J. & Pyne, N.J. Role of sphingosine kinases and lipid phosphate phosphatases in regulating spatial sphingosine 1-phosphate signalling in health and disease. *Cell Signal* **21**, 14-21 (2009).
13. Hannun, Y.A. & Obeid, L.M. Principles of bioactive lipid signalling: lessons from sphingolipids. *Nat Rev Mol Cell Biol* **9**, 139-150 (2008).
14. Futerman, A.H., Riezman, H. The ins and outs of sphingolipid synthesis. *Trends Cell Biol* **15**, 7 (2005).
15. Fugmann, T., *et al.* Regulation of secretory transport by protein kinase D-mediated phosphorylation of the ceramide transfer protein. *J Cell Biol* **178**, 15-22 (2007).
16. Hanada, K., *et al.* Molecular machinery for non-vesicular trafficking of ceramide. *Nature* **426**, 803-809 (2003).
17. Kolesnick, R.N., Goni, F.M. & Alonso, A. Compartmentalization of ceramide signaling: physical foundations and biological effects. *J Cell Physiol* **184**, 285-300 (2000).
18. Bartke, N. & Hannun, Y.A. Bioactive sphingolipids: metabolism and function. *J Lipid Res* **50 Suppl**, S91-96 (2009).
19. Spiegel, S. & Milstien, S. Sphingosine-1-phosphate: an enigmatic signalling lipid. *Nat Rev Mol Cell Biol* **4**, 397-407 (2003).

20. Pyne, S. & Pyne, N. Sphingosine 1-phosphate signalling via the endothelial differentiation gene family of G-protein-coupled receptors. *Pharmacol Ther* **88**, 115-131 (2000).
21. Kihara, A., Mitsutake, S., Mizutani, Y. & Igarashi, Y. Metabolism and biological functions of two phosphorylated sphingolipids, sphingosine 1-phosphate and ceramide 1-phosphate. *Prog Lipid Res* **46**, 126-144 (2007).
22. Rosen, H., Gonzalez-Cabrera, P.J., Sanna, M.G. & Brown, S. Sphingosine 1-phosphate receptor signaling. *Annu Rev Biochem* **78**, 743-768 (2009).
23. Pyne, N.J., *et al.* New aspects of sphingosine 1-phosphate signaling in mammalian cells. *Adv Enzyme Regul* **49**, 214-221 (2009).
24. Tani, M., *et al.* Sphingosine 1-phosphate (S1P) inhibits monocyte-endothelial cell interaction by regulating of RhoA activity. *FEBS Lett* **581**, 4621-4626 (2007).
25. Spiegel, S. & Milstien, S. Functions of a new family of sphingosine-1-phosphate receptors. *Biochim Biophys Acta* **1484**, 107-116 (2000).
26. Billich, A. & Baumruker, T. Sphingolipid metabolizing enzymes as novel therapeutic targets. *Subcell Biochem* **49**, 487-522 (2008).
27. Maceyka, M., Payne, S.G., Milstien, S. & Spiegel, S. Sphingosine kinase, sphingosine-1-phosphate, and apoptosis. *Biochim Biophys Acta* **1585**, 193-201 (2002).
28. Morita, Y., *et al.* Oocyte apoptosis is suppressed by disruption of the acid sphingomyelinase gene or by sphingosine-1-phosphate therapy. *Nat Med* **6**, 1109-1114 (2000).
29. Ikeda, M., Kihara, A. & Igarashi, Y. Sphingosine-1-phosphate lyase SPL is an endoplasmic reticulum-resident, integral membrane protein with the pyridoxal 5'-phosphate binding domain exposed to the cytosol. *Biochem Biophys Res Commun* **325**, 338-343 (2004).
30. Kumar, A. & Saba, J.D. Lyase to live by: sphingosine phosphate lyase as a therapeutic target. *Expert Opin Ther Targets* **13**, 1013-1025 (2009).
31. Van Veldhoven, P.P. & Mannaerts, G.P. Subcellular localization and membrane topology of sphingosine-1-phosphate lyase in rat liver. *J Biol Chem* **266**, 12502-12507 (1991).
32. Van Veldhoven, P.P., Gijsbers, S., Mannaerts, G.P., Vermeesch, J.R. & Brys, V. Human sphingosine-1-phosphate lyase: cDNA cloning, functional expression studies and mapping to chromosome 10q22(1). *Biochim Biophys Acta* **1487**, 128-134 (2000).
33. Mukhopadhyay, D., Howell, K.S., Riezman, H. & Capitani, G. Identifying key residues of sphinganine-1-phosphate lyase for function in vivo and in vitro. *J Biol Chem* **283**, 20159-20169 (2008).
34. Bourquin, F., Riezman, H., Capitani, G. & Grutter, M.G. Structure and function of sphingosine-1-phosphate lyase, a key enzyme of sphingolipid metabolism. *Structure* **18**, 1054-1065 (2010).
35. Genter, M.B., *et al.* Microarray-based discovery of highly expressed olfactory mucosal genes: potential roles in the various functions of the olfactory system. *Physiol Genomics* **16**, 67-81 (2003).
36. Van Veldhoven, P.P. Sphingosine-1-phosphate lyase. *Meth Enzymol* **311**, 244-254 (2000).
37. Yatomi, Y., *et al.* Sphingosine 1-phosphate breakdown in platelets. *J Biochem* **136**, 495-502 (2004).
38. Ito, K., *et al.* Lack of sphingosine 1-phosphate-degrading enzymes in erythrocytes. *Biochem Biophys Res Commun* **357**, 212-217 (2007).

39. Oskouian, B., *et al.* Sphingosine-1-phosphate lyase potentiates apoptosis via p53- and p38-dependent pathways and is down-regulated in colon cancer. *Proc Natl Acad Sci USA* **103**, 17384-17389 (2006).
40. Schmahl, J., Raymond, C.S. & Soriano, P. PDGF signaling specificity is mediated through multiple immediate early genes. *Nat Genet* **39**, 52-60 (2007).
41. Vogel, P., *et al.* Incomplete inhibition of sphingosine 1-phosphate lyase modulates immune system function yet prevents early lethality and non-lymphoid lesions. *PLoS One* **4**, e4112 (2009).
42. Saddoughi, S.A., Song, P. & Ogretmen, B. Roles of bioactive sphingolipids in cancer biology and therapeutics. *Subcell Biochem* **49**, 413-440 (2008).
43. Huwiler, A. & Pfeilschifter, J. Altering the sphingosine-1-phosphate/ceramide balance: a promising approach for tumor therapy. *Curr Pharm Des* **12**, 4625-4635 (2006).
44. Li, G., Alexander, H., Schneider, N. & Alexander, S. Molecular basis for resistance to the anticancer drug cisplatin in *Dictyostelium*. *Microbiology* **146** (Pt 9), 2219-2227 (2000).
45. Min, J., Stegner, A.L., Alexander, H. & Alexander, S. Overexpression of sphingosine-1-phosphate lyase or inhibition of sphingosine kinase in *Dictyostelium discoideum* results in a selective increase in sensitivity to platinum-based chemotherapy drugs. *Eukaryotic Cell* **3**, 795-805 (2004).
46. Reiss, U., *et al.* Sphingosine-phosphate lyase enhances stress-induced ceramide generation and apoptosis. *J Biol Chem* **279**, 1281-1290 (2004).
47. Min, J., *et al.* Sphingosine-1-phosphate lyase regulates sensitivity of human cells to select chemotherapy drugs in a p38-dependent manner. *Mol Cancer Res* **3**, 287-296 (2005).
48. Bhat, G.K., *et al.* Influence of a leptin deficiency on testicular morphology, germ cell apoptosis, and expression levels of apoptosis-related genes in the mouse. *J Androl* **27**, 302-310 (2006).
49. Phan, V.H., *et al.* Disruption of sphingolipid metabolism elicits apoptosis-associated reproductive defects in *Drosophila*. *Dev Biol* **309**, 329-341 (2007).
50. Fyrst, H. & Saba, J.D. Sphingosine-1-phosphate lyase in development and disease: sphingolipid metabolism takes flight. *Biochim Biophys Acta* **1781**, 448-458 (2008).
51. Hagen, N., *et al.* Subcellular origin of sphingosine 1-phosphate is essential for its toxic effect in lyase-deficient neurons. *J Biol Chem* **284**, 11346-11353 (2009).
52. Visentin, B., *et al.* Validation of an anti-sphingosine-1-phosphate antibody as a potential therapeutic in reducing growth, invasion, and angiogenesis in multiple tumor lineages. *Cancer Cell* **9**, 225-238 (2006).
53. Ramaswamy, S., Ross, K.N., Lander, E.S. & Golub, T.R. A molecular signature of metastasis in primary solid tumors. *Nat Genet* **33**, 49-54 (2003).
54. Colie, S., *et al.* Disruption of sphingosine 1-phosphate lyase confers resistance to chemotherapy and promotes oncogenesis through Bcl-2/Bcl-xL upregulation. *Cancer Res* **69**, 9346-9353 (2009).
55. Hibbs, K., *et al.* Differential gene expression in ovarian carcinoma: identification of potential biomarkers. *Am J Pathol* **165**, 397-414 (2004).
56. Schwab, S.R., *et al.* Lymphocyte sequestration through S1P lyase inhibition and disruption of S1P gradients. *Science* **309**, 1735-1739 (2005).

57. Bandhuvula, P., Fyrst, H. & Saba, J.D. A rapid fluorescence assay for sphingosine-1-phosphate lyase enzyme activity. *J Lipid Res* **48**, 2769-2778 (2007).
58. Pagano, R.E., Martin, O.C., Kang, H.C. & Haugland, R.P. A novel fluorescent ceramide analogue for studying membrane traffic in animal cells: accumulation at the Golgi apparatus results in altered spectral properties of the sphingolipid precursor. *J Cell Biol* **113**, 1267-1279 (1991).
59. Bandhuvula, P., Li, Z., Bittman, R. & Saba, J.D. Sphingosine 1-phosphate lyase enzyme assay using a BODIPY-labeled substrate. *Biochem Biophys Res Commun* **380**, 366-370 (2009).
60. Berdyshev, E.V., *et al.* Characterization of sphingosine-1-phosphate lyase activity by electrospray ionization-liquid chromatography/tandem mass spectrometry quantitation of (2E)-hexadecenal. *Anal Biochem* **408**, 12-18 (2011).
61. Serra, M. & Saba, J.D. Sphingosine 1-phosphate lyase, a key regulator of sphingosine 1-phosphate signaling and function. *Adv Enzyme Regul* **50**, 349-362 (2010).
62. Stoffel, W. & Grol, M. Chemistry and biochemistry of 1-desoxysphinganine 1-phosphonate (dihydrosphingosine-1-phosphonate). *Chem Phys Lipids* **13**, 372-388 (1974).
63. Schwab, S.R. & Cyster, J.G. Finding a way out: lymphocyte egress from lymphoid organs. *Nat Immunol* **8**, 1295-1301 (2007).
64. Bagdanoff, J.T., *et al.* Inhibition of sphingosine-1-phosphate lyase for the treatment of autoimmune disorders. *J Med Chem* **52**, 3941-3953 (2009).
65. Nussbaumer, P. Medicinal chemistry aspects of drug targets in sphingolipid metabolism. *ChemMedChem* **3**, 543-551 (2008).
66. Bandhuvula, P., Tam, Y.Y., Oskouian, B. & Saba, J.D. The immune modulator FTY720 inhibits sphingosine-1-phosphate lyase activity. *J Biol Chem* **280**, 33697-33700 (2005).
67. Mulgaonkar, S., *et al.* FTY720/cyclosporine regimens in de novo renal transplantation: a 1-year dose-finding study. *Am J Transplant* **6**, 1848-1857 (2006).
68. Salvadori, M., *et al.* FTY720 versus MMF with cyclosporine in de novo renal transplantation: a 1-year, randomized controlled trial in Europe and Australasia. *Am J Transplant* **6**, 2912-2921 (2006).
69. Tedesco-Silva, H., *et al.* Randomized controlled trial of FTY720 versus MMF in de novo renal transplantation. *Transplantation* **82**, 1689-1697 (2006).
70. Oravecz, T., Donoviel, M.S., Anderson, S.J., Carson, K., Swaffield, J., Liu, Q., Kimball, S.D., Piggott, J.R., Main, A.J., Zambrowicz, B.P., Sands, A.S., Turner, C.A., Augeri, D.J. . Genetic and Chemical Inhibition of Sphingosine Phosphate Lyase Results in Peripheral Lymphopenia and Alleviates Disease Development in Animal Models of Inflammation and Autoimmunity. in *Annual Meeting of the American Society of Hematology* (2007).
71. Brown, P., Augeri, D., Walke, D.W., Pappas, C., Brooks, B., Donoviel, M., Oravecz, T. LX2931: A Potential Small Molecule Treatment for Autoimmune Disorders. in *Annual Meeting of the American College of Rheumatology* (2008).
72. Fahy, E., *et al.* A comprehensive classification system for lipids. *J Lipid Res* **46**, 839-861 (2005).

73. Sot, J., Goni, F.M. & Alonso, A. Molecular associations and surface-active properties of short- and long-N-acyl chain ceramides. *Biochim Biophys Acta* **1711**, 12-19 (2005).
74. Ogretmen, B., *et al.* Biochemical mechanisms of the generation of endogenous long chain ceramide in response to exogenous short chain ceramide in the A549 human lung adenocarcinoma cell line. Role for endogenous ceramide in mediating the action of exogenous ceramide. *J Biol Chem* **277**, 12960-12969 (2002).
75. Gangoiti, P., *et al.* Control of metabolism and signaling of simple bioactive sphingolipids: Implications in disease. *Prog Lipid Res.*
76. Arana, L., Gangoiti, P., Ouro, A., Trueba, M. & Gomez-Munoz, A. Ceramide and ceramide 1-phosphate in health and disease. *Lipids Health Dis* **9**, 15.
77. Hannun, Y.A. & Obeid, L.M. The Ceramide-centric universe of lipid-mediated cell regulation: stress encounters of the lipid kind. *J Biol Chem* **277**, 25847-25850 (2002).
78. Mao, C. & Obeid, L.M. Ceramidases: regulators of cellular responses mediated by ceramide, sphingosine, and sphingosine-1-phosphate. *Biochim Biophys Acta* **1781**, 424-434 (2008).
79. Sun, W., *et al.* Upregulation of the human alkaline ceramidase 1 and acid ceramidase mediates calcium-induced differentiation of epidermal keratinocytes. *J Invest Dermatol* **128**, 389-397 (2008).
80. Xu, R., *et al.* Golgi alkaline ceramidase regulates cell proliferation and survival by controlling levels of sphingosine and S1P. *FASEB J* **20**, 1813-1825 (2006).
81. Okino, N., Tani, M., Imayama, S. & Ito, M. Purification and characterization of a novel ceramidase from *Pseudomonas aeruginosa*. *J Biol Chem* **273**, 14368-14373 (1998).
82. Ohnishi, Y., Okino, N., Ito, M. & Imayama, S. Ceramidase activity in bacterial skin flora as a possible cause of ceramide deficiency in atopic dermatitis. *Clin Diagn Lab Immunol* **6**, 101-104 (1999).
83. Tani, M., Sano, T., Ito, M. & Igarashi, Y. Mechanisms of sphingosine and sphingosine 1-phosphate generation in human platelets. *J Lipid Res* **46**, 2458-2467 (2005).
84. Kono, M., *et al.* Neutral ceramidase encoded by the *Asah2* gene is essential for the intestinal degradation of sphingolipids. *J Biol Chem* **281**, 7324-7331 (2006).
85. Mao, Z., *et al.* Alkaline ceramidase 2 (ACER2) and its product dihydro sphingosine mediate the cytotoxicity of N-(4-hydroxyphenyl)retinamide in tumor cells. *J Biol Chem* **285**, 29078-29090 (2010).
86. Mao, C., *et al.* Cloning and characterization of a novel human alkaline ceramidase. A mammalian enzyme that hydrolyzes phytoceramide. *J Biol Chem* **276**, 26577-26588 (2001).
87. Gatt, S. Enzymic Hydrolysis and Synthesis of Ceramides. *J Biol Chem* **238**, 3131-3133 (1963).
88. Bernardo, K.H., R. Zenk, T. Desnick, R. Ferlinz, K. Schuchman, E. Sandhoff, K. Purification, Characterization, and Biosynthesis of Human Acid Ceramidase. *J Biol Chem* **270**, 5 (1995).
89. Shtraizent, N., *et al.* Autoproteolytic cleavage and activation of human acid ceramidase. *J Biol Chem* **283**, 11253-11259 (2008).
90. Okino, N., *et al.* The reverse activity of human acid ceramidase. *J Biol Chem* **278**, 29948-29953 (2003).

91. Li, C.M., *et al.* Insertional mutagenesis of the mouse acid ceramidase gene leads to early embryonic lethality in homozygotes and progressive lipid storage disease in heterozygotes. *Genomics* **79**, 218-224 (2002).
92. Park, J.H. & Schuchman, E.H. Acid ceramidase and human disease. *Biochim Biophys Acta* **1758**, 2133-2138 (2006).
93. Ramsubir, S., *et al.* In vivo delivery of human acid ceramidase via cord blood transplantation and direct injection of lentivirus as novel treatment approaches for Farber disease. *Mol Genet Metab* **95**, 133-141 (2008).
94. Medin, J.A., *et al.* Retrovirus-mediated correction of the metabolic defect in cultured Farber disease cells. *Hum Gene Ther* **10**, 1321-1329 (1999).
95. Park, J.-H., Yoon, Suk. Ceramide, a crucial functional lipid, and its metabolic regulation by acid ceramidase. *Food Sci Biotechnol* **19**, 6 (2010).
96. Duan, R.D. & Nilsson, A. Metabolism of sphingolipids in the gut and its relation to inflammation and cancer development. *Prog Lipid Res* **48**, 62-72 (2009).
97. Zeidan, Y.H., *et al.* Molecular targeting of acid ceramidase: implications to cancer therapy. *Curr Drug Targets* **9**, 653-661 (2008).
98. Liu, X., *et al.* Acid ceramidase inhibition: a novel target for cancer therapy. *Front Biosci* **13**, 2293-2298 (2008).
99. Elojeimy, S., *et al.* Role of acid ceramidase in resistance to FasL: therapeutic approaches based on acid ceramidase inhibitors and FasL gene therapy. *Mol Ther* **15**, 1259-1263 (2007).
100. Seelan, R.S., *et al.* Human acid ceramidase is overexpressed but not mutated in prostate cancer. *Genes Chromosomes Cancer* **29**, 137-146 (2000).
101. Perry, D.K., *et al.* Serine palmitoyltransferase regulates de novo ceramide generation during etoposide-induced apoptosis. *J Biol Chem* **275**, 9078-9084 (2000).
102. Ruckhaberle, E., *et al.* Microarray analysis of altered sphingolipid metabolism reveals prognostic significance of sphingosine kinase 1 in breast cancer. *Breast Cancer Res Treat* **112**, 41-52 (2008).
103. Saad, A.F., *et al.* The functional effects of acid ceramidase overexpression in prostate cancer progression and resistance to chemotherapy. *Cancer Biol Ther* **6**, 1455-1460 (2007).
104. Ruckhaberle, E., *et al.* Acid ceramidase 1 expression correlates with a better prognosis in ER-positive breast cancer. *Climacteric* **12**, 502-513 (2009).
105. Sawai, H., *et al.* Ceramide-induced translocation of protein kinase C-delta and -epsilon to the cytosol. Implications in apoptosis. *J Biol Chem* **272**, 2452-2458 (1997).
106. Thon, L., Mathieu, S., Kabelitz, D. & Adam, D. The murine TRAIL receptor signals caspase-independent cell death through ceramide. *Exp Cell Res* **312**, 3808-3821 (2006).
107. Huang, Y., *et al.* Elevation of the level and activity of acid ceramidase in Alzheimer's disease brain. *Eur J Neurosci* **20**, 3489-3497 (2004).
108. He, X., Huang, Y., Li, B., Gong, C.X. & Schuchman, E.H. Deregulation of sphingolipid metabolism in Alzheimer's disease. *Neurobiol Aging* **31**, 398-408 (2010).
109. Greenberg, S.M., Koo, E.H., Selkoe, D.J., Qiu, W.Q. & Kosik, K.S. Secreted beta-amyloid precursor protein stimulates mitogen-activated protein kinase

- and enhances tau phosphorylation. *Proc Natl Acad Sci U S A* **91**, 7104-7108 (1994).
110. Grassme, H., Becker, K.A., Zhang, Y. & Gulbins, E. Ceramide in bacterial infections and cystic fibrosis. *Biol Chem* **389**, 1371-1379 (2008).
 111. Teichgraber, V., *et al.* Ceramide accumulation mediates inflammation, cell death and infection susceptibility in cystic fibrosis. *Nat Med* **14**, 382-391 (2008).
 112. Riethmuller, J., *et al.* Therapeutic efficacy and safety of amitriptyline in patients with cystic fibrosis. *Cell Physiol Biochem* **24**, 65-72 (2009).
 113. Stratford, S., Hoehn, K.L., Liu, F. & Summers, S.A. Regulation of insulin action by ceramide: dual mechanisms linking ceramide accumulation to the inhibition of Akt/protein kinase B. *J Biol Chem* **279**, 36608-36615 (2004).
 114. Chavez, J.A., Holland, W.L., Bar, J., Sandhoff, K. & Summers, S.A. Acid ceramidase overexpression prevents the inhibitory effects of saturated fatty acids on insulin signaling. *J Biol Chem* **280**, 20148-20153 (2005).
 115. Samad, F., Hester, K.D., Yang, G., Hannun, Y.A. & Bielawski, J. Altered adipose and plasma sphingolipid metabolism in obesity: a potential mechanism for cardiovascular and metabolic risk. *Diabetes* **55**, 2579-2587 (2006).
 116. Kolesnick, R. The therapeutic potential of modulating the ceramide/sphingomyelin pathway. *J Clin Invest* **110**, 3-8 (2002).
 117. Houben, E., *et al.* Kinetic characteristics of acidic and alkaline ceramidase in human epidermis. *Skin Pharmacol Physiol* **20**, 187-194 (2007).
 118. Bedia, C., *et al.* Cytotoxicity and acid ceramidase inhibitory activity of 2-substituted aminoethanol amides. *Chem Phys Lipids* **156**, 33-40 (2008).
 119. Selzner, M., *et al.* Induction of apoptotic cell death and prevention of tumor growth by ceramide analogues in metastatic human colon cancer. *Cancer Res* **61**, 1233-1240 (2001).
 120. Raisova, M., *et al.* Bcl-2 overexpression prevents apoptosis induced by ceramidase inhibitors in malignant melanoma and HaCaT keratinocytes. *FEBS Lett* **516**, 47-52 (2002).
 121. Samsel, L., *et al.* The ceramide analog, B13, induces apoptosis in prostate cancer cell lines and inhibits tumor growth in prostate cancer xenografts. *Prostate* **58**, 382-393 (2004).
 122. Szulc, Z.M., *et al.* Novel analogs of D-e-MAPP and B13. Part 1: synthesis and evaluation as potential anticancer agents. *Bioorg Med Chem* **16**, 1015-1031 (2008).
 123. Bielawska, A., *et al.* Novel analogs of D-e-MAPP and B13. Part 2: signature effects on bioactive sphingolipids. *Bioorg Med Chem* **16**, 1032-1045 (2008).
 124. Holman, D.H., *et al.* Lysosomotropic acid ceramidase inhibitor induces apoptosis in prostate cancer cells. *Cancer Chemother Pharmacol* **61**, 231-242 (2008).
 125. Liu, X., *et al.* Involvement of sphingolipids in apoptin-induced cell killing. *Mol Ther* **14**, 627-636 (2006).
 126. Granot, T., *et al.* Caspase-dependent and -independent cell death of Jurkat human leukemia cells induced by novel synthetic ceramide analogs. *Leukemia* **20**, 392-399 (2006).
 127. Elojeimy, S., *et al.* New insights on the use of desipramine as an inhibitor for acid ceramidase. *FEBS Lett* **580**, 4751-4756 (2006).
 128. Bai, A., *et al.* Synthesis and bioevaluation of omega-N-amino analogs of B13. *Bioorg Med Chem* **17**, 1840-1848 (2009).

129. Nikolova-Karakashian, M., Merrill, H. Ceramidases. *Methods in Enzymology* **311**, 8 (1999).
130. Babia, T., Kok, J.W., Hulstaert, C., de Weerd, H. & Hoekstra, D. Differential metabolism and trafficking of sphingolipids in differentiated versus undifferentiated HT29 cells. *Int J Cancer* **54**, 839-845 (1993).
131. Tani, M., Kita, K., Komori, H., Nakagawa, T. & Ito, M. Enzymatic synthesis of omega-amino-ceramide: preparation of a sensitive fluorescent substrate for ceramidase. *Anal Biochem* **263**, 183-188 (1998).
132. Tani, M.O., N. Mitsuke, S. Ito, M. Specific and Sensitive Assay for Alkaline and Neutral Ceramidases Involving C12-NBD-Ceramide. *J Biochem* **125**, 4 (1999).
133. Nieuwenhuizen, W.F., van Leeuwen, S., Gotz, F. & Egmond, M.R. Synthesis of a novel fluorescent ceramide analogue and its use in the characterization of recombinant ceramidase from *Pseudomonas aeruginosa* PA01. *Chem Phys Lipids* **114**, 181-191 (2002).
134. He, X., Dagan, A., Gatt, S. & Schuchman, E.H. Simultaneous quantitative analysis of ceramide and sphingosine in mouse blood by naphthalene-2,3-dicarboxyaldehyde derivatization after hydrolysis with ceramidase. *Anal Biochem* **340**, 113-122 (2005).
135. Momoi, T., Ben-Yoseph, Y. & Nadler, H.L. Substrate-specificities of acid and alkaline ceramidases in fibroblasts from patients with Farber disease and controls. *Biochem J* **205**, 419-425 (1982).
136. El Bawab, S., Bielawska, A. & Hannun, Y.A. Purification and characterization of a membrane-bound nonlysosomal ceramidase from rat brain. *J Biol Chem* **274**, 27948-27955 (1999).
137. Mitsutake, S., Kita, K., Okino, N. & Ito, M. [¹⁴C]ceramide synthesis by sphingolipid ceramide N-deacylase: new assay for ceramidase activity detection. *Anal Biochem* **247**, 52-57 (1997).
138. Nikolova-Karakashian, M., Morgan, E.T., Alexander, C., Liotta, D.C. & Merrill, A.H., Jr. Bimodal regulation of ceramidase by interleukin-1beta. Implications for the regulation of cytochrome p450 2C11. *J Biol Chem* **272**, 18718-18724 (1997).
139. Wu, B.X., Zeidan, Y.H. & Hannun, Y.A. Downregulation of neutral ceramidase by gemcitabine: Implications for cell cycle regulation. *Biochim Biophys Acta* **1791**, 730-739 (2009).
140. Nieuwenhuizen, W.F., van Leeuwen, S., Jack, R.W., Egmond, M.R. & Gotz, F. Molecular cloning and characterization of the alkaline ceramidase from *Pseudomonas aeruginosa* PA01. *Protein Expr Purif* **30**, 94-104 (2003).
141. Bedia, C., Casas, J., Garcia, V., Levade, T. & Fabrias, G. Synthesis of a novel ceramide analogue and its use in a high-throughput fluorogenic assay for ceramidases. *Chembiochem* **8**, 642-648 (2007).
142. Alberts, P.W.A.J.J.L.M.R.K.R.a.B. *Molecular Biology of the Cell*, (Garland Science, New York, 2002).
143. Foster, I. Cancer: A cell cycle defect. *Radiography* **14**, 5 (2008).
144. Vermeulen, K., Berneman, Z.N. & Van Bockstaele, D.R. Cell cycle and apoptosis. *Cell Prolif* **36**, 165-175 (2003).
145. Vermeulen, K., Van Bockstaele, D.R. & Berneman, Z.N. The cell cycle: a review of regulation, deregulation and therapeutic targets in cancer. *Cell Prolif* **36**, 131-149 (2003).
146. Maira, M.S., Pearson, M., Fabbro, D., and García-Echeverría C. *Cancer Biology*, (Elsevier, Basel, Switzerland, 2007).

147. Gülow, K., Kaminski, M., Krammer, H. *Apoptosis and Cancer Therapy*, (WILEY-VCH, Weinheim, Germany, 2006).
148. Walczak, H. & Sprick, M.R. Biochemistry and function of the DISC. *Trends Biochem Sci* **26**, 452-453 (2001).
149. Movassagh, M. & Foo, R.S. Simplified apoptotic cascades. *Heart Fail Rev* **13**, 111-119 (2008).
150. Korsmeyer, S.J., *et al.* Pro-apoptotic cascade activates BID, which oligomerizes BAK or BAX into pores that result in the release of cytochrome c. *Cell Death Differ* **7**, 1166-1173 (2000).
151. Youle, R.J. & Strasser, A. The BCL-2 protein family: opposing activities that mediate cell death. *Nat Rev Mol Cell Biol* **9**, 47-59 (2008).
152. Goldstein, J.C., Kluck, R.M. & Green, D.R. A single cell analysis of apoptosis. Ordering the apoptotic phenotype. *Ann N Y Acad Sci* **926**, 132-141 (2000).
153. Cory, S. & Adams, J.M. The Bcl2 family: regulators of the cellular life-or-death switch. *Nat Rev Cancer* **2**, 647-656 (2002).
154. Li, H., *et al.* Activation of caspase-2 in apoptosis. *J Biol Chem* **272**, 21010-21017 (1997).
155. Taha, T.A., Mullen, T.D. & Obeid, L.M. A house divided: ceramide, sphingosine, and sphingosine-1-phosphate in programmed cell death. *Biochim Biophys Acta* **1758**, 2027-2036 (2006).
156. Ogretmen, B. & Hannun, Y.A. Biologically active sphingolipids in cancer pathogenesis and treatment. *Nat Rev Cancer* **4**, 604-616 (2004).
157. Lee, J.Y., Leonhardt, L.G. & Obeid, L.M. Cell-cycle-dependent changes in ceramide levels preceding retinoblastoma protein dephosphorylation in G2/M. *Biochem J* **334 (Pt 2)**, 457-461 (1998).
158. Dbaibo, G.S., *et al.* Retinoblastoma gene product as a downstream target for a ceramide-dependent pathway of growth arrest. *Proc Natl Acad Sci U S A* **92**, 1347-1351 (1995).
159. Lin, S.S., *et al.* PP2A regulates BCL-2 phosphorylation and proteasome-mediated degradation at the endoplasmic reticulum. *J Biol Chem* **281**, 23003-23012 (2006).
160. Ogretmen, B. Sphingolipids in cancer: regulation of pathogenesis and therapy. *FEBS Lett* **580**, 5467-5476 (2006).
161. Bose, R., *et al.* Ceramide synthase mediates daunorubicin-induced apoptosis: an alternative mechanism for generating death signals. *Cell* **82**, 405-414 (1995).
162. Lin, C.F., Chen, C.L. & Lin, Y.S. Ceramide in apoptotic signaling and anticancer therapy. *Curr Med Chem* **13**, 1609-1616 (2006).
163. Xin, M. & Deng, X. Protein phosphatase 2A enhances the proapoptotic function of Bax through dephosphorylation. *J Biol Chem* **281**, 18859-18867 (2006).
164. Reynolds, C.P., Maurer, B.J. & Kolesnick, R.N. Ceramide synthesis and metabolism as a target for cancer therapy. *Cancer Lett* **206**, 169-180 (2004).
165. Verheij, M., *et al.* Requirement for ceramide-initiated SAPK/JNK signalling in stress-induced apoptosis. *Nature* **380**, 75-79 (1996).
166. Stancevic, B. & Kolesnick, R. Ceramide-rich platforms in transmembrane signaling. *FEBS Lett* **584**, 1728-1740 (2010).
167. Oskouian, B. & Saba, J.D. Cancer treatment strategies targeting sphingolipid metabolism. *Adv Exp Med Biol* **688**, 185-205 (2010).

168. Grassme, H., Cremesti, A., Kolesnick, R. & Gulbins, E. Ceramide-mediated clustering is required for CD95-DISC formation. *Oncogene* **22**, 5457-5470 (2003).
169. Schutze, S., Tchikov, V. & Schneider-Brachert, W. Regulation of TNFR1 and CD95 signalling by receptor compartmentalization. *Nat Rev Mol Cell Biol* **9**, 655-662 (2008).
170. Grassme, H., Schwarz, H. & Gulbins, E. Molecular mechanisms of ceramide-mediated CD95 clustering. *Biochem Biophys Res Commun* **284**, 1016-1030 (2001).
171. Cancer Facts and Figures. in *American Cancer Society* (2008).
172. Vogelstein, B. & Kinzler, K.W. Cancer genes and the pathways they control. *Nat Med* **10**, 789-799 (2004).
173. Hanahan, D. & Weinberg, R.A. The hallmarks of cancer. *Cell* **100**, 57-70 (2000).
174. Wendell-Smith, C. Terminology of the prostate and related structures. *Clin Anat* **13**, 207-213 (2000).
175. McNeal, J.E. Normal histology of the prostate. *Am J Surg Pathol* **12**, 619-633 (1988).
176. Timms, B.G. Prostate development: a historical perspective. *Differentiation* **76**, 565-577 (2008).
177. Cunha, G.R., *et al.* The endocrinology and developmental biology of the prostate. *Endocr Rev* **8**, 338-362 (1987).
178. Capasso, L.L. Antiquity of cancer. *Int J Cancer* **113**, 2-13 (2005).
179. Lilja, H., Ulmert, D. & Vickers, A.J. Prostate-specific antigen and prostate cancer: prediction, detection and monitoring. *Nat Rev Cancer* **8**, 268-278 (2008).
180. Epstein, J.I. An update of the Gleason grading system. *J Urol* **183**, 433-440 (2010).
181. Ohori, M., Wheeler, T.M. & Scardino, P.T. The New American Joint Committee on Cancer and International Union Against Cancer TNM classification of prostate cancer. Clinicopathologic correlations. *Cancer* **74**, 104-114 (1994).
182. Stages of prostate cancer. in <http://www.cancer.gov/cancertopics/pdq/treatment/prostate/Patient/page2> (National Cancer Institute, USA, 2010).
183. Shen, M.M. & Abate-Shen, C. Molecular genetics of prostate cancer: new prospects for old challenges. *Genes Dev* **24**, 1967-2000 (2010).
184. Petrylak, D.P. New paradigms for advanced prostate cancer. *Rev Urol* **9 Suppl 2**, S3-S12 (2007).
185. Pashayan, N., Powles, J., Brown, C. & Duffy, S.W. Excess cases of prostate cancer and estimated overdiagnosis associated with PSA testing in East Anglia. *Br J Cancer* **95**, 401-405 (2006).
186. Prostate Cancer -UK incidence statistics. in <http://info.cancerresearchuk.org/cancerstats/types/prostate/incidence/>, (Cancer Research UK, 2008).
187. Liu, X., *et al.* Acid ceramidase upregulation in prostate cancer: role in tumor development and implications for therapy. *Expert Opin Ther Targets* **13**, 1449-1458 (2009).
188. Park, J.H., *et al.* KLF6 is one transcription factor involved in regulating acid ceramidase gene expression. *Biochim Biophys Acta* **1732**, 82-87 (2005).

189. Dong, J.T. Chromosomal deletions and tumor suppressor genes in prostate cancer. *Cancer Metastasis Rev* **20**, 173-193 (2001).
190. Mahdy, A.E., *et al.* Acid ceramidase upregulation in prostate cancer cells confers resistance to radiation: AC inhibition, a potential radiosensitizer. *Mol Ther* **17**, 430-438 (2009).
191. Maceyka, M., Alvarez, S.E., Milstien, S. & Spiegel, S. Filamin A links sphingosine kinase 1 and sphingosine-1-phosphate receptor 1 at lamellipodia to orchestrate cell migration. *Mol Cell Biol* **28**, 5687-5697 (2008).
192. Oskouian, B. & Saba, J. Sphingosine-1-phosphate metabolism and intestinal tumorigenesis: lipid signaling strikes again. *Cell Cycle* **6**, 522-527 (2007).
193. Goddard P, R.J. Recent advances in enzyme assays. *TRENDS in Biotechnology* **22**, 7 (2004).
194. Kikuchi K, T.S., and Hilvert D. Albumin-Catalyzed Proton Transfer. *J. Am. Chem. Soc.* **118**, 2 (1996).
195. Fedor LR, G.W. Base-Catalyzed B-Elimination Reactions in Aqueous Solution.
- V. Elimination from 4- (p-Substituted-phenoxy) -2-butanones'. *J Am Chem Soc* **93**, 5 (1971).
196. Tani, M., *et al.* Molecular cloning of the full-length cDNA encoding mouse neutral ceramidase. A novel but highly conserved gene family of neutral/alkaline ceramidases. *J Biol Chem* **275**, 11229-11234 (2000).
197. Bedia, C., Camacho, L., Abad, J.L., Fabrias, G. & Levade, T. A simple fluorogenic method for determination of acid ceramidase activity and diagnosis of Farber disease. *J Lipid Res* (2010).
198. Hara, S., *et al.* p53-Independent ceramide formation in human glioma cells during gamma-radiation-induced apoptosis. *Cell Death Differ* **11**, 853-861 (2004).
199. Morselli, E., *et al.* Mutant p53 protein localized in the cytoplasm inhibits autophagy. *Cell Cycle* **7**, 3056-3061 (2008).
200. Nieves, I.G., M.; Abad, J. L.; Delgado, A. An Unexpected Access to a New Sphingoid Base Containing a Vinyl Sulfide Unit. *Synlett*, 2 (2010).
201. Kraveka, J.M., *et al.* Involvement of dihydroceramide desaturase in cell cycle progression in human neuroblastoma cells. *J Biol Chem* **282**, 16718-16728 (2007).
202. Schiffmann, S., *et al.* The selective COX-2 inhibitor celecoxib modulates sphingolipid synthesis. *J Lipid Res* **50**, 32-40 (2009).
203. Signorelli, P., *et al.* Dihydroceramide intracellular increase in response to resveratrol treatment mediates autophagy in gastric cancer cells. *Cancer Lett* **282**, 238-243 (2009).
204. Triola, G., Fabrias, G., Casas, J. & Llebaria, A. Synthesis of cyclopropene analogues of ceramide and their effect on dihydroceramide desaturase. *J Org Chem* **68**, 9924-9932 (2003).
205. Triola, G., Fabrias, G. & Llebaria, A. Synthesis of a Cyclopropene Analogue of Ceramide, a Potent Inhibitor of Dihydroceramide Desaturase This work was supported by the Direccion General de Ensenanza Superior e Investigacion Cientifica (grant PB97-1171) and the Departament d'Universitats, Recerca i Societat de la Informacio, Generalitat de Catalunya (grant 1999-SGR 00187 and a Predoctoral fellowship to G.T.). We thank Dr. J. Casas, Dr. A. Delgado, and Dr. J. Joglar for their help in different aspects of this work. *Angew Chem Int Ed Engl* **40**, 1960-1962 (2001).

206. Munoz-Olaya, J.M., *et al.* Synthesis and biological activity of a novel inhibitor of dihydroceramide desaturase. *ChemMedChem* **3**, 946-953 (2008).
207. Antoon JW, L.J., Ponnappakkam AP, Gestaut M, Foroozesh M and Beckman B. Novel d-erythro N-octanoyl sphingosine analogs as chemo- and endocrine-resistant breast cancer therapeutics *Cancer Chemother and Pharmacol* **65**, 5 (2010).
208. Antoon JW, L.J., Gestaut MM, Burow ME, Beckman BS, Foroozesh M. Design, Synthesis, and Biological Activity of a Family of Novel Ceramide Analogs in Chemoresistant Breast Cancer Cells. *J Med Chem* **52**, 5 (2009).
209. Sims, K.F., K.; Symolon, H.; Zheng, W.; Munter, E.; Momin, A.; Pack, C.; Haynes, C.; Kelly, S.; Allegood, J.; Wang, E.; Merrill, A. H. Fenretinide induces lethal autophagy via a novel ensemble of life and death regulators: dihydroceramide and sphinganine versus sphinganine 1-phosphate. in *ASBMB Annual Meeting*, Vol. 21 779.776 (FASEB J, Washington D.C., 2007).
210. Turner LS, C.J., Beckham TH, Keane TE, Norris JS, Liu X. Autophagy is increased in prostate cancer cells overexpressing acid ceramidase and enhances resistance to C(6) ceramide. *Prostate Cancer Prostatic Dis* (2010).
211. El Hilali, N., Rubio, N., Martinez-Villacampa, M. & Blanco, J. Combined noninvasive imaging and luminometric quantification of luciferase-labeled human prostate tumors and metastases. *Lab Invest* **82**, 1563-1571 (2002).
212. Kozlowski, J.M., *et al.* Metastatic behavior of human tumor cell lines grown in the nude mouse. *Cancer Res* **44**, 3522-3529 (1984).
213. Lee, S.A., *et al.* Tetraspanin TM4SF5 mediates loss of contact inhibition through epithelial-mesenchymal transition in human hepatocarcinoma. *J Clin Invest* **118**, 1354-1366 (2008).
214. Hannun, Y.A. & Luberto, C. Ceramide in the eukaryotic stress response. *Trends Cell Biol* **10**, 73-80 (2000).
215. Kanno, T. & Nishizaki, T. Sphingosine induces apoptosis in hippocampal neurons and astrocytes by activating caspase-3/-9 via a mitochondrial pathway linked to SDK/14-3-3 Protein/Bax/Cytochrome c. *J Cell Physiol* (2010).
216. Ohta, H., *et al.* Induction of apoptosis by sphingosine in human leukemic HL-60 cells: a possible endogenous modulator of apoptotic DNA fragmentation occurring during phorbol ester-induced differentiation. *Cancer Res* **55**, 691-697 (1995).
217. Shirahama, T., *et al.* Sphingosine induces apoptosis in androgen-independent human prostatic carcinoma DU-145 cells by suppression of bcl-X(L) gene expression. *FEBS Lett* **407**, 97-100 (1997).
218. Tsuji, T., *et al.* Epithelial-mesenchymal transition induced by growth suppressor p12CDK2-AP1 promotes tumor cell local invasion but suppresses distant colony growth. *Cancer Res* **68**, 10377-10386 (2008).
219. Hermann, P.C., *et al.* Distinct populations of cancer stem cells determine tumor growth and metastatic activity in human pancreatic cancer. *Cell Stem Cell* **1**, 313-323 (2007).

VII.RESUMEN

Introducción

Los esfingolípidos son los principales componentes de la membrana plasmática de las células eucariotas. Inicialmente fueron considerados simples componentes estructurales de la membrana, sin embargo, actualmente se sabe que participan en la regulación de importantes procesos celulares como proliferación, crecimiento, migración, diferenciación, senescencia y apoptosis. Algunos miembros de la familia de los esfingolípidos que poseen actividad biológica son: la ceramida (Cer), la ceramida-1-fosfato (C1P), la esfingosina (So) y la esfingosina-1-fosfato (S1P) entre otros. Estructuralmente los esfingolípidos están compuestos por una molécula de esfingosina o esfinganina unida a través de un enlace amida a un ácido graso. Los esfingolípidos más complejos (p. ej. esfingomielina, cerebrósidos, gangliósidos, etc.) contienen sustituyentes polares unidos al grupo hidroxilo en C1.

Metabolismo de los esfingolípidos

La ceramida está considerada como la molécula central del metabolismo de los esfingolípidos. La ceramida puede ser generada por dos mecanismos principales: a) la síntesis *de novo*, la cual es una ruta anabólica que comienza con la condensación de una molécula de serina con el palmitoil-CoA para formar 3-cetoesfinganina. Esta reacción es catalizada por la enzima serina palmitoiltransferasa. Posteriormente, la reducción de la 3-cetoesfinganina para formar esfinganina es catalizada por la cetoesfinganina reductasa. A continuación la ceramida sintasa cataliza la unión de la esfinganina con un ácido graso para formar dihidroceramida, la cual a su vez es transformada a ceramida por la dihidroceramida desaturasa.

b) la vía catabólica es otra vía de formación de la ceramida. Esta vía necesita de la activación de la enzima esfingomielinasa, que cataliza la degradación de esfingomielina a ceramida y fosfocolina. La ceramida también puede formarse a partir de la degradación de esfingolípidos complejos, principalmente glicosfingolípidos.

La ceramida, independientemente de la vía por la cual es generada, puede ser hidrolizada por las enzimas ceramidasa, dando como resultado esfingosina. La esfingosina puede ser fosforilada por las enzimas esfingosina quinasa 1 o 2, produciendo esfingosina-1-fosfato. Finalmente la esfingosina-1-fosfato puede ser desfosforilada por fosfatasas específicas regenerando la esfingosina, que puede dar lugar a ceramida mediante las ceramida sintasas. Finalmente, la esfingosina-1-fosfato también puede ser metabolizada de manera irreversible por la enzima esfingosina-1- fosfato liasa (SPL).

Algunas de las funciones biológicas de la esfingosina-1-fosfato (S1P) son: la regulación de la migración celular, la diferenciación y la supervivencia celular. La señalización mediada por la S1P tiene un papel muy importante promoviendo la maduración y permeabilidad vascular, además de regular la salida de los linfocitos del timo y de los órganos linfoides periféricos. La S1P ejerce sus funciones actuando como ligando de receptores extracelulares y como segundo mensajero intracelular.

Este trabajo esta centrado particularmente en las enzimas esfingosina-1- fosfato liasa y ceramidasa ácida, de las cuales se hablará más a fondo.

Esfingosina fosfato liasa

La esfingosina-1-fosfato liasa (SPL) es la enzima responsable de la degradación de la esfingosina-1-fosfato, formando hexadecenal y etanolamina, regulando los niveles de este esfingolípido bioactivo. La SPL se localiza en el retículo endoplásmico como una proteína de membrana, con el dominio catalítico de unión al piridoxal fosfato de cara al citosol. En diversos tejidos de ratas y ratones se ha observado una alta expresión de la SPL en el intestino delgado, colon, timo y bazo, mientras que en el corazón, músculo y cerebro se expresa poco. Esta enzima está codificada por el gen *SGPL1*.

Como se ha dicho, los niveles de S1P son determinantes en la regulación de la supervivencia celular, por lo que es necesario un estricto control de sus niveles intra y extracelulares. Así, un descontrol de la función de la SPL puede contribuir a la patofisiología de algunas enfermedades como el cáncer.

Se ha encontrado una reducción significativa en la expresión y la actividad de la SPL en cortes histológicos de cáncer de colon humano. Adicionalmente, se ha encontrado una disminución en la expresión del gen *SGPL1* en tejidos de tumores metastáticos. Estos hallazgos sugieren que la SPL puede actuar como supresor de tumores y quizá este relacionada con las vías de supervivencia de las células tumorales.

Por su papel en la migración de los linfocitos, la SPL también ha sido señalada como posible diana terapéutica en enfermedades inflamatorias y autoinmunes, así como en inmunosupresión en trasplantes. De esta manera, es importante disponer de ensayos de actividad sencillos y confiables, tanto para la determinación de los niveles de actividad de SPL en tejidos como para la identificación y caracterización bioquímica de inhibidores. En este sentido se han hecho muchos esfuerzos para desarrollar métodos para determinar la actividad de la SPL. Los primeros que fueron utilizados se basaban en el empleo de sustratos radioactivos análogos a la S1P. Posteriormente se desarrollaron dos métodos que empleaban sustratos fluorescentes (BODIPY y NBD), pero dichos métodos no son convenientes para el cribado de quimiotecas, ya que no son adaptables como métodos de alto rendimiento.

La modulación de la actividad de la SPL a través de inhibidores parece prometedora para el desarrollo de terapias que requieran inmunomodulación, como en el caso de las enfermedades autoinmunes. Sin embargo, hasta la fecha hay muy pocas moléculas descritas que inhiban a la SPL, entre ellas se encuentran los compuestos DOP, THI y FTY720, todos ellos inhibidores no específicos de la SPL. Además, su intervalo de acción se encuentra en concentraciones muy elevadas. Recientemente la compañía farmacéutica LEXICON ha sintetizado el compuesto LX2931, que está siendo evaluado en pruebas clínicas para el tratamiento de la artritis reumatoide. Es sorprendente que hasta el momento, el avance en el desarrollo de nuevos inhibidores esté tan retrasado, por lo que la disponibilidad de un ensayo que permita realizar un gran número de ensayos en poco tiempo permitirá un avance sustancial en la búsqueda de dichos inhibidores.

Ceramida

Diversos estudios han demostrado que la Cer está implicada en la regulación de la apoptosis, el paro del ciclo celular, la diabetes, la resistencia a la insulina, algunos desordenes neurodegenerativos y la aterosclerosis. Los niveles de Cer están controlados por diversas enzimas encargadas de su síntesis y degradación, en particular explicaremos la función de las enzimas ceramidasa (CDasas). Las CDasas están encargadas de la hidrólisis de la ceramida, produciendo esfingosina y un ácido graso.

Para su estudio, las CDasas se han dividido en tres grupos de acuerdo a su pH óptimo; ceramidasa ácida, neutras o alcalinas.

Ceramidasa ácida

Esta enzima se encuentra principalmente en el lisosoma. Esta formada por dos subunidades y se encuentra codificada por el gen *ASAH1* en humanos. La deficiencia genética de la ceramidasa ácida produce una acumulación de esfingolípidos en el lisosoma, causando la enfermedad de Farber. Los síntomas típicos de este padecimiento son: articulaciones deformadas, nódulos subcutáneos y muerte a una edad temprana. El diagnóstico de la enfermedad de Farber se realiza comprobando la reducción de la actividad de la ceramidasa ácida o niveles anormalmente altos de ceramida en células cultivadas, muestras de biopsias u orina. Actualmente no existe tratamiento para esta enfermedad.

La ceramidasa ácida también ha sido asociada a otras enfermedades; por ejemplo la enfermedad de Alzheimer, en la cual se ha reportado una disminución significativa de la actividad y expresión de la ceramidasa ácida.

Adicionalmente, en diversos estudios se ha relacionado la inhibición de la ceramidasa ácida con la inducción de la apoptosis en condiciones de estrés celular. La ceramidasa ácida es una de las enzimas clave en el control del metabolismo de los esfingolípidos. Su inhibición produce la acumulación de ceramida desencadenando la apoptosis, por lo que su ha convertido en una posible diana terapéutica en el cáncer. En este sentido se han realizado diversos esfuerzos en la búsqueda de inhibidores.

Dentro de estos compuestos la *N*-oleoiletanolamina (NOE) ha sido el más utilizado en las publicaciones científicas. Sin embargo, presenta una baja potencia y pobre selectividad, por lo que no presenta utilidad terapéutica.

Además de la NOE, se han sintetizado algunos derivados de esta molécula en un esfuerzo por aumentar su potencia. En particular, nuestro grupo ha identificado algunos de ellos. Existe otro importante grupo de inhibidores de la ceramidasa ácida: el compuesto B13 y sus derivados, que han probado no ser específicos al afectar la actividad de las ceramidasa neutra o alcalinas.

Algunos de estos inhibidores han sido utilizados en experimentos *in vitro* de sensibilización a radioterapia en modelos de cáncer de próstata y melanoma, obteniéndose resultados muy prometedores. Por esto es importante el descubrimiento y caracterización de nuevos y mejores inhibidores y para este fin se han descrito muchas maneras de determinar la actividad de la ceramidasa ácida. Entre los métodos más antiguos se encuentra el uso de ceramida con marcaje radioactivo como sustrato. Para evitar los inconvenientes de trabajar con radiactividad, se han desarrollado métodos que emplean sustratos fluorescentes como Cer-NBD, Cer-BODIPY y recientemente nuestro grupo ha publicado el uso del sustrato del compuesto RBM14 adaptado a un ensayo de alto rendimiento.

El sustrato RBM14 puede ser hidrolizado por las ceramidasa *in vitro* e *in situ*, liberando un grupo aminodiol que es oxidado por vías químicas produciendo un aldehído cumarínico susceptible de β -oxidación espontánea que finalmente libera el compuesto fluorescente umbeliferona, que puede ser detectado en un fluorímetro.

Por otro lado, la sobre-expresión de la ceramidasa ácida se ha documentado en diversos tipos de cánceres, como el cáncer de próstata y melanoma. En particular, en un 60 % de tumores de pacientes con cáncer de próstata avanzados se ha demostrado por Western blot la sobre-expresión de la ceramidasa ácida. Este hecho también ha sido detectado en líneas derivadas de cáncer de próstata, como PC3 y DU145.

Las consecuencias funcionales del aumento en la expresión y función de la ceramidasa ácida se han estudiado en diversos trabajos en los cuales se demostraba que las células que expresaban altos niveles de ceramidasa ácida mostraban un aumento de la proliferación en condiciones de bajas concentraciones de nutrientes, así como un aumento en el grado de migración en estudios de invasividad. La administración de inhibidores de la ceramidasa ácida o el silenciamiento del gen *ASAH1* mediante siARN revierten este comportamiento, relacionando directamente a la ceramidasa ácida con estos cambios fenotípicos.

Sin embargo, el mecanismo exacto de la tumorigenicidad aumentada, así como del incremento de la migración celular inducida por la sobre-expresión de la ceramidasa ácida aún no ha sido dilucidado.

Objetivos

Los objetivos generales de este trabajo fueron:

1. Desarrollar ensayos de actividad para la ceramidasa ácida y la esfingosina fosfato liasa y explorar sus posibles aplicaciones como biomarcadores, así como en la identificación de nuevos inhibidores enzimáticos. Este último punto incluye los siguientes objetivos específicos:

- a) Desarrollar ensayos enzimáticos para la esfingosina fosfato liasa
- b) Optimizar el ensayo fluorogénico para la ceramidasa ácida y utilizar el ensayo optimizado en: el diagnóstico de la enfermedad de Farber, como una herramienta en la caracterización fenotípica de las células tumorales y en la búsqueda de inhibidores por cribado masivo de quimiotecas.

2. Investigar el papel de la ceramidasa ácida en un modelo de cáncer de próstata y explorar los usos terapéuticos de los inhibidores de la ceramidasa ácida.

Resultados y Discusión

1. Desarrollo de ensayos enzimáticos para la enzima esfingosina-1-fosfato liasa

1.1. Determinación de la enzima esfingosina-1-fosfato liasa por fluorimetría.

Se ha desarrollado un ensayo para determinar la actividad de esta enzima basado en la utilización del compuesto RBM13, un análogo del sustrato natural en el cual la cadena C6-C18 de la esfinganina es reemplazada por un sistema cumarínico. La hidrólisis del RBM13 catalizada por la esfingosina-1-fosfato liasa produce un aldehído cumarínico, el cual sufre beta eliminación espontánea a un pH neutro o alcalino, liberando umbeliferona, que es fluorescente. Este método permite el uso de microplacas facilitando la búsqueda a gran escala de potenciales inhibidores de la esfingosina fosfato liasa.

Expresión de la enzima recombinante esfingosina fosfato liasa. Esta enzima se encuentra poco expresada en la mayor parte de los tejidos y, además posee una baja actividad. Para solventar la falta de una buena fuente enzimática, las bacterias *E. coli* TOP10 fueron transformadas con la construcción PVB001, que contiene un fragmento activo del gen *SGPL1*, reduciendo significativamente las cantidades de proteína necesarias para obtener una buena respuesta utilizando el ensayo fluorogénico.

1.2. Determinación de la actividad de la esfingosina-1-fosfato liasa por cromatografía de gases acoplada a espectrometría de masas

Como resultado de la moderada afinidad de la esfingosina fosfato liasa por el sustrato RBM13, el ensayo fluorogénico permite una rápida identificación de los inhibidores de la esfingosina fosfato liasa, pero no su caracterización cinética. Esta debe llevarse a cabo con un sustrato mínimamente modificado, por lo que nos propusimos desarrollar un nuevo ensayo para medir la actividad de la esfingosina fosfato liasa utilizando C17-esfinganina-1-fosfato como sustrato y que detecta el producto de la hidrólisis enzimática, el aldehído C17, por medio de cromatografía de gases acoplada a espectrometría de masas.

Este ensayo permitirá la caracterización cinética de los inhibidores identificados por medio del ensayo fluorogénico.

2. Optimización y uso del ensayo fluorogénico para la ceramidasa ácida.

En las condiciones del ensayo fluorogénico publicado para la determinación de la ceramidasa ácida, la relación respuesta/ruido fondo no era óptima. Para incrementarla, se abordó la mejora de la etapa de oxidación del aminodiol a aldehído, variando las concentraciones del agente oxidante, NaIO_4 , así como las condiciones de pH de la reacción. Las condiciones óptimas encontradas para esta reacción de oxidación fueron: medio básico, 25 μL de MeOH y 25 μL de NaIO_4 2.5 mg/mL.

A fin de mejorar aún más las prestaciones del ensayo, se abordó la determinación de la actividad de la ceramidasa ácida en función de la longitud de la cadena del sustrato RBM14. Para ello, se sintetizaron análogos del RBM14 (C16) con cadenas de *N*-acilo de 4, 8, 10, 12, 14 y 24 átomos de carbono. Seguidamente, se determinó su hidrólisis por las distintas ceramidases, a fin de conocer su especificidad.

2.1. Hidrólisis de los sustratos RBM14 por la ceramidasa ácida.

Los primeros experimentos se llevaron a cabo en células Moh pAS (enfermedad de Farber), comparándolas con las mismas células transducidas para expresar ceramidasa ácida funcional (Moh pAS 10X), tanto utilizando lisados celulares como células intactas. Como era esperado, en las células Moh la fluorescencia liberada fue significativamente más baja que la producida por las Moh pAS 10X, indicando que la ceramidasa ácida es la enzima responsable de la hidrólisis de los análogos de RBM14. Además, los resultados concuerdan con los datos descritos previamente en la literatura para la especificidad de sustrato de la ceramidasa ácida. Los mejores sustratos en las células Moh pAS 10x fueron los análogos de RBM14 de C10, C12 y C14, tanto *in vitro* como en células intactas. Los tres compuestos fueron hidrolizados más eficientemente que el original de C16 *in vitro*, mientras que la hidrólisis en células intactas fue mejor para RBM14 C12 y C14, pero similar a C10.

Es posible que en células intactas, el grupo *N*-acilo del sustrato administrado, sea modificado por la ruta metabólica de desacilación/reacilación, de forma que el sustrato enzimático real sea una mezcla de análogos de RBM14 con diferente longitud de cadena acilo. Esto explicaría la diferencia de los resultados obtenidos *in vitro* y en las células intactas

2.2. Hidrólisis de los análogos RBM14 por otras ceramidases en células intactas e *in vitro*

Las evidencias experimentales sugieren que las 5 ceramidases descritas tienen diferentes especificidades de sustrato. Para investigar si los análogos de RBM14 son hidrolizados por las ceramidases neutra o alcalinas, las células Moh pAS fueron transfectadas para sobreexpresar la ceramidasa neutra y las ceramidases alcalinas 1, 2 y 3 (ACER1, ACER2 y ACER3). Ninguno de los sustratos RBM14 fue metabolizado por las ACER1, ACER2 ó ACER3 ni en células intactas ni *in vitro*. Sin embargo, existen artículos que afirman que estas enzimas prefieren ceramidas de cadena larga. Por el contrario, los compuestos RBM14 C8, C10, C12, C14, C16 fueron hidrolizados por la ceramidasa neutra, siendo el derivado de C10 el mejor sustrato en células intactas. Cabe resaltar al sustrato C8 como específico para la ceramidasa neutra, ya que no es hidrolizado por ninguna otra ceramidasa. En los experimentos realizados *in vitro* para la ceramidasa neutra los resultados fueron semejantes a los obtenidos en células intactas.

2.3. Aplicación del ensayo fluorogénico al diagnóstico de la enfermedad de Farber

Una vez concluido el estudio previo de optimización del ensayo, se decidió utilizar el sustrato RBM14 C12 como herramienta en el diagnóstico de la enfermedad de Farber. Hasta ahora el diagnóstico de la enfermedad de Farber se basa en la confirmación bioquímica de la actividad deficiente de la ceramidasa ácida y, posteriormente, por la caracterización de los defectos moleculares en el gen *ASAH1*. Los métodos existentes para determinar la actividad de la ceramidasa ácida presentan muchas desventajas, ya que es necesario trabajar con sustratos marcados radiactivamente, los cuales son muy pocos solubles en medio acuoso, requiriendo el uso de detergentes.

Otro método empleado es la determinación de la acumulación de ceramida, pero requiere de tediosos métodos cromatográficos. El uso del ensayo fluorogénico de la ceramidasa ácida en el diagnóstico de la enfermedad de Farber fue realizado en colaboración con el grupo del Dr. T. Levade (INSERM, Toulouse). Utilizando células derivadas de enfermos de Farber y comparándolas con células normales se comprobó que la fluorescencia liberada por las primeras era prácticamente indetectable, mientras que en células con ceramidasa ácida activa el sustrato liberaba fluorescencia tanto en células intactas como en lisados celulares.

Al medir la actividad en lisados celulares, sólo se detectaba fluorescencia a pH ácido. Además, los resultados de actividad de distintas líneas de enfermos de Farber coincidieron con los obtenidos mediante otros ensayos. Todo ello confirmó la utilidad del sustrato RBM14 C12 en el diagnóstico de la enfermedad de Farber.

Las principales ventajas de este método incluyen: no requiere sustancias radiactivas ni instrumentos para la detección de radioactividad, el sustrato es soluble en medio acuoso y es estable cuando se almacena a -20°C hasta por lo menos 6 meses y finalmente, no requiere de la separación de producto y sustrato evitando así procesos tediosos como cromatografía de capa fina, o más complejos, como cromatografía de líquidos o cromatografía de gases

2.4. Aplicación del ensayo fluorogénico de actividad de la ceramidasa ácida en células cancerosas

Las alteraciones en el metabolismo de los esfingolípidos han sido descritas en gran cantidad de procesos cancerosos. Por ejemplo, en cánceres de colon, gliomas y cáncer de ovario la cantidad de ceramida se encuentra disminuida, y las ceramidases contribuyen a este desequilibrio.

En este contexto, la hidrólisis de los análogos RBM14 fue evaluada en diversas líneas celulares tumorales para poder identificar diferencias en la actividad ceramidasa ácida que pudieran ser relevantes en el diagnóstico o pronóstico del cáncer. Los ensayos se realizaron en células intactas y en lisados celulares. Las líneas celulares utilizadas fueron a) MDA-MB231, derivada de cáncer de mama, negativa para el receptor de estrógenos alfa y altamente invasiva;

b) IMR-32, derivada de neuroblastoma humano; c) HCT116, derivada de cáncer de colon.

De esta línea se pudo disponer de dos clones diferentes: el 379 (p53^{-/-}) y el 40-16 (p53^{+/+}); d) PC3/Mc (altamente metastásica y poco invasiva) y PC3/S (no metastásica y altamente invasiva), ambas derivadas de cáncer de próstata. La hidrólisis de los sustratos cumarínicos en las células HCT116 379 fue 3-4 veces menor a la obtenida con las células HCT116 40-16, mientras que las células PC3/S presentaron una actividad 2-4 veces menor que las PC3/Mc tanto en experimentos *in vitro* como en células intactas. Las células MDA MB231 y las IMR32 no mostraron una actividad ceramidasa importante comparado con otras líneas. Así, las células PC3/Mc fueron seleccionadas para investigar más a fondo las consecuencias de la inhibición de la ceramidasa ácida.

2.5. Aplicación del ensayo fluorogénico de la ceramidasa ácida a la búsqueda, identificación y caracterización de inhibidores enzimáticos.

La inhibición específica de la ceramidasa ácida incrementa las señales pro-apoptóticas a través de la acumulación de ceramida, por lo que la ceramidasa ácida ha sido señalada como diana terapéutica en el cáncer, utilizándose inhibidores de esta enzima en conjunto con la quimioterapia, particularmente en los casos de resistencia a los fármacos. Por lo tanto, la búsqueda y caracterización de inhibidores potentes y específicos para la ceramidasa ácida es de vital importancia y el ensayo fluorogénico de la ceramidasa ácida permite la búsqueda eficiente de inhibidores dentro de quimiotecas.

En nuestro laboratorio se han identificado diversos inhibidores de la ceramidasa ácida, entre los que destacan los compuestos pertenecientes a las familias RBM1 y RBM2. En particular, los compuestos RBM1-12, RBM1-13 y SABRAC, que mostraron una IC₅₀ de 0.3, 60 y 0.05 μM respectivamente.

Los compuestos RBM2-B y RBM2-D fueron los mejores inhibidores de la familia RBM2, con valores de IC₅₀ de 77 y 51 μM.

Es importante señalar que ninguno de los compuestos tuvo efecto sobre la ceramidasa neutra, aunque a concentraciones más altas son inhibidores de la enzima dihidroceramida desaturasa, con una IC_{50} de 18 y 100 μ M respectivamente.

Adicionalmente se estudio el efecto de los compuestos más activos como inhibidores de la ceramidasa ácida en el esfingolipidoma de las células PC3/Mc y HCT 116. Los resultados mostraron claramente la acumulación de las diversas especies de ceramidas, como consecuencia de la inhibición de la ceramidasa ácida. Sin embargo, este incremento en la concentración de ceramidas estaba acompañado de un aumento de la dihidroceramida, así como de otros esfingolípidos como la dihidroesfingomielina y la glucosil-dihidroceramida.

3. Estudio de la contribución de la ceramidasa ácida a la invasividad de las células de cáncer de próstata.

En colaboración con el Dr. T. Thomson (IBMB, CSIC, Barcelona), las células PC3/Mc fueron seleccionadas como modelo para investigar el papel de la ceramidasa ácida en la tumorigenicidad y metástasis en células cancerosas.

Como se ha mencionado, en diversos trabajos se ha descrito la sobre-expresión de la ceramidasa ácida en diversos tejidos tumorales de próstata, así como en las líneas celulares humanas de cáncer de próstata DU145, LNCaP y PC3, por lo que se decidió investigar cómo influye la actividad de la ceramidasa ácida en las diferencias fenotípicas de las células PC3/S y PC3/Mc.

En resultados anteriores se demostró que las células PC3/Mc muestran una elevada actividad de la ceramidasa ácida, comparadas con las células PC3/S. De acuerdo a reportes previos, una actividad de la ceramidasa ácida elevada disminuye los niveles de ceramida incrementando la proliferación celular bajo condiciones de pocos nutrientes, además de aumentar la tumorigenicidad in vivo y promover la migración en ensayos de invasividad.

Las células PC3/Mc fueron aisladas por el grupo del Dr. Thomson como un clon de características particulares a partir de las células PC3.

Estas células presentan un crecimiento rápido y son poco invasivas y altamente clonogénicas *in vitro*. Además, forman tumores de gran tamaño cuando son inyectadas de manera intramuscular en ratones y son altamente metastásicas al inyectarse por vía intravenosa en ratones NOD-SCID. Para conocer si la inhibición de la ceramidasa ácida ayuda a disminuir estas características, se abordó la inhibición de la actividad enzimática a través de dos estrategias: la inhibición con ARN de interferencia y la inhibición química.

Primero, se generó una línea celular estable knockdown para *ASAH1*, por medio de la transducción con lentivirus de las células PC3/Mc con shARN. Para lograr este fin, fueron evaluadas cinco secuencias diferentes complementarias al gen *ASAH1*. La inhibición más efectiva de la expresión de *ASAH1* fue obtenida con las secuencias denominadas 399 y 402.

Estos resultados fueron comprobados por qPCR, ensayos de actividad y Western Blot. Adicionalmente se realizó un análisis del contenido intracelular de esfingolípidos, confirmándose la acumulación de ceramidas en los clones 399 y 402.

3.1. Efecto del silenciamiento del gen *ASAH1* en el crecimiento celular.

El crecimiento de las células normales se detiene cuando entran en contacto entre ellas, un proceso conocido como inhibición por contacto. Esta característica se pierde durante la tumorigénesis, dando como resultado el crecimiento descontrolado.

Para conocer si el knockdown en el gen *ASAH1* permitía a las células PC3/Mc recuperar la inhibición por contacto se realizaron curvas de crecimiento en dos condiciones, 10 y 0.5% de SFB. Los resultados indicaron que las células knockdown crecían más lentamente que las PC3M/c control, cuando se utilizaban bajas concentraciones de suero; por el contrario, cuando crecían con un 10% de suero no había cambios significativos.

De acuerdo con lo descrito en trabajos anteriores, en los cuales la inhibición de la ceramidasa ácida producía una disminución del crecimiento de las células cancerosas cultivadas en condiciones de bajos nutrientes.

3.2. Efecto del silenciamiento de *ASAH1* en la invasividad

Para que las células sean capaces de formar metástasis deben cruzar la membrana basal y penetrar el estroma. La vía utilizada por las células es la producción elevada de proteasas que degradan la matriz extracelular. Para evaluar esta capacidad celular *in vitro*, se han desarrollado diversos ensayos de invasión, en los que se utiliza una placa con un filtro en la base cubierto con matrigel, un compuesto que mimetiza las características de la matriz extracelular. Utilizando este método se observó que las células knockdown en el gen *ASAH1* presentaban un aumento de la invasividad.

3.3. Efecto del silenciamiento del gen *ASAH1* en el crecimiento en 3D y formación de tumores

La habilidad de las células tumorales de formar colonias en agar está estrechamente relacionada con su capacidad para producir metástasis. En ensayos de crecimiento en agar, las células knockdown en el gen *ASAH1* presentaron una disminución significativa de su capacidad para formar colonias comparadas con las células PC3/Mc.

Estos datos coinciden con reportes previos, en los cuales se ha descrito que el silenciamiento por medio de ARN de interferencia en combinación con la radiación ionizante reduce significativamente la clonogenicidad de las células tumorales, comparadas con las células tratadas con un ARN de interferencia inespecífico.

En base a esos resultados, se decidió continuar con los experimentos de crecimiento tumoral en animales.. Las células PC3/Mc y sus derivadas knockdown en el gen *ASAH1* fueron inyectadas por vía intramuscular en las patas traseras de ratones NOD-SCID machos (6 por grupo). El crecimiento fue evaluado por medio de la producción de luminiscencia después de la inyección intraperitoneal de luciferina, ya que las células PC3/Mc expresan constitutivamente la enzima luciferasa.

El seguimiento se llevó a cabo durante 20 días y se observó que las células deficientes en ceramidasa ácida produjeron tumores significativamente menores comparados con las células control.

Después de estos experimentos se realizó una evaluación de la capacidad de estas células para colonizar los pulmones. Con este fin, los ratones NOD-SCID machos fueron inyectados en la vena caudal con células PC3/Mc o PC3/Mc knockdown en ASAH1 y el seguimiento fue similar al del experimento de crecimiento tumoral, pero la aparición de tumores en los pulmones se evaluó durante 55 días.

Los resultados mostraron que en los ratones inyectados con células knockdown en ASAH1 la aparición de tumores en los pulmones fue retrasada en comparación con las células intactas.

3.4. Inhibición química de la ceramidasa ácida en células PC3/Mc

Después de estudiar el efecto del bloqueo de la expresión y actividad de la ceramidasa ácida por medio de ARN de interferencia, se determinó el efecto de la inhibición química. Para este fin, se utilizaron los inhibidores RBM1-12, RBM1-13 y SABRAC a una dosis de 1 y 5 μ M. Mediante determinación de la cantidad de esfingolípidos intracelulares se confirmó la acumulación de ceramidas en las células tratadas con RBM1-12 y SABRAC, pero no así con RBM1-13, que parece no tener efecto sobre esta línea celular.

En este sentido, cabe resaltar que mientras la inhibición genética de la ceramidasa ácida produce un aumento en los niveles intracelulares de glucoesfingolípidos, la inhibición química no afecta las concentraciones de estos compuestos. Estas diferencias pueden estar relacionadas con el tiempo de incubación de las células con los inhibidores (48h), de manera que a tiempos de incubación mayores también se podrían acumular glucoesfingolípidos al utilizar los inhibidores.

3.5. Efecto de los inhibidores de la ceramidasa ácida en el crecimiento celular

Las células PC3/Mc fueron tratadas con los inhibidores a 5 μ M durante 7 días. Los resultados indicaron que los compuestos RBM1-12 y SABRAC, disminuyeron el crecimiento celular, mostrando el mismo efecto presentado en las células knockdown.

Por el contrario, no sucedió así con el compuesto RBM1-13, que mostró tener un efecto moderado en la inhibición del crecimiento. Lo cual coincide con la baja actividad que presenta este compuesto en células intactas, para inhibir a la ceramidasa ácida.

También llama la atención el hecho de que con el uso de inhibidores el crecimiento celular disminuye incluso en condiciones normales de cantidad de nutrientes, mientras que como se mencionó anteriormente la inhibición de la expresión de *ASAH1* solo tiene efecto en el crecimiento celular cuando las células son cultivadas en medio bajo en nutrientes.

3.6. Efecto de los inhibidores de la ceramidasa ácida en la invasividad.

La capacidad de las células PC3/Mc se redujo significativamente con el tratamiento con RBM1-12 y SABRAC. Estos resultados no coincidían con los obtenidos mediante silenciamiento, en los cuales la invasividad aumentaba con la inhibición de la expresión del gen *ASAH1*.

Una explicación posible a este fenómeno es la acumulación de esfingosina en las células silenciadas, posiblemente derivada de actividad aumentada de otra ceramidasa, pero no en las células sometidas a tratamiento con inhibidores.

La conversión de la esfingosina en esfingosina-1-fosfato explicaría el aumento de invasividad en las células silenciadas, pero no en las tratadas con inhibidores. Sin embargo, serán necesarios más experimentos para determinar las causas de esta importante diferencia.

3.7. Efecto de los inhibidores de ceramidasa ácida en la clonogenicidad.

Para continuar con la comparación de los efectos del silenciamiento genético y la inhibición química, las células PC3/Mc fueron incubadas en agar en presencia de 1 o 5 μM de los inhibidores RBM1-12 o SABRAC. Cuando las células fueron tratadas con 1 μM la formación de colonias fue igual a la de las células control, mientras que a 5 μM la invasividad disminuyó

3.8. Evaluación de la toxicidad del SABRAC.

Un paso previo a la determinación del efecto del inhibidor de la ceramidasa ácida SABRAC, en la tumorigenesis in vivo y la colonización pulmonar en ratones NOD-SCID, la toxicidad de la administración aguda y crónica de los compuestos fue determinada en ratones CD1. La LD_{50} del tratamiento agudo fue de 200 mg/Kg, así que para el tratamiento crónico se selecciono la dosis de 75 mg / Kg

Conclusiones

1. El compuesto RBM13 es sustrato de la enzima esfingosina fosfato liasa. Sin embargo, a pesar de que la afinidad por la enzima es baja, su uso en combinación con el extracto bacteriano enriquecido en SPL permite la identificación de inhibidores de la SPL a través del cribado de quimiotecas.
2. La cuantificación del pentadecanal por cromatografía de gases masas acoplada a espectrometría de masas después de la conversión a la oxima correspondiente es un procedimiento sensible para medir la actividad de la SPL utilizando el análogo C17 de la esfinganina-1-fostato como sustrato.
3. Los compuestos RBM14 C10 al C16 son hidrolizados por la ceramidasa ácida y la ceramidasa neutra, pero no por las ceramidases alcalinas ACER1, ACER2 y ACER3. El RBM14 C4 no es sustrato ni de la ceramidasa neutra ni de la ácida, mientras que el sustrato RBM14 C8 es hidrolizado exclusivamente por la ceramidasa neutra.

4. El compuesto RBM14 C12 es una herramienta excelente para el diagnóstico de la enfermedad de Farber.
5. Las células HCT116 379, deficientes en p53, hidrolizan de manera menos eficientes los sustratos de ceramidasa RBM14 comparadas con la línea silvestre HCT116 40-16. Las células de cáncer de próstata PC3/S (muy invasivas, poco metastásicas) son menos activas hidrolizando los sustratos RBM14, comparadas con las células PC3/Mc (muy metastásicas, poco invasivas).
6. Los compuestos RBM14 son poco metabolizados por otras enzimas del metabolismo de los esfingolípidos en comparación con la hidrólisis producida por las ceramidasa neutra y ácida.
7. Los compuestos RBM2-1B y RBM2-1D son inhibidores de la ceramidasa ácida y de la dihidroceramida desaturasa, aunque con distintas potencias.
8. La inhibición genética o química de la ceramidasa ácida reduce el crecimiento celular y la clonogenicidad de las células PC3/Mc. Sin embargo, la inhibición genética aumenta la migración celular, mientras que la inhibición química la reduce.
9. El compuesto RBM1-13 inhibe la ceramidasa ácida en las células Moh pAS, pero no en las células PC3/Mc.
10. Los ratones NOD-SCID inoculados con células knockdown en *ASAH1* producen tumores significativamente más pequeños comparados con los inyectados con las células PC3/Mc y muestran una capacidad reducida de desarrollar tumores metastásicos en pulmón.
11. El SABRAC es el inhibidor de la ceramidasa ácida más potente descrito hasta el momento. Su baja toxicidad en ratones lo resalta como un posible candidato para la terapia antitumoral conjunta con agentes de quimioterapia.